Simulations of 2016 Hydrodynamics and Water Quality in the Massachusetts Bay System using the Bays Eutrophication Model

Massachusetts Water Resources Authority
Environmental Quality Department
Report 2017-13

Citation:

Zhao L, Beardsley RC, Chen C, Codiga DL, Wang L. 2017. **Simulations of 2016 Hydrodynamics and Water Quality in the Massachusetts Bay System using the Bays Eutrophication Model.** Boston: Massachusetts Water Resources Authority. Report 2017-13. 111pp.

Acronyms

Related to models used

BEM	Bays Eutrophication Model (water quality model UG-RCA and hydrodynamics model MB-FVCOM together)
FVCOM	Finite-Volume Community Ocean Model
Global-FVCOM	FVCOM applied to the global oceans
GOM4-FVCOM	FVCOM for Gulf of Maine (GOM), Scotian and southern New England shelves, and Georges Bank: 45 vertical layers, nested in Global-FVCOM
MB-FVCOM	FVCOM applied to Massachusetts Bay
RCA	Row Column Advanced (RCA), a water quality model originally developed by Hydroqual
UG-RCA	Unstructured-grid version of RCA
WRF	Weather Research and Forecast meteorological model

Related to modeled quantities

DIN	Dissolved Inorganic Nitrogen (Sum of Nitrogen in NH_4^+, NO_3^-, and NO_2^-)
DO	Dissolved Oxygen
DOC, DON, DOP	Dissolved Organic Carbon, Nitrogen, and Phosphorous
NH_4^+, NO_3^-, NO_2^-	Ammonium, Nitrate, Nitrite
PO_4^{3-}, SiO_3^{2-}	Phosphate, Silicate
POC, PON, POP	Particulate Organic Carbon, Nitrogen, and Phosphorous
SOD	Sediment Oxygen Demand

Simulations of 2016 Hydrodynamics and Water Quality

in the Massachusetts Bay System using the Bays Eutrophication Model

Submitted to

Massachusetts Water Resources Authority
Environmental Quality Department
100 First Avenue
Charlestown Navy Yard
Boston, MA 02129
(617) 242-6000

Prepared by

Liuzhi Zhao[1], Robert C. Beardsley[2], Changsheng Chen[1], Daniel L. Codiga[3], and Lu Wang[1]

[1]School for Marine Science and Technology
University of Massachusetts-Dartmouth
New Bedford, MA 02744

[2]Woods Hole Oceanographic Institution
Woods Hole, MA 02543

[3]Massachusetts Water Resources Authority
Boston, MA 02129

January 2018

EXECUTIVE SUMMARY

The hydrodynamics (including temperature, salinity, and currents) and water quality (including nutrients, chlorophyll, and dissolved oxygen) of Massachusetts Bay, Cape Cod Bay, and Boston Harbor during 2016 were simulated by University of Massachusetts Dartmouth. Methods were the same as in simulations of 2015 (MWRA Technical Report, http://www.mwra.state.ma.us/harbor/enquad/pdf/2016-16.pdf) except that the grid resolution in the northern Gulf of Maine portion of the regional hydrodynamic model was increased. Hydrodynamic results were in good agreement with available observations for the geographic and vertical structure, and temporal variability, of temperature and salinity distributions (including density stratification) and currents (non-tidal and tidal).

The water quality simulation captured general patterns in observed seasonal variations, geographic distributions, and vertical structure for many variables. This included the late spring reduction in near-surface dissolved inorganic nitrogen (DIN), due to phytoplankton uptake, and its replenishment when stratification broke down in fall. It also included seasonal dissolved oxygen variations, with peak values in spring at shallow depths due to colder water and phytoplankton growth, and late summer minima deep in the water column where stratification inhibits reaeration by air-sea exchange. In addition to those more bay-wide patterns, DIN was elevated near the seafloor within 10-20 km of the outfall. Model-observation agreement was modest for dissolved and particulate organic nitrogen and weakest for particulate organic carbon, particularly its vertical structure, and for chlorophyll. In general, as in prior years, most modeled water quality variables exhibited a smaller range of values, and smaller surface-bottom differences during stratified conditions, than did field observations. The simulations support the conclusion of the field monitoring program, that bay-wide ecological function is not appreciably influenced by the outfall.

Potential outfall nutrient load influences were examined using two runs with effluent nutrients increased/decreased 20% relative to observed 2016 levels; the 2016 nitrogen load was just below the 12,500 metric tons per year (MT/yr) caution threshold in the Contingency Plan attached to the outfall permit. The 20% increase caused minor (about 8%) nutrient increases at depth near the outfall, much smaller chlorophyll increases, and imperceptible effects on oxygen. The results suggest bays ecology would be unharmed even for nitrogen load above the 14,000 MT/yr warning threshold (the projected 2020 load for anticipated population increases). Bay nutrients mostly come from exchange with Gulf of Maine waters and only a small fraction is contributed by the outfall.

Table of Contents

List of Figures

List of Tables

1. Introduction

1.1 *Project overview*

The Massachusetts Water Resources Authority (MWRA) has established a long-term monitoring program to evaluate the impact of MWRA sewage treatment plant effluent on the water quality and ecosystem function of Massachusetts Bay, Cape Cod Bay, and Boston Harbor. The monitoring program primarily consists of a series of ongoing field observation surveys and includes complementary water quality modeling as required by the permit for effluent discharge into Massachusetts Bay. The water quality simulations are carried out using the Bays Eutrophication Model (BEM), which consists of the Unstructured Grid Row Column Advanced (UG-RCA) water quality model and the Massachusetts Bay Finite Volume Community Ocean Model (MB-FVCOM) hydrodynamic model. This report presents simulation results for the 2016 calendar year.

1.2 *Background on oceanographic processes influencing water quality*

Massachusetts Bay and Cape Cod Bay (Figure 1-1) comprise a temperate coastal embayment system. Readers unfamiliar with the geography and/or the current understanding of the physical and biological oceanographic processes characterizing the system are referred to the introductory summaries found in sections 1.2 and 1.3 of MWRA Technical Report 2011-13 (Zhao et al., 2012), in the annual MWRA water column monitoring report (e.g., for calendar year 2016, Libby et al., 2017), and in references cited by them. (All MWRA Technical Reports, including those just cited, are available online at http://www.mwra.state.ma.us/harbor/enquad/trlist.html.) A brief summary follows here.

System hydrodynamics are characterized by a persistent general circulation pattern driving the flow of offshore Gulf of Maine waters into Massachusetts Bay via the Western Maine Coastal Current off Cape Ann, then southward before returning offshore just to the north of Cape Cod, with a portion of the flow first passing through Cape Cod Bay to the south. Rough estimates of the water residence time are about a month based on the surface currents, somewhat longer at mid-depth or deeper, where currents are weaker, and also longer in Cape Cod Bay than in Massachusetts Bay. While this slow general circulation is important in determining long-term average transport pathways, superposed on it are stronger and more variable wind-driven currents, and oscillatory tidal motions. Temperatures follow the characteristic temperate seasonal pattern of minima in late winter and peaks in late summer. Salinities are freshest inshore and in the upper several meters; in

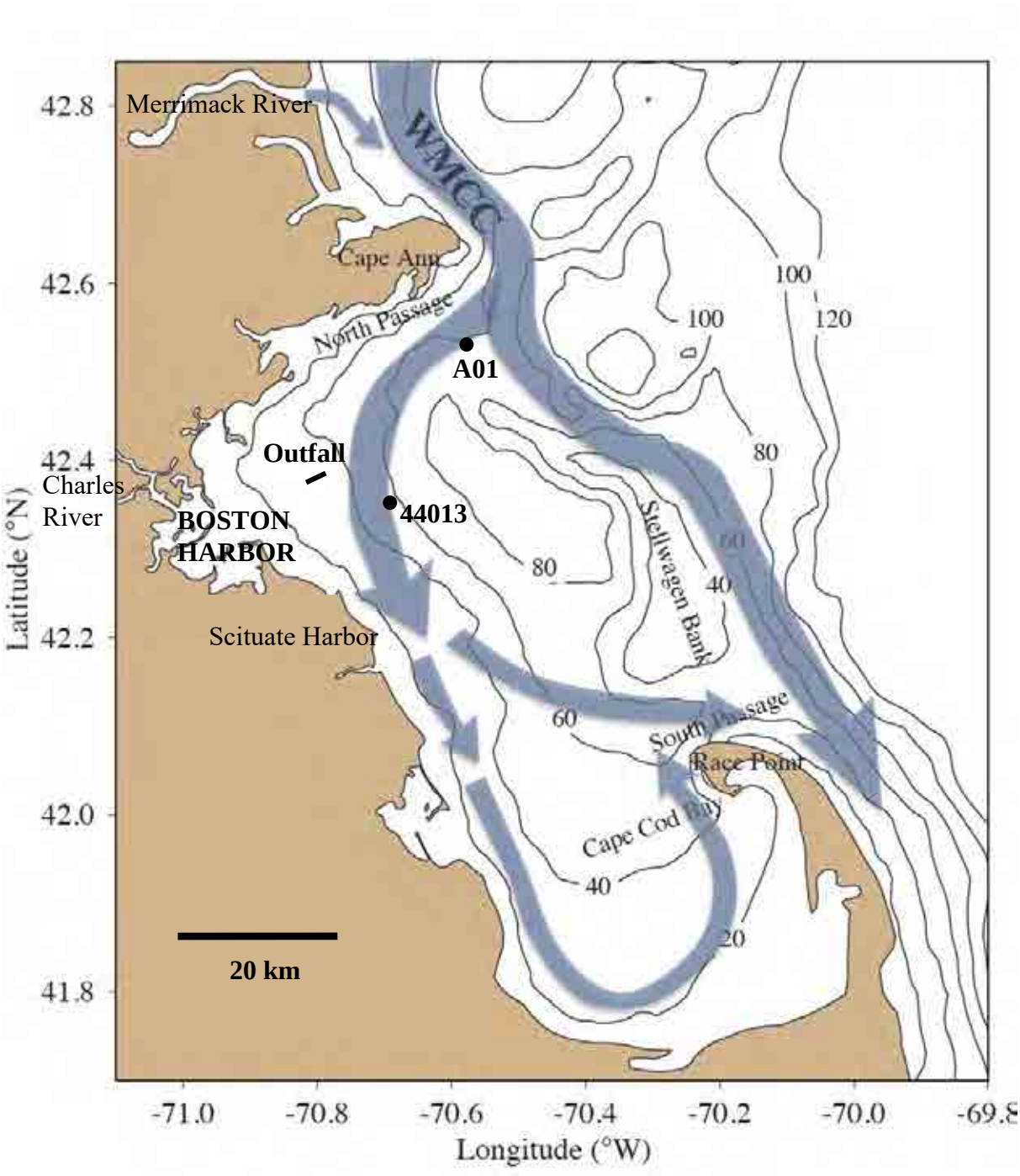

Figure 1-1. Geography, bathymetry, schematic long-term mean circulation.

WMCC = Western Maine Coastal Current.
A01 = Oceanographic mooring (Northeastern Regional Association of Coastal Ocean Observing Systems).
44013 = Weather buoy (National Data Buoy Center).
Contours = water depth in meters.
Figure adapted from Xue et al. (2014).

addition to the influence of offshore oceanographic conditions, they vary mainly in response to riverine inputs including primarily those brought by the Western Maine Coastal Current and the Merrimack River outflow to the north, and to a lesser extent the smaller amounts delivered via Boston Harbor. There is a seasonal cycle in vertical structure that includes transitions between well-mixed conditions, present from fall through early spring due to higher winds and atmospheric cooling, and strong density stratification during the late spring and summer due mainly to increased surface temperatures resulting from atmospheric heating.

The biology of the system is plankton-based and exhibits clear seasonal cycles that are tied closely to those hydrodynamic features, but with more pronounced spatial and interannual variability. Phytoplankton abundance typically peaks most strongly during bloom-favorable conditions in the late winter and early spring, as temperatures rise, light increases, and nutrients remain plentiful near the surface due to the active vertical mixing. Following the transition from spring to summer, near-surface nutrient concentrations become depleted as density stratification impedes the vertical mixing that replenishes them. Zooplankton abundance and biomass generally peak in late summer, following the spring increase in phytoplankton prey levels. Primary productivity is commonly sustained at modest levels through summer and typically there is a second increase in phytoplankton during fall, when vertical mixing increases again and delivers nutrients to the surface while temperature and light conditions are still favorable before winter. Dissolved oxygen concentrations are influenced by a combination of biological and physical processes; the net result is a seasonal peak in late spring, due to phytoplankton production increasing winter levels already high due to strong reaeration, then steady decreases to a late summer minimum due to respiration and reduced reaeration. The summer oxygen minimum is lower at depth, where stratification limits reaeration.

1.3 *Summary of observed 2016 conditions*

To provide context for descriptions of model simulations of 2016 throughout this report, a brief summary is given here of observed 2016 conditions based on MWRA monitoring results (Libby et al., 2017). Temperatures in 2016 were warmer than normal and it was an unusually dry year. The Merrimack and Charles Rivers had the lowest flows observed during the past 25 years of MWRA monitoring. Winter 2016 was the fifth year in a row with relatively low to moderate nutrient concentrations during the February survey, and slightly elevated and steady chlorophyll concentrations over the wintertime (based on satellite observations), which suggests the possibility

that the system may have remained more biologically productive through the winter than in typical years prior to the past five. Due to strong springtime winds, stratification developed later than in a typical year. The spring bloom, in late April or early May, was relatively small and predominantly *Phaeocystis*, not diatoms as is more typical. Nutrient levels were comparable to past years, including slightly elevated ammonium at depth within about 10-20 km of the outfall. Summer chlorophyll levels were relatively high compared to past years. In fall, when phytoplankton blooms are typical, none were observed during MWRA vessel-based surveys. Consequently, annual total phytoplankton abundance estimates were low compared to typical years. In contrast, zooplankton abundances were at high or maximal levels compared to previous years for most of the year, including during their summertime peak. Bottom water dissolved oxygen concentration minima were relatively low in 2016 compared to past years. They might have been lower if not for a late May mixing event, which raised them prior to the summertime drawdown, and also if not for a September storm with winds that broke down stratification earlier than in a typical year.

2. Methods

2.1 *Overview*

The present-day BEM is the result of extensive development begun in the early 1990s. Complete background information is in MWRA technical reports, where the model development and updating process has been documented. MWRA Technical Report 2015-02 (Zhao et al., 2015a) provides a comprehensive listing (their Table 1.1) of MWRA technical reports about the modeling (up to and including simulations of 2011), including for each report a summary of its topic, highlighted aspects of its content, the full citation, and (when viewed electronically) a hyperlink to the downloadable PDF file in the online repository. Section 1.4 of Zhao et al. (2012) reviews some of the key improvements incorporated to modeling methods, with emphasis on the several years leading up to the simulations of 2011. Simulations of years 2008 and later use MB-FVCOM for hydrodynamics and UG-RCA for water quality. The methods used in the simulations of 2016 are the same as for simulations of 2015 (Zhao et al., 2016b), except for the use of a grid with minor improvements, as described in Section 2.2 below. A brief overview of the methods is as follows.

The model grids consist of four domains. The largest domain is the Global-FVCOM simulation, with worldwide coverage (Figure 2-1; Chen et al., 2016). Nested within Global-FVCOM is the regional Gulf of Maine (GOM) FVCOM hydrodynamic model (GOM4-FVCOM; lower panel, Figure 2-2). Circulation in GOM4-FVCOM along its offshore boundary, including tidal variability, is driven ("forced") by circulation of the Global-FVCOM simulation. Nested within the GOM4-FVCOM domain is the higher-resolution grid of the Massachusetts Bay FVCOM (MB-FVCOM) hydrodynamic model (upper panel, Figure 2-2). The MB-FVCOM domain extends offshore to an open boundary along an arc southeastward from north of Portsmouth, New Hampshire that passes about 25 km offshore from Cape Cod. Circulation in MB-FVCOM along this boundary, including tidal variability, is driven by circulation of the GOM4-FVCOM simulation. The fourth and smallest domain is that for the UG-RCA water quality model, which is the same as the MB-FVCOM grid except that it extends less far offshore, having an open boundary along an arc from near Cape Ann to the eastern shore of Cape Cod (upper panel, Figure 2-2). In MB-FVCOM and UG-RCA, horizontal resolution ranges from about 0.29 km near the coast to 0.7-2.5 km at the eastern boundary of UG-RCA and 5-10 km near the offshore MB-FVCOM nested boundary. In the vertical, the models have 45 grid levels. In areas shallower than 225 m deep, the levels are uniformly distributed; in deeper areas, the shallowest and deepest levels are concentrated

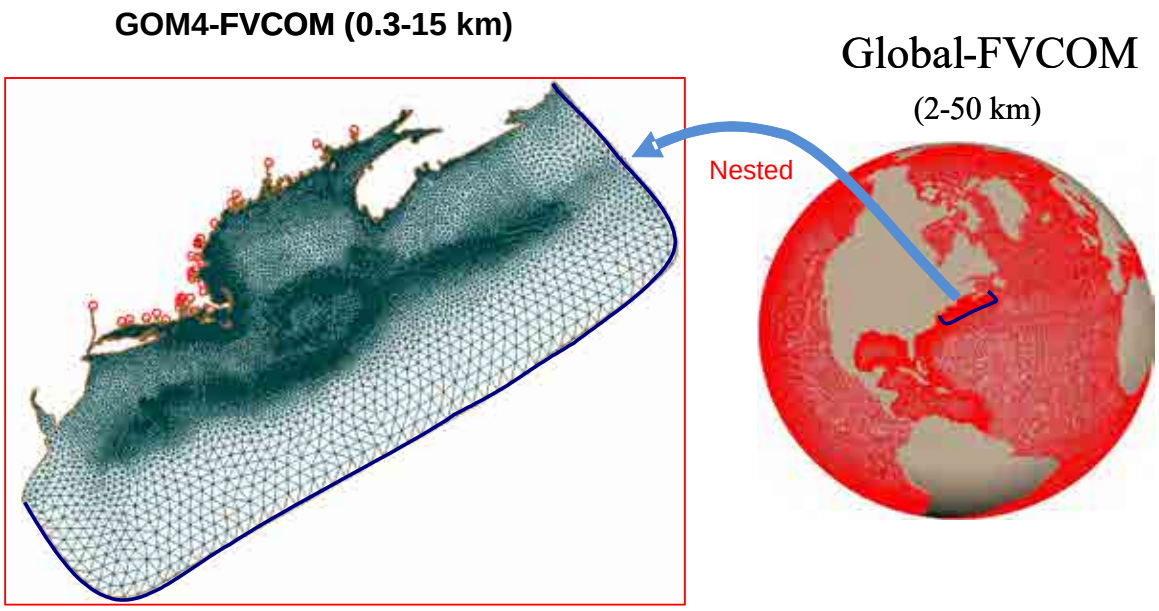

Figure 2-1. GOM4-FVCOM grid and Global-FVCOM grid.

GOM4-FVCOM is the new regional grid introduced for the 2016 simulation. It includes higher resolution in the northern Gulf of Maine, as compared to the GOM3-FVCOM grid used for simulations of 2015 conditions (the latter is shown in Figure 2-1 of Zhao et al., 2016b; because of the fine resolution, differences between GOM4 and GOM3 are hardly visible in this presentation). The higher resolution improves model fidelity for conditions in the northern Gulf of Maine, which influence offshore conditions that drive the Mass Bay model. Red dots in left panel show locations of freshwater input.

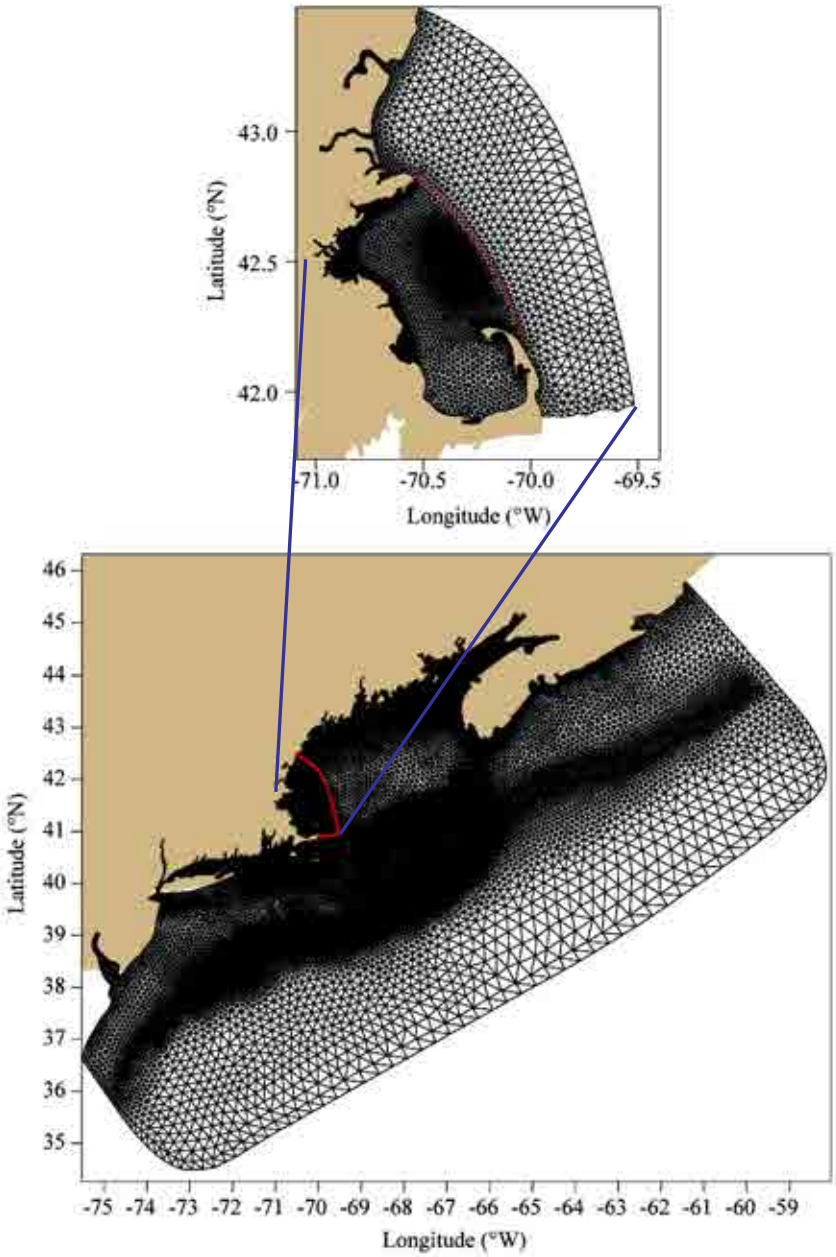

Figure 2-2. Model grids: GOM4-FVCOM, MB-FVCOM, and UG-RCA.

Lower panel: Gulf of Maine grid, GOM4-FVCOM; the red line shows the offshore boundary of the nested Massachusetts Bay grid, MB-FVCOM. Upper panel: nested MB-FVCOM domain; red line shows offshore boundary of the smaller domain of the water quality model, UG-RCA.

in constant-thickness boundary layers, between which the remaining levels are uniformly distributed. The GOM4-FVCOM and MB-FVCOM hydrodynamic models are forced at the surface by the data-assimilative Weather Research and Forecast (WRF) meteorological model, along the coast by freshwater inputs from rivers, and at the seafloor by the MWRA outfall. In addition to satellite sea surface temperature, the models assimilate all available observed temperature and salinity profiles and moored timeseries collected throughout their geographic coverage areas (as described in Zhao et al., 2016a).

The water quality model UG-RCA is driven using the circulation and eddy diffusivity from the MB-FVCOM hydrodynamic model output. UG-RCA is an unstructured grid version of RCA-v3.0 (Hydroqual, 2004), which simulates 26 water column parameters and 23 sediment variables, a subset of which are shown in a schematic diagram of modeled processes (Figure 2-3). Three phytoplankton functional groups are included: a winter-spring group favoring low temperatures, low light, and high nutrients (representative of diatoms); a summer group that favors higher temperature and light conditions, and tolerates lower nutrients (representative of a mixture of species including dinoflagellates); and a fall group most responsive to moderate temperatures and lower nutrients (representative of a second diatom group). Growth of phytoplankton is based on solar radiation and nutrient availability. Grazing by zooplankton, which are not directly modeled, is treated as a transformation of mass in the phytoplankton groups to particulate and dissolved organic matter at rates that increase linearly with temperature. Nutrients (including nitrate NO_3^-, nitrite NO_2^-, ammonium NH_4^+, phosphate PO_4^{3-}, and dissolved silica SiO_3^{2-}) are formed through mineralization of organic substances in the water column and at the sea floor. Cycling of labile and refractory forms of dissolved and particulate organic carbon, nitrogen, and phosphorous is included. Dissolved oxygen concentration is computed by the reaeration flux at the sea surface, sediment oxygen demand at the bottom, and biological and biogeochemical dynamics in the water column including phytoplankton photosynthetic production, consumption by respiration, biogeochemical oxygen demand through the mineralization of particulate and dissolved organic matter, and nitrification. Open boundary condition fields are specified using MWRA monitoring program observations and the method of objective analysis (e.g., Tian et al., 2009). MWRA outfall nutrient and carbon loadings are specified using Deer Island Treatment Plant data.

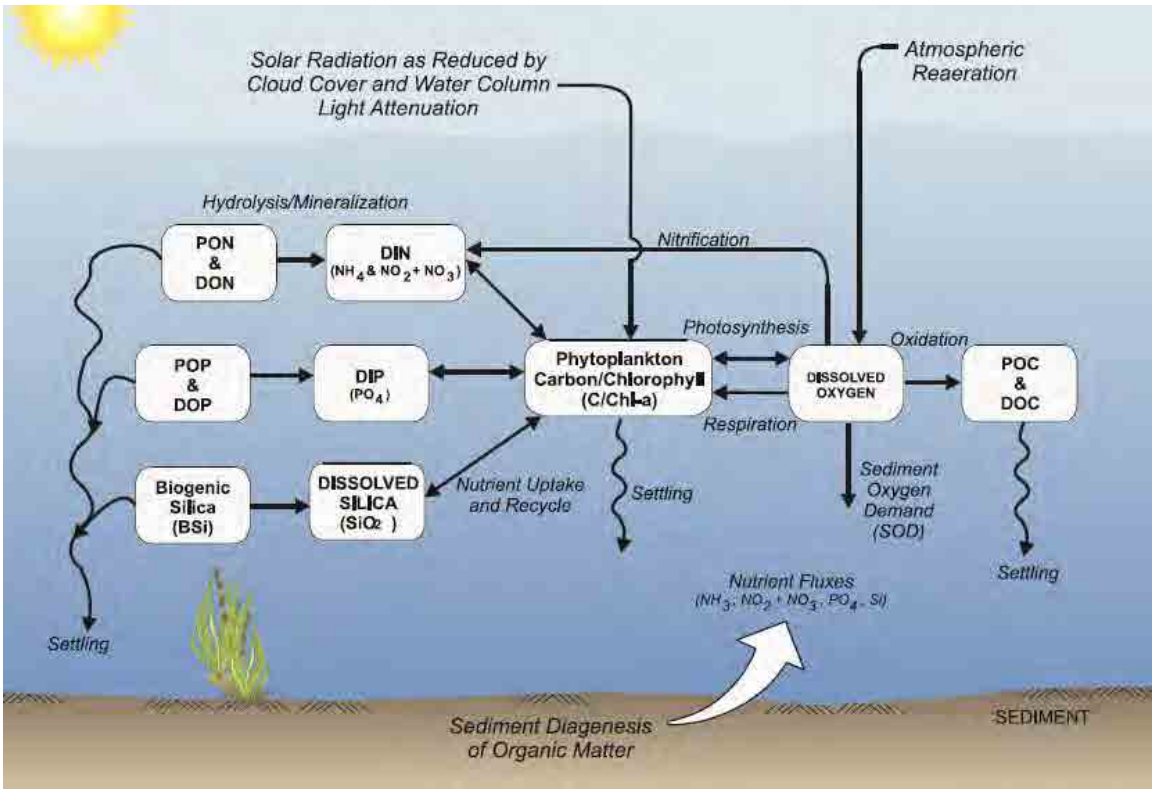

Figure 2-3. Water quality model dynamics, schematic (reproduced from Hydroqual, 2004).

2.2 *Replacement of GOM3-FVCOM by GOM4-FVCOM*

For the 2016 simulation the Bays Eutrophication Model was updated by replacing the GOM3-FVCOM regional hydrodynamics model, used in 2015 simulations, by GOM4-FVCOM. The latter has higher grid resolution in the northern Gulf of Maine, which improves the model fidelity there and thus provides a more accurate offshore forcing influence on the MB-FVCOM simulations.

3. Forcing conditions

3.1 *Wind, heat flux, light, and rivers*

The main characteristics of 2016 wind forcing are revealed by comparisons with the long-term mean and standard deviation of previous years from 1995 to 2015 (Figure 3-1). The seasonal pattern of vector-averaged velocities (top frame) was generally similar to the long-term mean; in the month of August the wind was relatively strong and from the southwest, in contrast to the long-term mean which is from the northeast and weaker. The wind speeds (second frame) in 2016 are comparable to the long-term mean most of the year and up to about one standard deviation higher in some months, for example June through August. The wind stress magnitude (third frame) was higher than the long term average during nearly all of the year, and particularly high in January and December. The north-south wind stress (bottom frame), a diagnostic for upwelling, was substantially stronger than typical, and southward, in August and September.

The main attributes of the 2016 air-sea heat flux are seen on comparisons with the long-term mean and standard deviation (Figure 3-2). The seasonal pattern in 2016 (top frame) had negative heat flux (loss of heat from surface; cooling of ocean) during winter and positive heat flux (heating of ocean) during summer, as does the long-term mean. The cumulative flux (middle frame) results emphasize that winter/spring cooling in 2016 was relatively weak, such that the cumulative flux was higher than the long-term mean in spring; by early summer, weaker warming than typical had compensated, and for the remainder of the year the cumulative flux was lower than typical. The anomaly of 2016 relative to the long-term mean (bottom frame) highlights this change in sign in mid-spring, with the cumulative anomaly becoming positive in spring and then negative later in the fall, and the end of year anomaly being negative.

The largest riverine influence on Massachusetts Bay is the Merrimack River. On entering coastal waters north of the bay it joins the Western Maine Coastal Current, which can flow into the bay off Cape Ann (Figure 1-1). The 2016 Merrimack volume transport (Figure 3-3) was substantially lower than the long-term mean throughout the entire year, with the exception of a few events in the winter and early spring. The cumulative values (middle frame) were above typical for approximately the month of March and distinctly lower than the long-term average for the rest of the year. The cumulative anomaly (bottom frame) was large and negative.

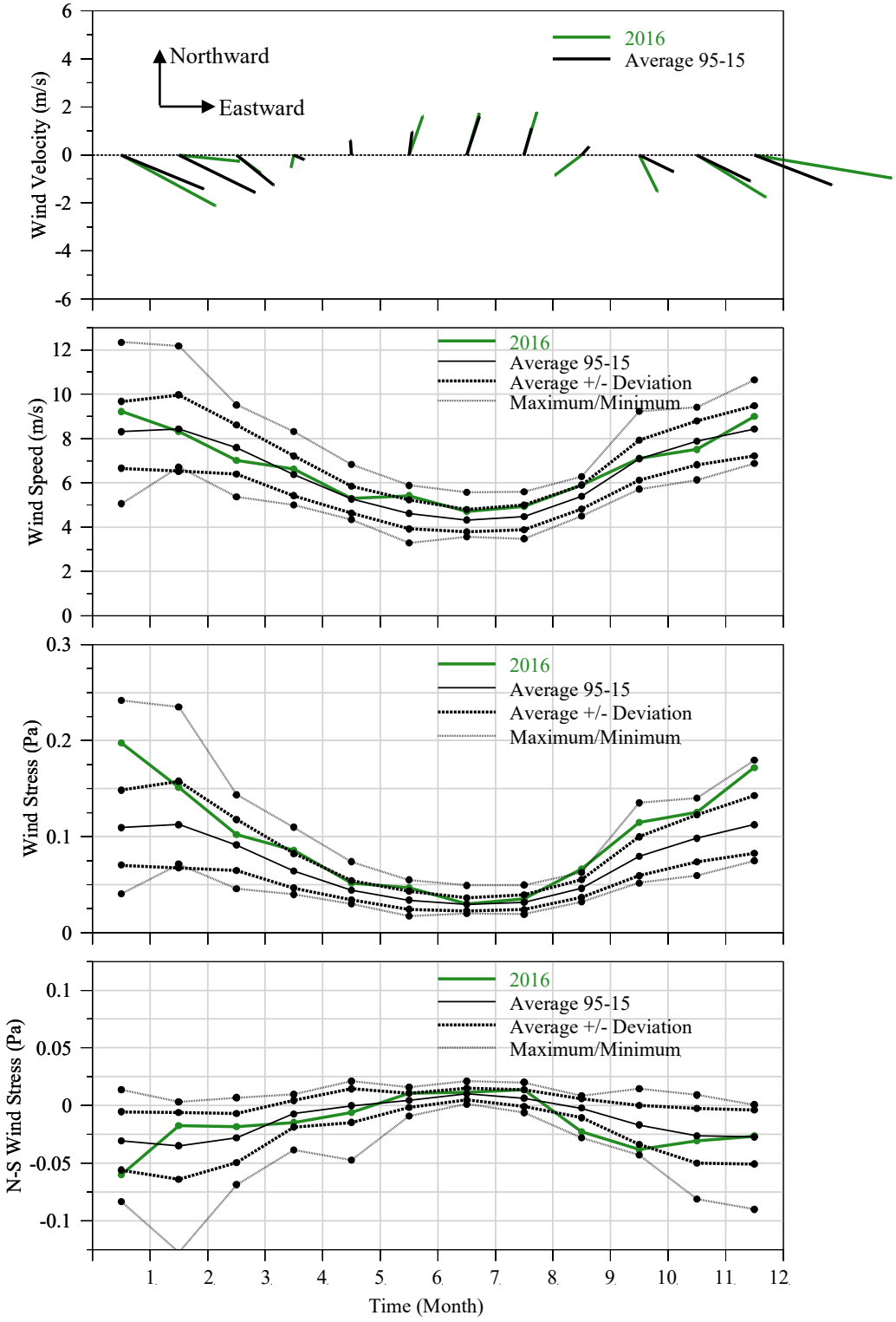

Figure 3-1. Surface wind forcing, monthly averages.

Top frame: Vector-averaged wind velocities. Second frame: Wind speed. Third frame: Wind stress magnitude. Bottom frame: North-south component of wind stress, an indicator for wind-driven upwelling.

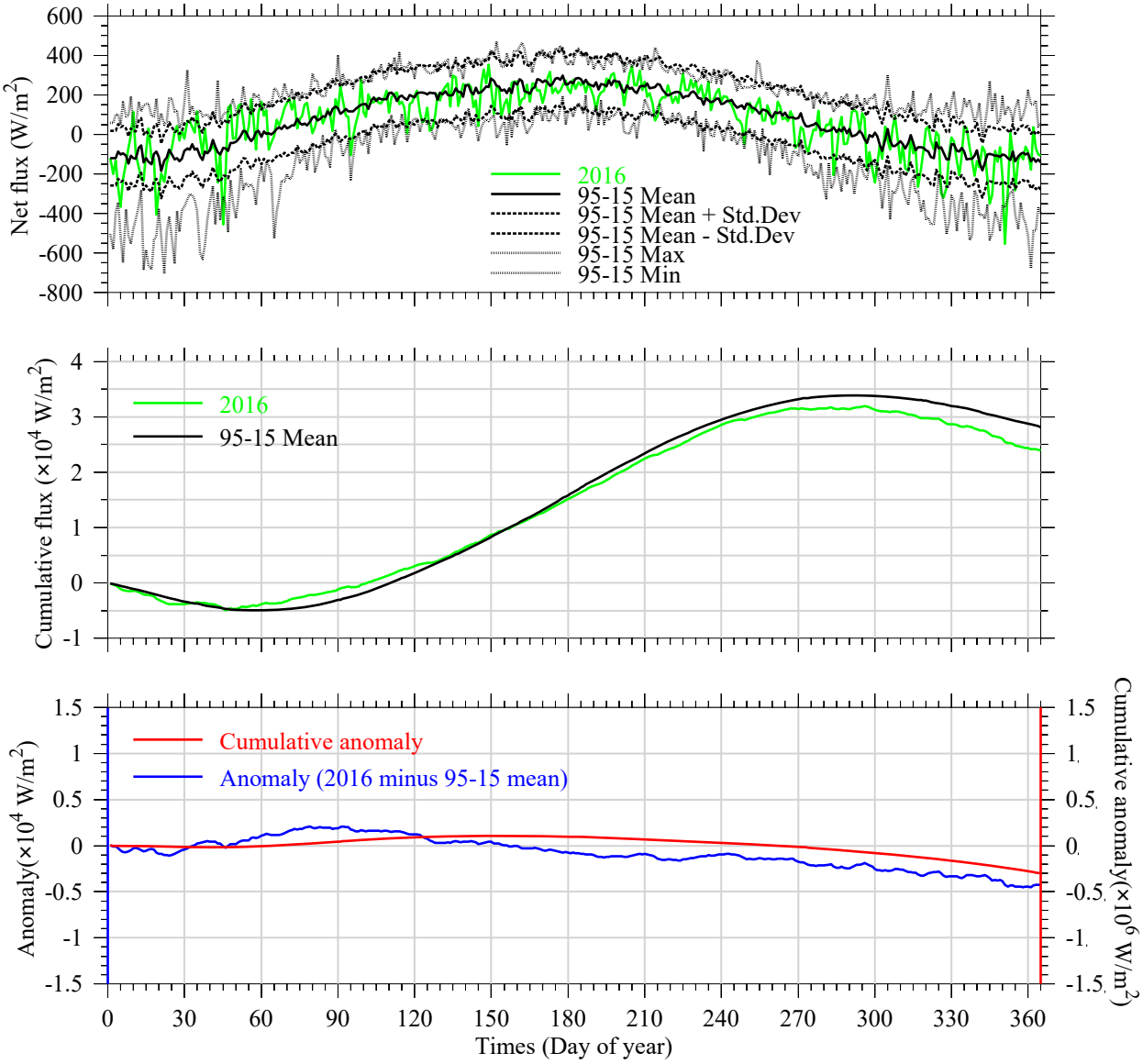

Figure 3-2. Surface heat flux.

Top frame: Net heat flux into ocean. Middle frame: Cumulative net heat flux relative to January 1. Bottom frame: Anomaly of 2016 net heat flux (blue, left vertical axis) relative to 1995-2015 average; cumulative anomaly relative to January 1 (red, right vertical axis).

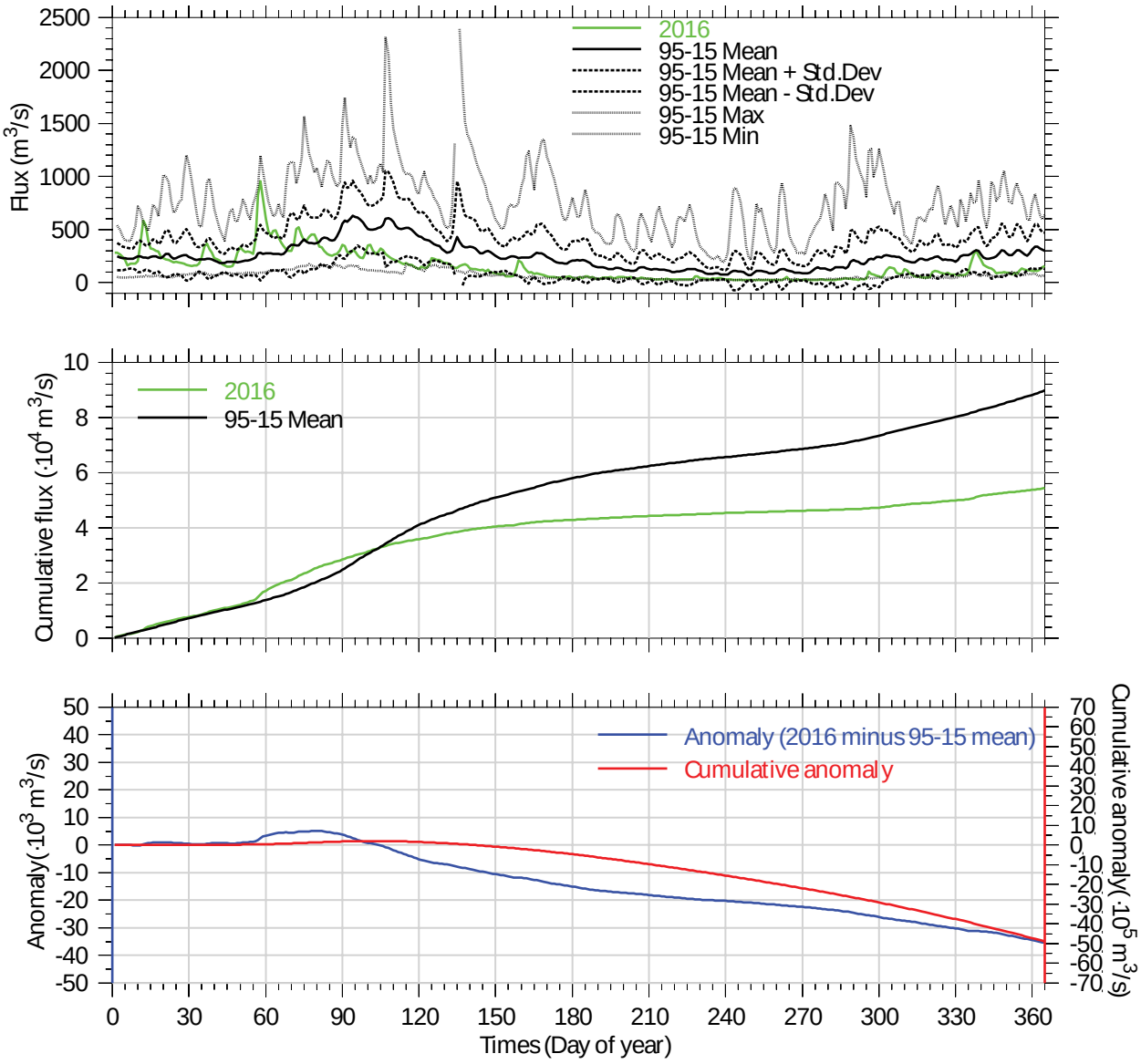

Figure 3-3. Merrimack River daily/cumulative flux, and anomaly relative to long-term mean.

Top frame: Merrimack River volume flux. Middle frame: Cumulative flux relative to January 1. Bottom frame: Anomaly of flux in 2016 relative to 1995-2015 average (blue, left vertical axis); cumnulative anomaly relative to January 1 (red, right vertical axis).

3.2 *Loading of organic carbon, nitrogen, and phosphorous*

There are both oceanic and non-oceanic sources of organic materials and nutrients to the bays. The oceanic component stems from exchange with adjacent offshore waters of the Gulf of Maine. These offshore waters are not characterized by particularly high concentrations, but the volume of the exchange is very large. A systemwide budget for total nitrogen in the bays, based in part on results from BEM simulations of 1992 conditions, concluded that approximately 93% originated offshore in the Gulf of Maine (Hunt et al., 1999; Hydroqual, 2000). Consequently, oceanic input is by far the single largest source of organic materials and nutrients to the bays. While conditions change from year to year and it is recognized there have been long-term changes to loads since 1992, the estimated 93% oceanic fraction for total nitrogen remains broadly representative of today's conditions, and is likely roughly applicable to all organic materials and nutrients.

The smaller non-oceanic sources include rivers, terrestrial runoff other than rivers (referred to as non-point sources), atmospheric deposition, and sewage outfalls (referred to as point sources). Point sources include both the MWRA outfall and non-MWRA outfalls. To help put the MWRA outfall contribution in context, estimates of the non-oceanic sources have been made and compared (Figure 3-4). In 2016 the non-MWRA outfalls contributed most to organic carbon loading, followed by the MWRA outfall, atmospheric deposition, non-point sources and rivers. The MWRA outfall was the largest input to nitrogen loading (ammonium, nitrate, and nitrite), followed by atmospheric deposition, non-MWRA outfalls, non-point sources, and rivers. For phosphorus loading, the MWRA outfall contributed the largest portion, followed by non-MWRA outfalls, non-point sources, rivers, and atmospheric deposition. Note that for non-MWRA outfalls, use has been made of the only available dataset for conditions across the Massachusetts Bays system (Menzie-Cura and Associates, 1991), for which there are recognized limitations to applicability given that treatment levels at some non-MWRA outfalls have changed since that study.

For the MWRA outfall the annual mean volume flow in 2016 (Figure 3-5) was the lowest recorded to date, and substantially lower than the average over the past 10 years. The 2016 outfall carbon load was below the average over the past 10 years, while the 2016 nitrogen load was higher than the average over the past 10 years. The 2016 phosphorous load was comparable to the long-term mean.

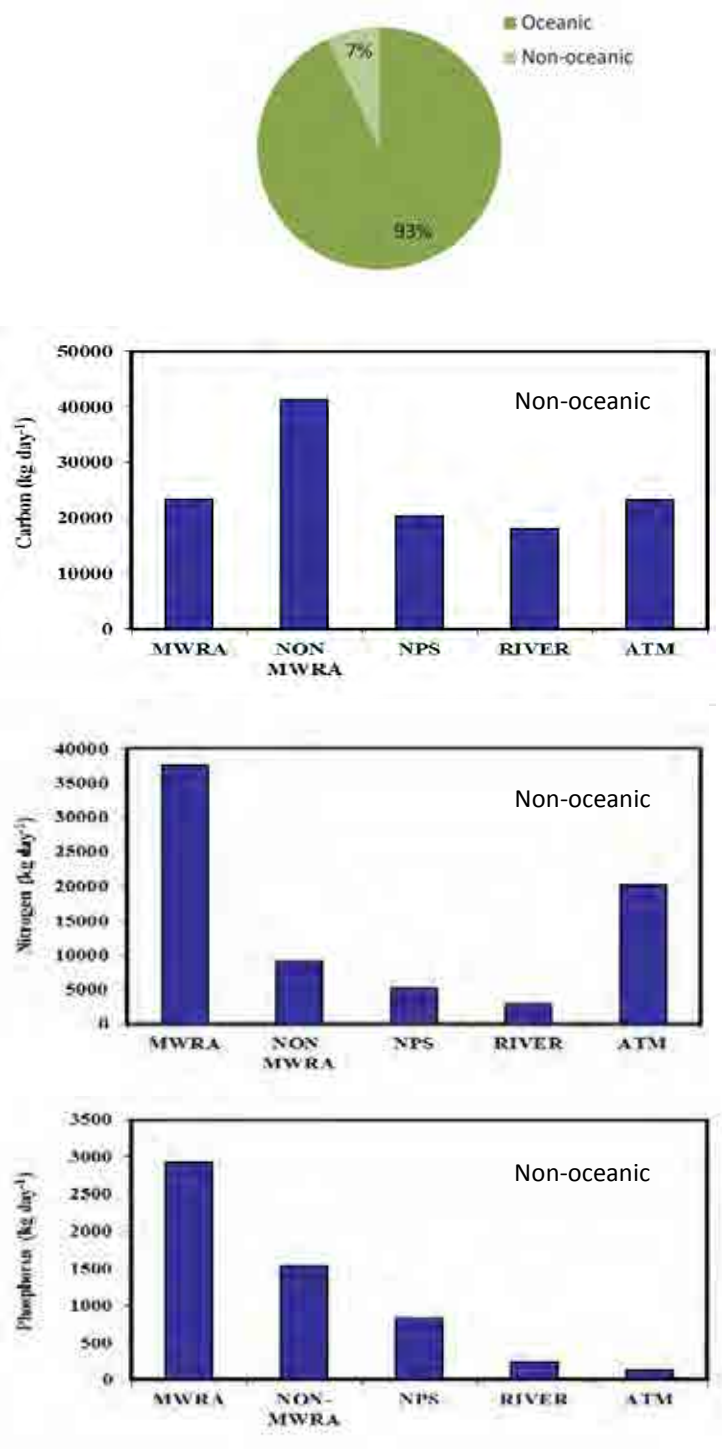

Figure 3-4. Mean daily 2016 non-oceanic loads (carbon, nitrogen, phosphorous).

MWRA = MWRA Outfall; NON-MWRA = Non-MWRA point sources; NPS = Non-point sources; RIVER = River loadings. ATM = Atmospheric deposition.

Top pie chart: Representative estimate of oceanic/non-oceanic sources of total nitrogen (see text).

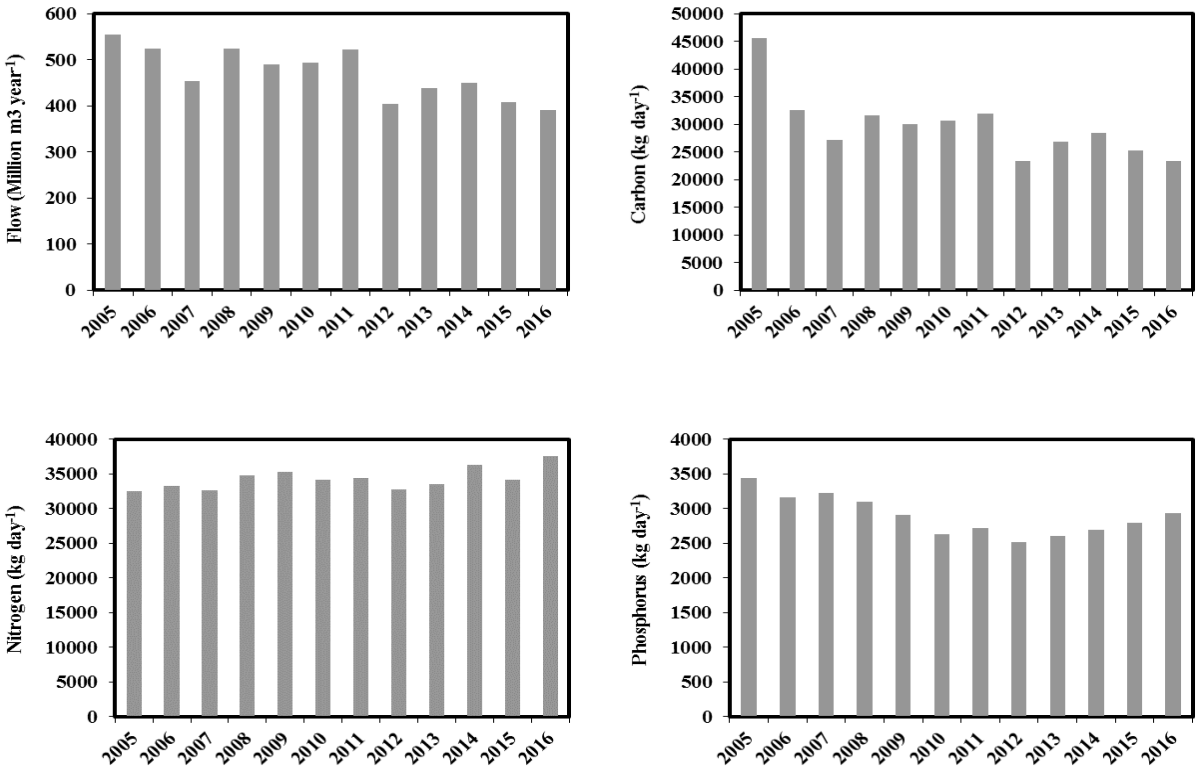

Figure 3-5. MWRA outfall mean annual flow and carbon/nitrogen/phosphorous loads, 2005-16.

3.3 *Open boundary of the UG-RCA water quality model*

The open boundary condition values for UG-RCA at the offshore edge of its grid domain (red line in upper frame of Figure 2-2) are determined using field survey observations from the MWRA monitoring program in Massachusetts and Cape Cod Bays and an objective analysis method (Tian et al., 2009). These observations are collected mainly during 9 routine surveys annually, at 14 stations in the two bays. Figure 3-6 shows the representative subset (10 stations; with N and F prefixes) of these 14 stations that is used, for clarity of presentation, below in Section 5 on water quality. (All 14 stations are shown, for example, in Figure 3-1 on page 8 of Werme et al. 2017.) Observations collected during a small number of non-routine springtime surveys, undertaken for harmful algal bloom monitoring, were also used in calculating the boundary values and included additional stations not shown here (stations AF9, AF8, AF6, AF4, AF2, and AF1, as seen, e.g., in Figure 1 on page 7 of Libby et al., 2017).

Open boundary condition results for April 15, June 15, August 15, and October 15 illustrate representative seasonal changes (Figure 3-7 and Figure 3-8; colorscale ranges are the same as in earlier reports for ease of comparison). As explained in Zhao et al. (2012), for dissolved organic carbon and biogenic silica (not shown), which are no longer being sampled, a seasonal cycle constructed by averaging observations from 1992-2010 is used. The field observations on which the objective analysis method is based are collected relatively infrequently, and located at large distances from the open boundary, particularly for the South Passage portion of it near Cape Cod. It is therefore recognized that, while the method is appropriate and effective, the results include a high degree of uncertainty.

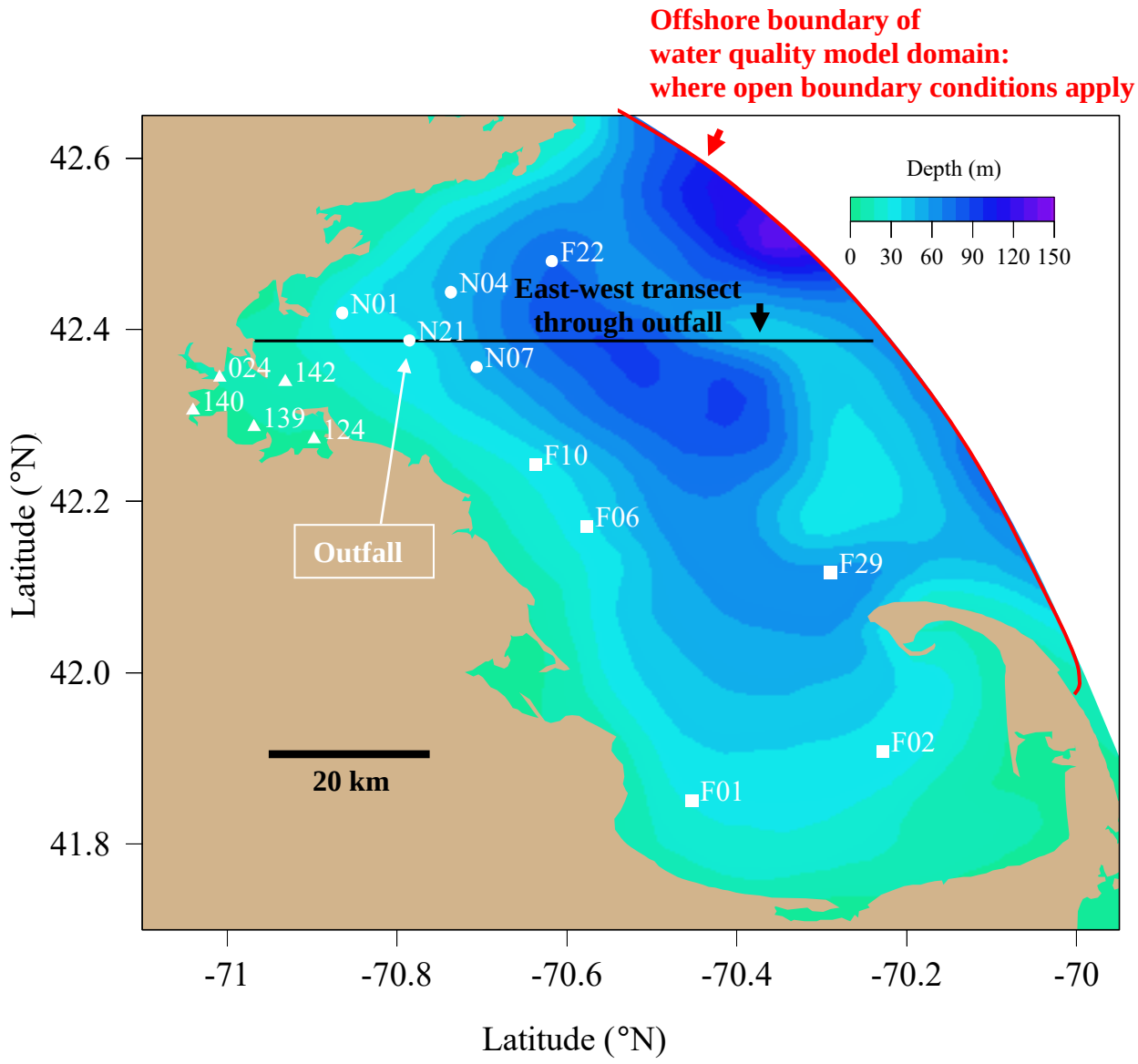

Figure 3-6. Station groups: northern (circles), southern (squares), and harbor (triangles).

For reference in later figures:
Red arc = Offshore boundary, water quality model domain, where open boundary conditions apply.
Black line = East-west transect through outfall.

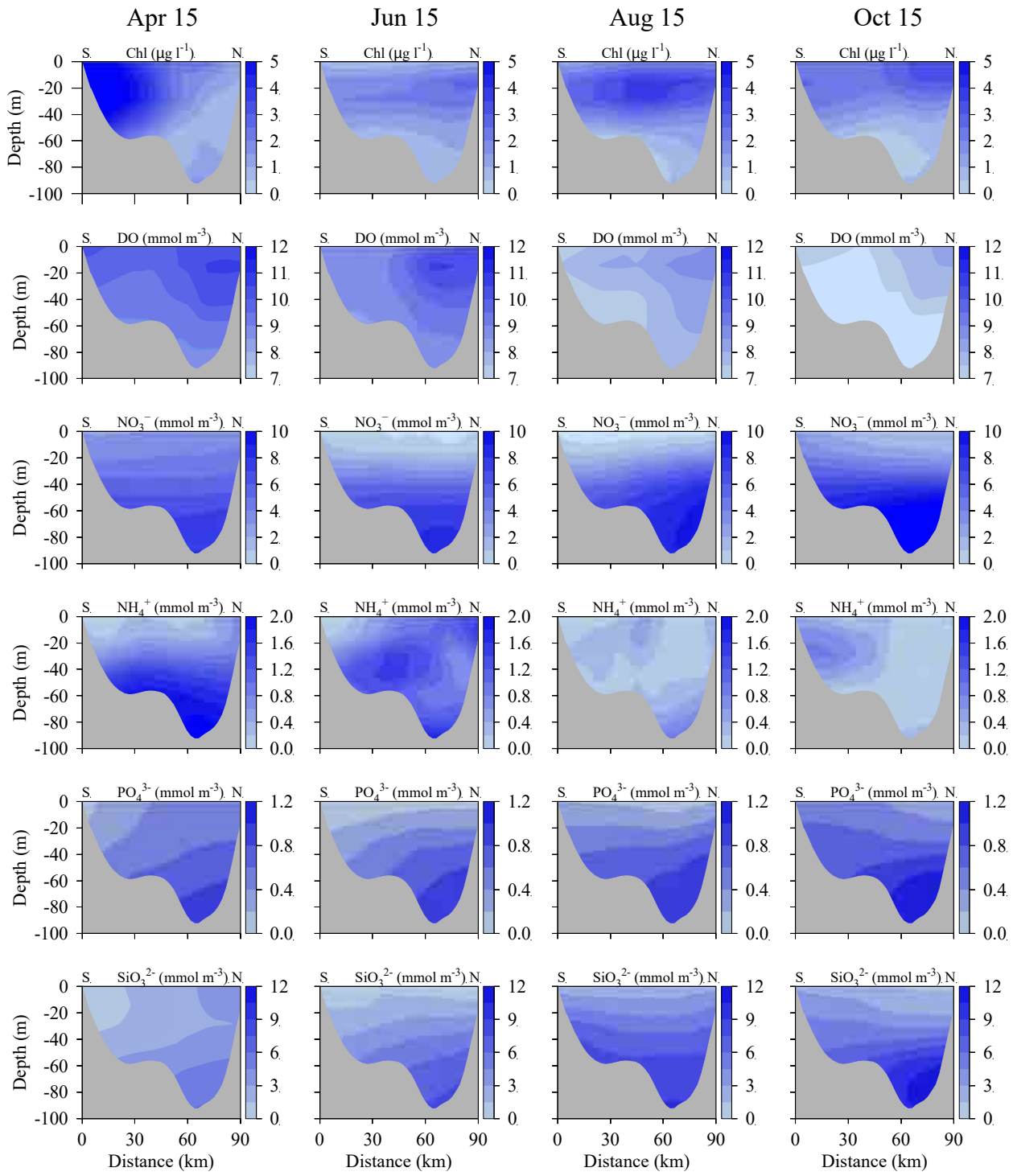

Figure 3-7. Open boundary forcing, water quality model: chlorophyll, oxygen, and nutrients.

Horizontal axis: distance along offshore arc (red in Figure 3-6) of open boundary, from its southernmost point; left endpoint ("S", distance 0 km) is the southernmost end of arc at Cape Cod and right endpoint ("N", distance 90 km) is the northernmost end of arc off Cape Ann.

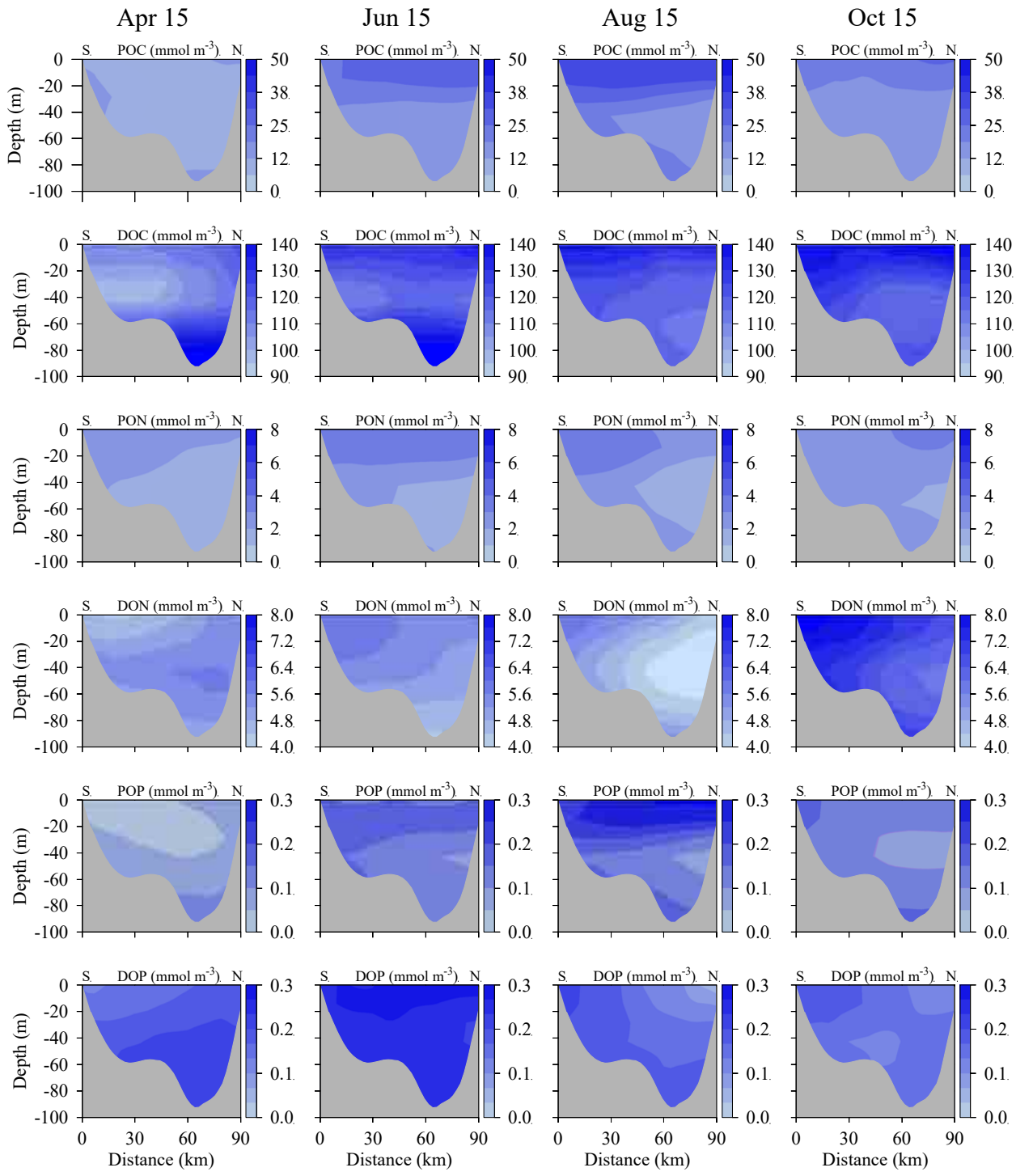

Figure 3-8. Open boundary forcing, water quality model: organics. Presented as in Figure 3-7.

POC = Particulate Organic Carbon, DOC = Dissolved Organic Carbon
PON = Particulate Organic Nitrogen, DON = Dissolved Organic Nitrogen
POP = Particulate Organic Phosphorus, DOP = Dissolved Organic Phosphorus

4. Hydrodynamics

The focus of BEM is water quality, which is strongly influenced by physical processes such as the evolution of temperature and salinity patterns and water circulation. The fidelity of the UG-RCA water quality simulations therefore depends on the capability of the MB-FVCOM hydrodynamic model to capture realistic physical processes of the bays. This section describes the hydrodynamic model characteristics and performance.

4.1 *Model-observation comparisons*

Comparisons between the model results and observations from 2016 make clear the level of agreement between them for the time evolution of the geographic and vertical structure of temperature (Figure 4-1) and salinity (Figure 4-2). Salinity is given in units on the Practical Salinity Scale throughout this report. Stations in these figures include locations spanning Massachusetts Bay (N01, F22, N07, F06), in and near Cape Cod Bay (F01, F02, F29), and at the mouth of Boston Harbor (F23; Figure 5-5 shows the location of F23, 1 km west of station 142 which is shown in Figure 3-6). Vessel-based observations from 9 survey dates in 2016 are shown as individual symbols, from both shallow (near-surface, less than 5m deep) and deep (near-bottom, within 5 m of seafloor) depths, at each station in Figure 4-1 and Figure 4-2. In addition, in the panels for Station F22, time series observations are shown from Mooring A01 (located about 5 km northeast of F22, see Figure 1-1, operated by University of Maine as part of the Northeast Regional Association of Coastal and Ocean Observing Systems) at 1m and 51 m deep.

The model generally captured the seasonal cycle, and most event-timescale characteristics, of observed temperature and salinity. This indicates the effectiveness of data assimilation of both satellite sea surface temperature and *in situ* hydrographic measurements. Stratification developed in April, peaked in July or August at most stations, and was mixed away during October. For temperatures the most notable model-observation differences were model temperatures not cold enough to match observations in February and November at station F23 at the mouth of Boston Harbor; there was also a general tendency at most stations for deep temperatures to be warmer than observed by up to several degrees except within a few days of observation dates, when the model values are reduced to nearer the observed values by data assimilation as expected. For salinities the most notable model-observation difference was the tendency for deep salinities to be higher than

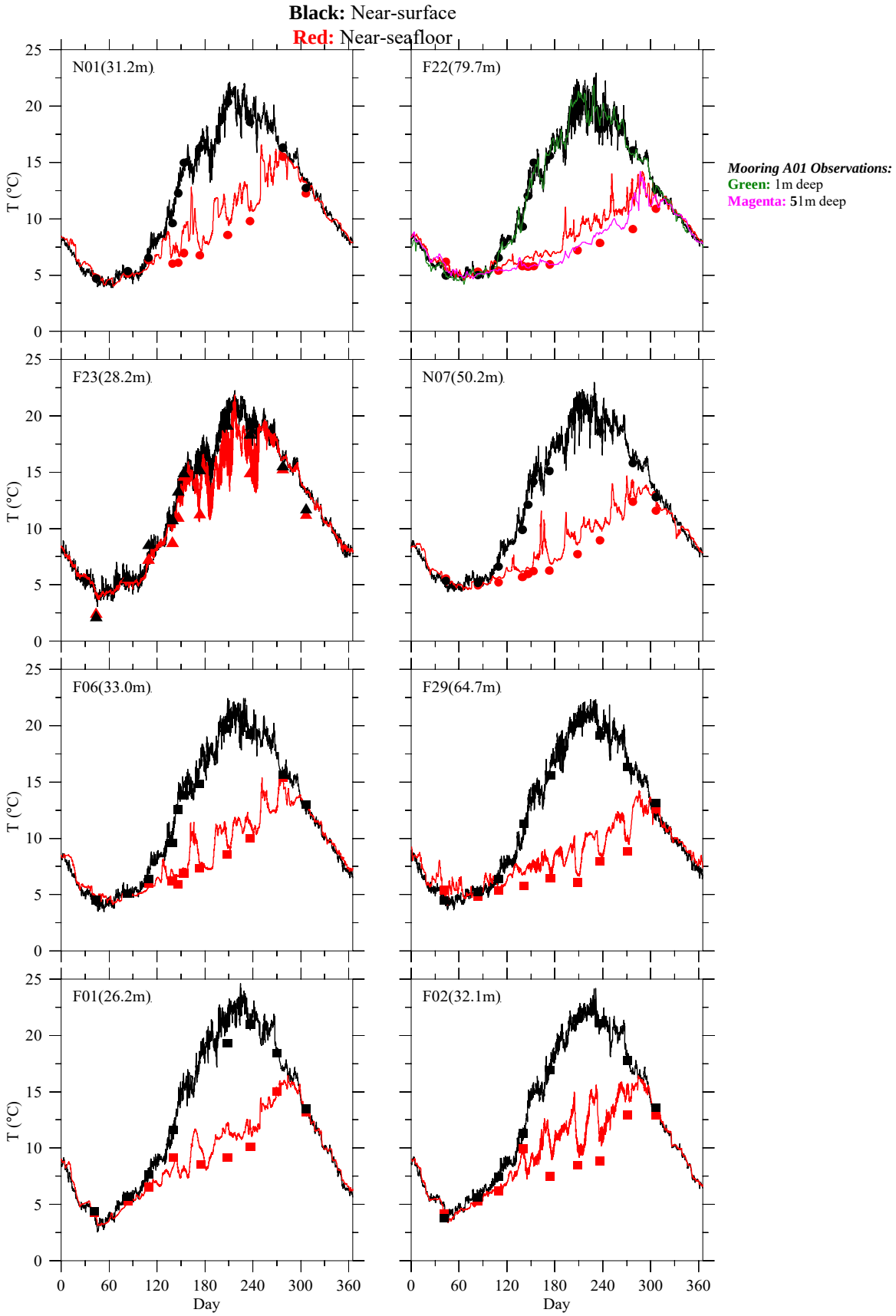

Figure 4-1. Temperature time series, model-observation comparison.

Model results: black/red lines. MWRA vessel-based survey observations: black/red symbols.

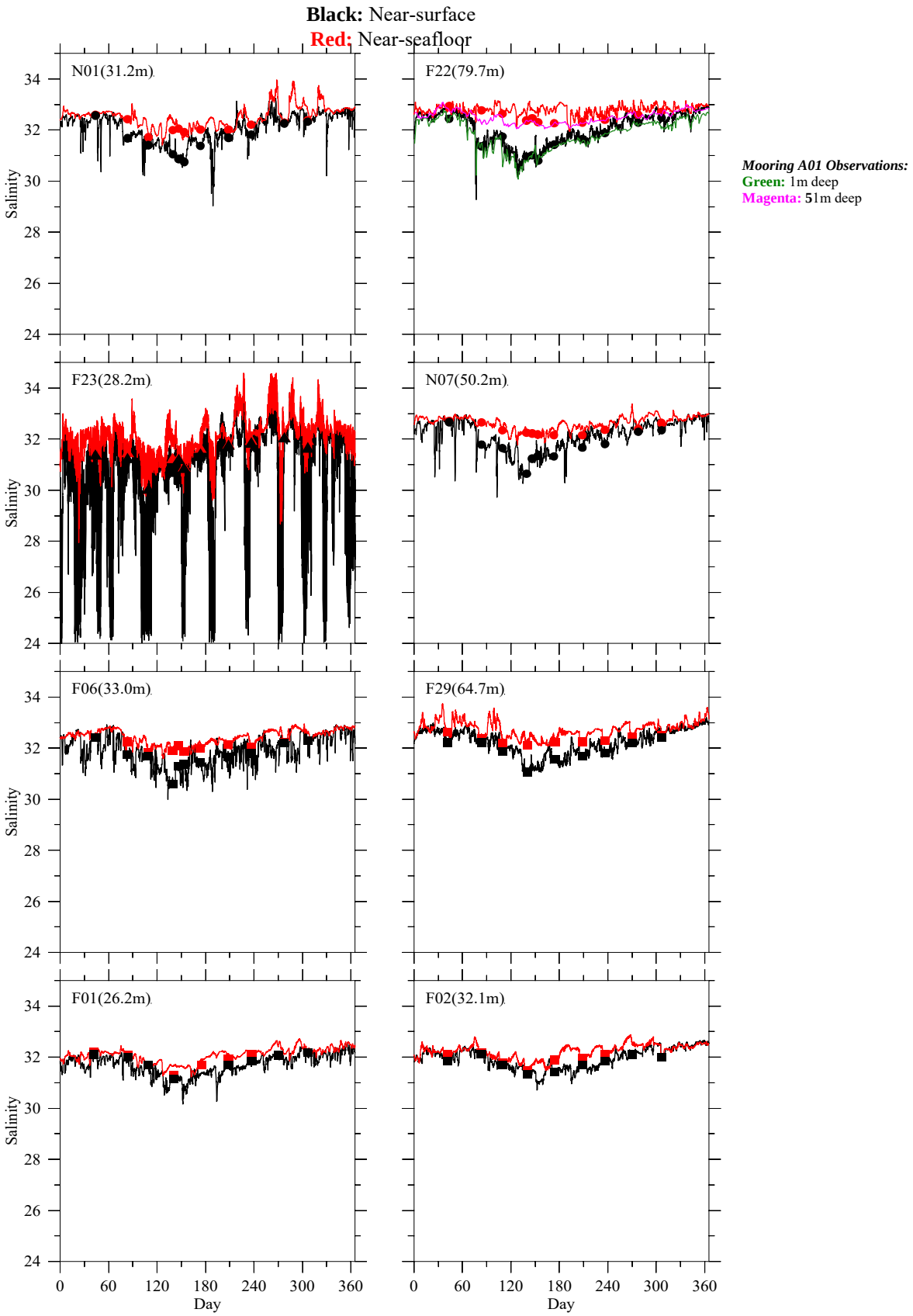

Figure 4-2. Salinity time series, model-observation comparison.

Shown as in Figure 4-1. Salinity units: Practical Salinity Scale.

observed by about 0.5, at some stations (for example, F22) after the first few months of the year. This difference was reduced by the data assimilation, as expected, within a few days of the dates of observations.

For more complete spatial information, model-observation comparisons have been made of the monthly-mean geographic structure, during a series of months spanning the seasonal cycle, of near-surface and near-bottom temperature (Figure 4-3a,b) and salinity (Figure 4-4a,b). The observed fields in these figures are computed using measurements from all stations (black dots) sampled during each month-long period. For most months there was a one-day survey in Massachusetts Bay and Cape Cod Bay, and Boston Harbor stations were sampled weekly or biweekly (for more detail on harbor station locations see, e.g., Taylor, 2015). The model fields in these figures are computed using the subset of model outputs from the dates and locations corresponding to the associated set of observations. (Consequently they are not expected to match exactly the monthly-means of all modeled times, which are shown in Figure 4-7 and Figure 4-8 below.)

The seasonal cycle and general spatial structure of the model fields is in reasonably good agreement with the observations. The most notable model-observation differences for shallow temperatures (Figure 4-3a) were that model results were typically more spatially uniform than the observations; relative to observations the model results were also notably warmer in February, June, and October. For deep temperatures (Figure 4-3b) the agreement was somewhat better, with the most notable differences being higher temperatures in February and June. The model shallow salinities (Figure 4-4a) match nearly all characteristics of the observations, with a slightly farther offshore extent of relatively fresh water in June. The model deep salinities (Figure 4-4b) agreed almost as well with observations, with inshore values saltier than observed during April and fresher than observed in October. The model captured the general spatial pattern of onshore freshening throughout the year.

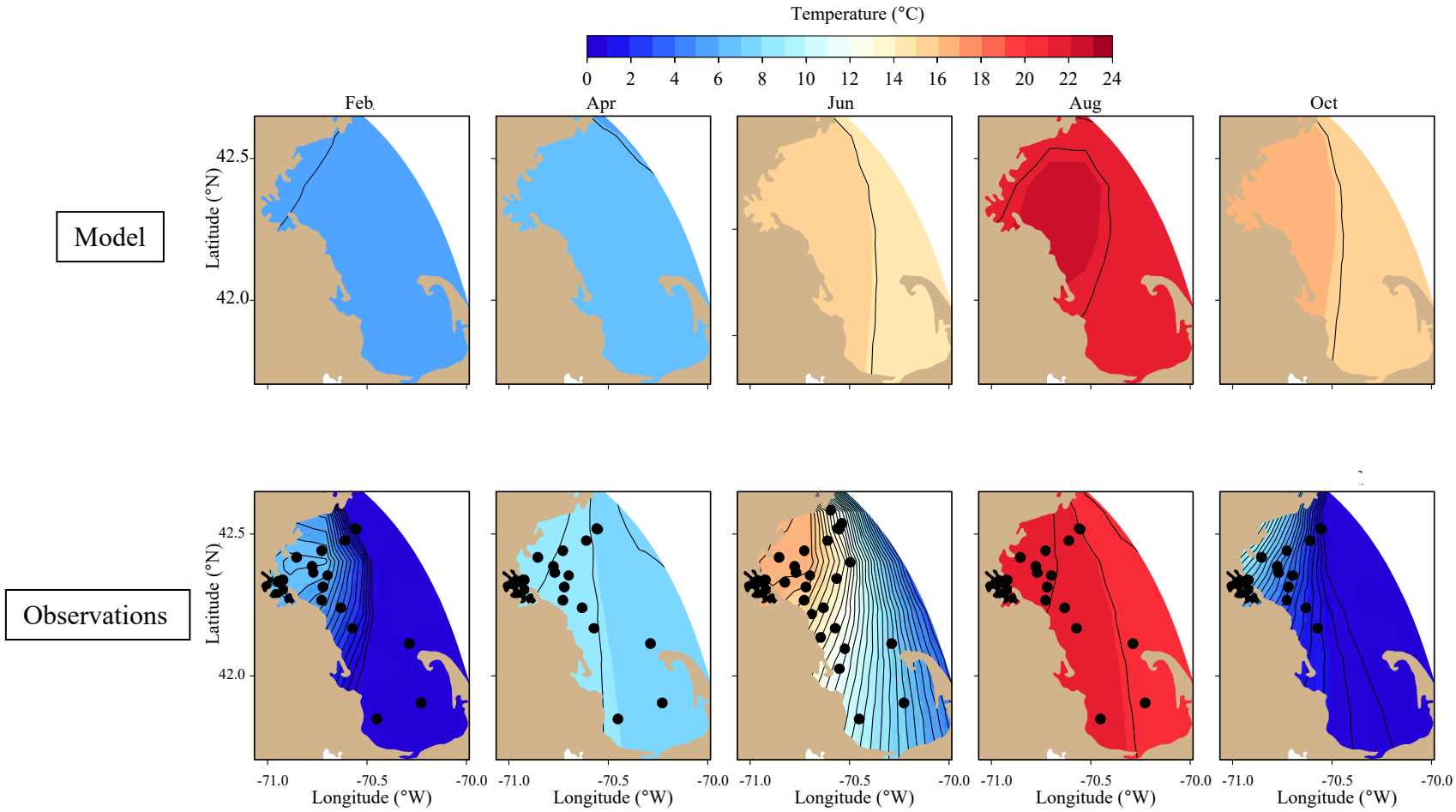

Figure 4-3a. Temperature spatial structure, at/near sea surface, model-observation comparison.

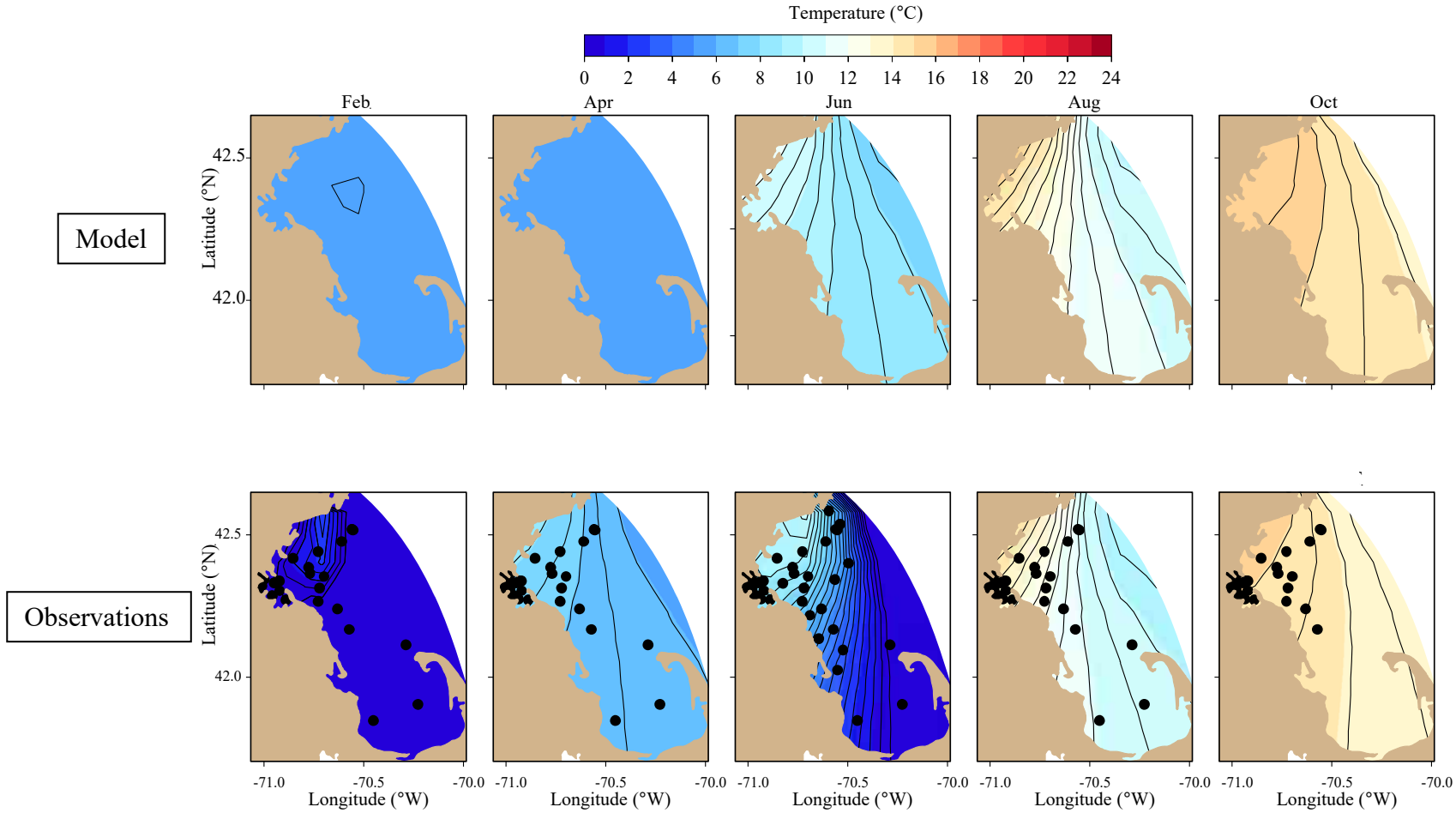

Figure 4-3b. Temperature spatial structure, at/near seafloor, model-observation comparison.

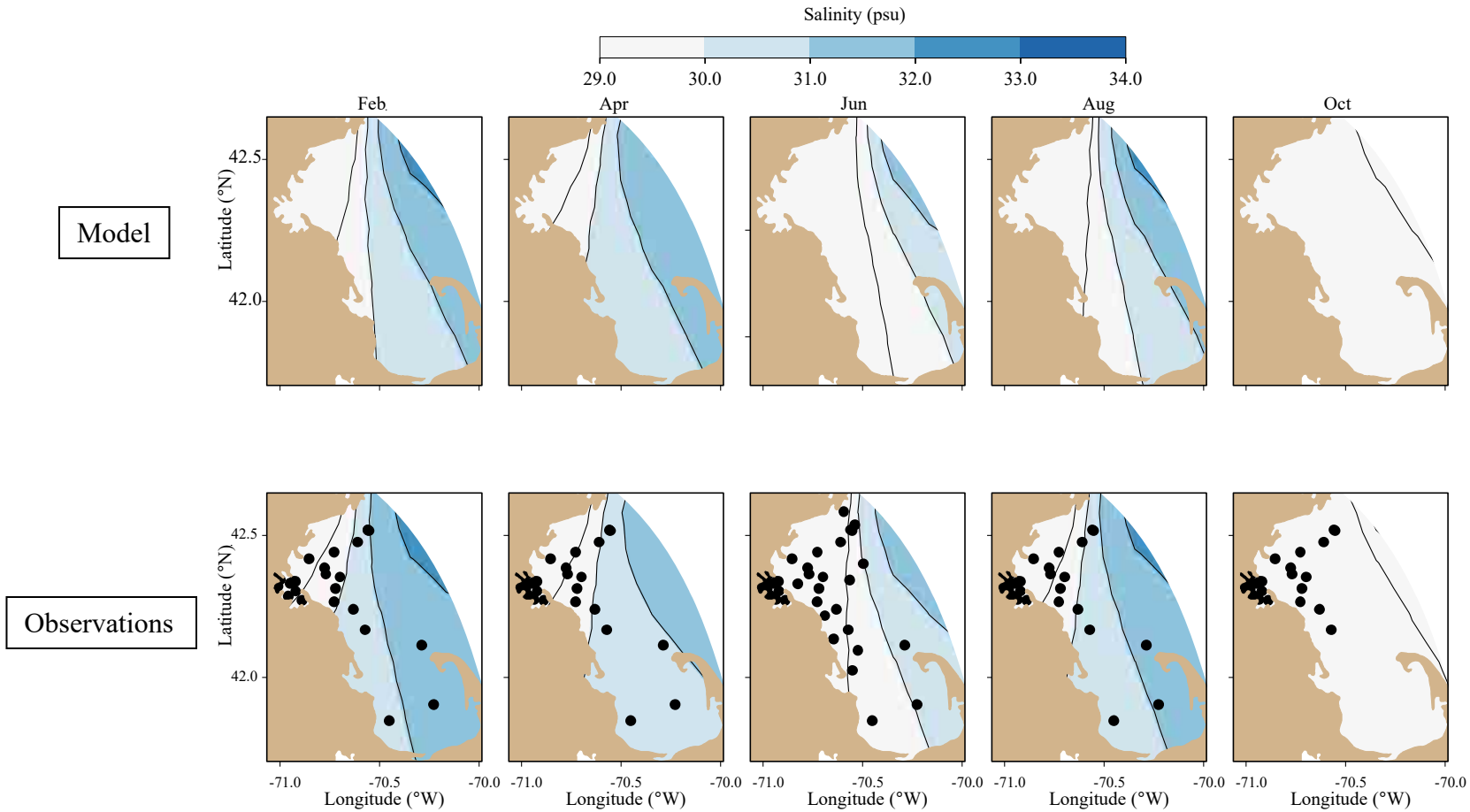

Figure 4-4a. Salinity spatial structure, at/near sea surface, model-observation comparison.

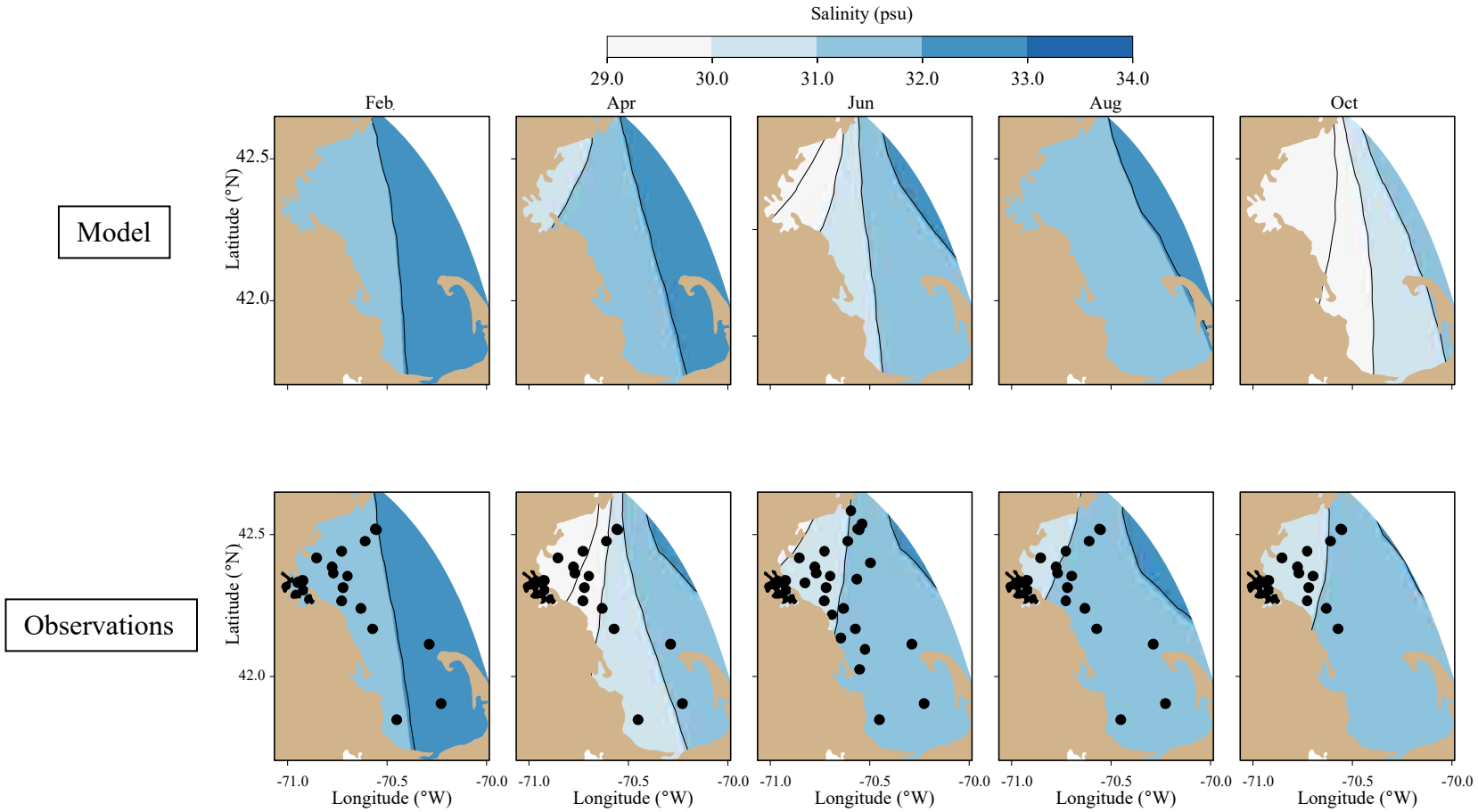

Figure 4-4b. Salinity spatial structure, at/near seafloor, model-observation comparison.

For more complete temporal information, model-observation comparisons have been made for temperature and salinity (Figure 4-5) using the time series measurements at three depths (1 m, 20 m, and 50 m) at Mooring A01 located (see Figure 1-1) in the northeast part of Massachusetts Bay (the only location where high-frequency time series observations are available). The comparisons are favorable with regard to the vertical structure and demonstrate that the model captures well the general characteristics of the strength and temporal evolution of stratification. This is true with regard to both the seasonal pattern and events on weather-band timescales of days to weeks. The most noticeable model-observation differences are at 50 m deep, where the model temperatures are warmer than observed and the model salinities are higher than observed.

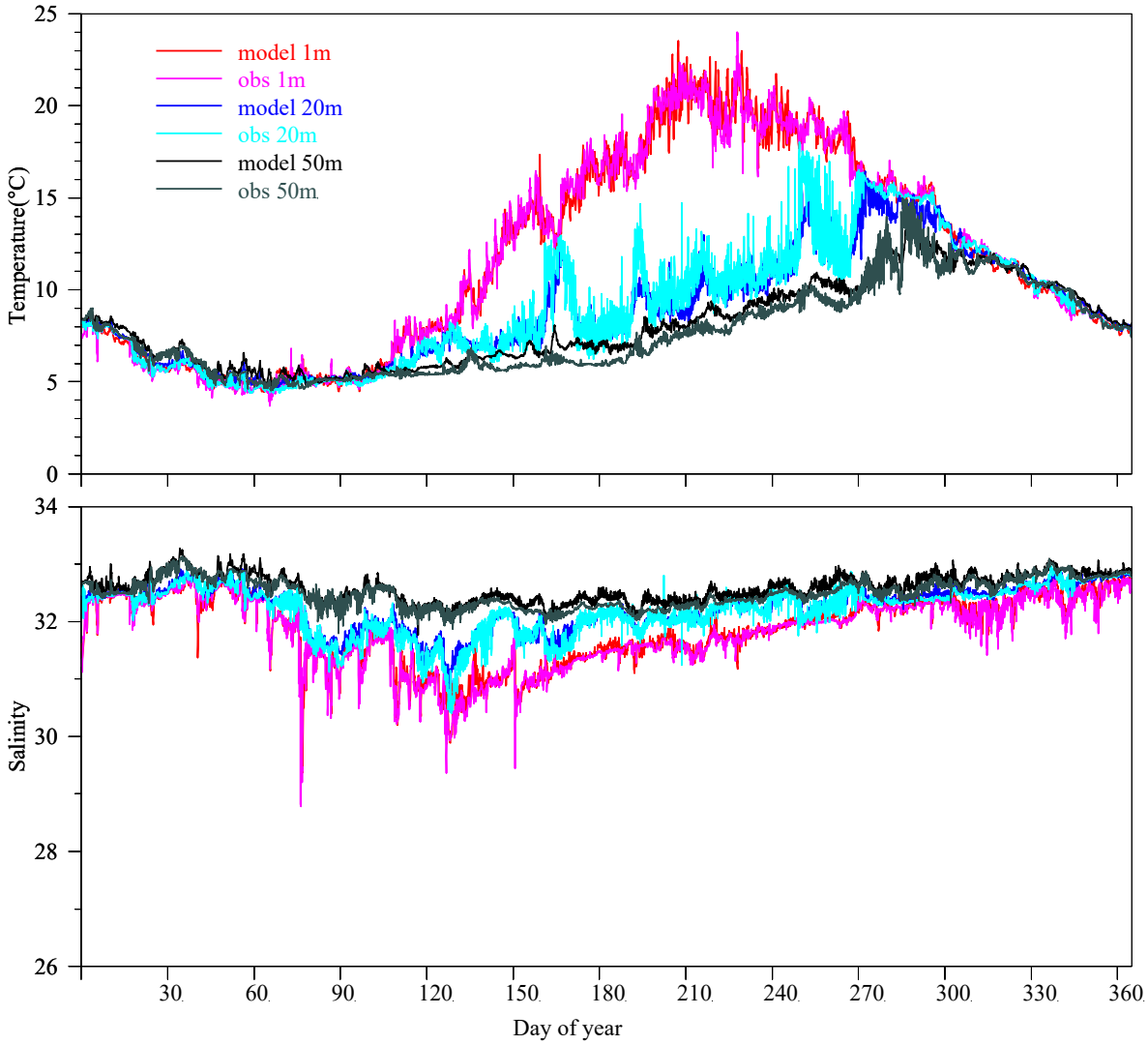

Figure 4-5. Time series Mooring A01 temperature/salinity model comparison, three depths. Temperature (upper frame), salinity (lower frame).

Comparisons between modeled and observed 2016 non-tidal currents at Mooring A01 are shown in Figure 4-6a,b. (Tidal currents, while important in controlling vertical mixing and dispersal of materials, are not examined in this report. Tidal currents in these simulations are similar to tidal currents in other similarly-configured FVCOM simulations spanning the Gulf of Maine, and have been shown—e.g., see the appendix of Chen et al., 2011—to be in good agreement with observed tidal currents.) The model-observation comparisons of non-tidal currents include time variations and vertical structure, with wind forcing included for context. In order to isolate the non-tidal variability of interest, consisting mainly of weather-related and seasonal changes, the tidal variability has been removed using a low-pass filter (38-hr half-power period, PL66TN; e.g., Limeburner 1985) and the results subsampled to 6 hour resolution.

As expected, the main features of the winds (from the WRF model) are weather-band changes on timescales of about 3-10 days. These features include: wind directions spanning the full compass range; generally weaker magnitudes in the summer; and a tendency for longer-term (monthly or longer) average winds to be weaker than weather-band changes, and directed towards the east year round, with a southward component in winter and a northward component in summer.

Observed currents are generally toward the south and west at this location (see Figure 1-1) and the model adequately captures this feature. The most prominent model-observation difference is that the model currents tend to have slightly larger magnitudes than observed; there is also evidence that at 50 m the model currents have a northward component that is stronger than observed. Most of the individual storm events seen in the observed currents occur in the model currents, and for most events the timing and direction of the flow is similar in the model and observations. These detailed comparisons of the time variations and vertical structure of currents in the model to direct observations at a particular site form a challenging test of the hydrodynamic simulation performance. Agreement is sufficient to conclude that the hydrodynamic model represents observed processes adequately to support the water quality modeling.

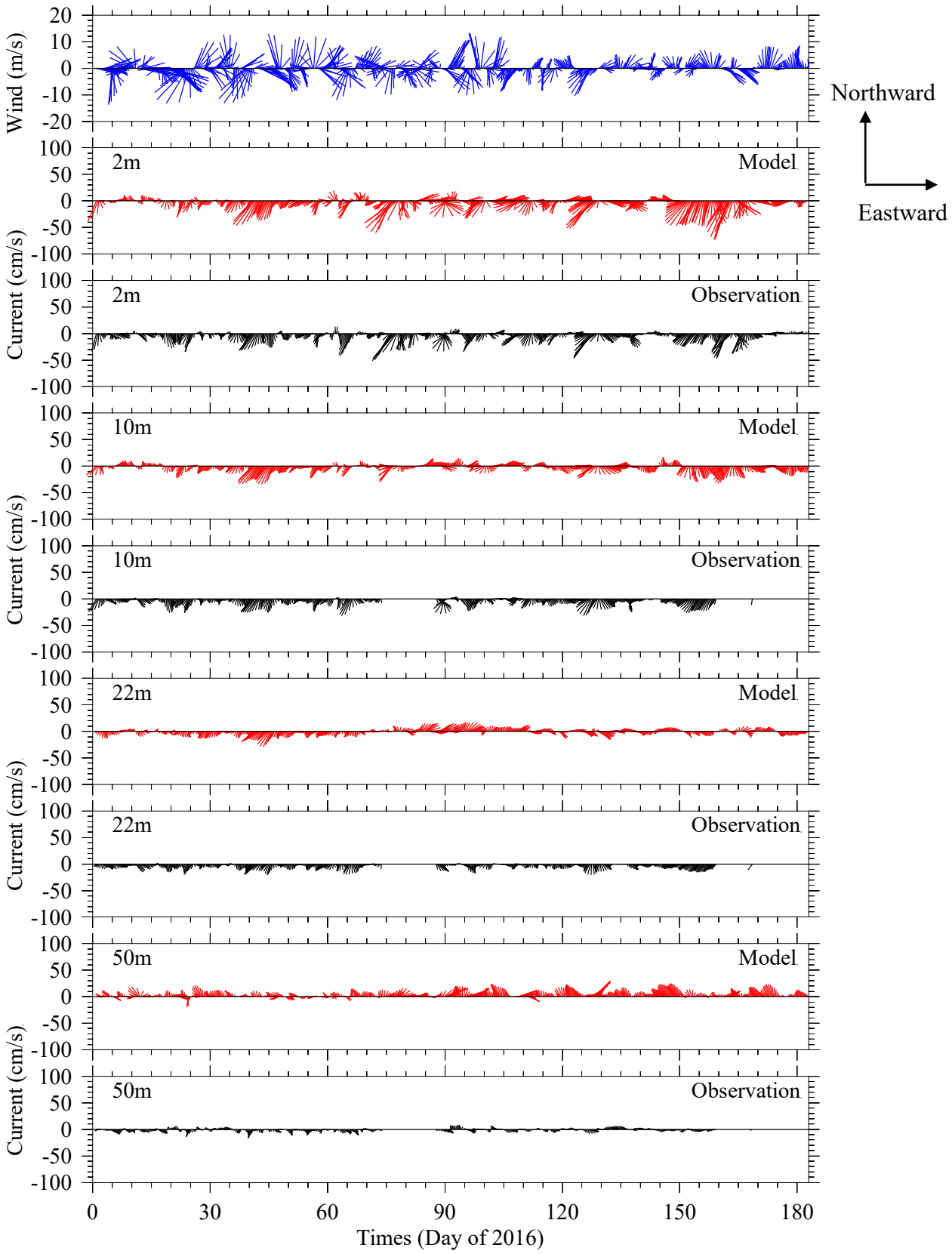

Figure 4-6a. Currents time series model-observation comparison, Jan – Jun.

Sticks point in the direction of flow, away from zero line; north/eastward flow up/rightward.

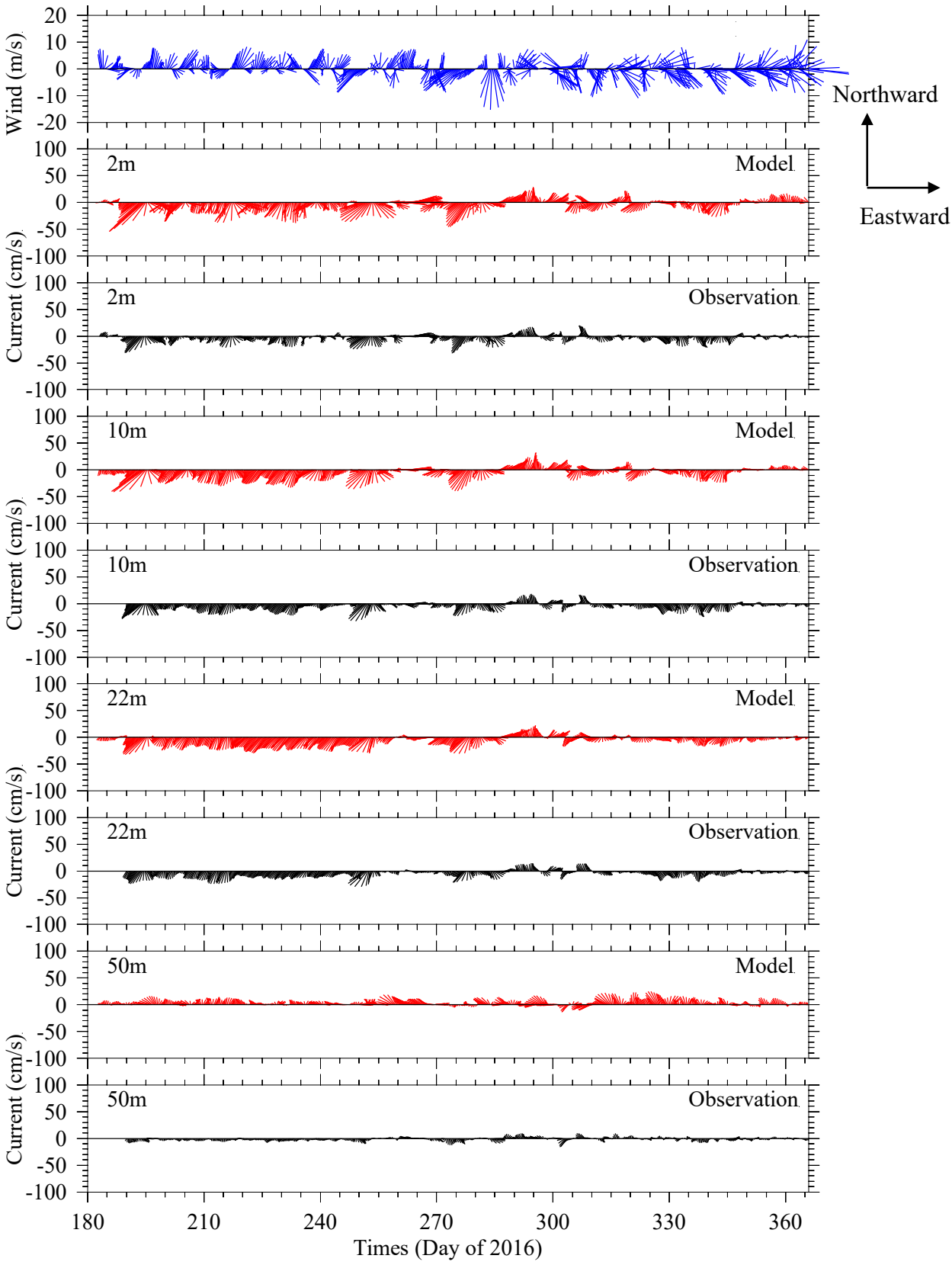

Figure 4-6b. Currents time series model-observation comparison, Jul - Dec.

4.2 *Model monthly-mean temperature, salinity, and circulation*

Based on the above comparisons having demonstrated a level of agreement between the 2016 simulation and available observations, this subsection presents a more complete view of the monthly-averaged simulation temperature, salinity, and circulation throughout the year.

Model temperatures followed the expected seasonal cycle (Figure 4-7a,b) with peak values in summer and early fall and minima in late winter. Horizontal gradients are notable, with inshore temperatures generally colder during winter and spring and warmer during summer and fall. From about April/May to October/November the surface temperatures (Figure 4-7a) are markedly higher than bottom temperatures (Figure 4-7b). Model salinities (Figure 4-8a,b) have a weaker seasonal cycle than temperature, particularly at depth. Water near the coastlines is generally fresher year-round, both at the surface (Figure 4-8a) and the seafloor (Figure 4-8b). At the surface, from April to June the offshore extent of relatively fresh water increased, first in the southern Gulf of Maine and then in Massachusetts Bay, where it then decreased from July to September.

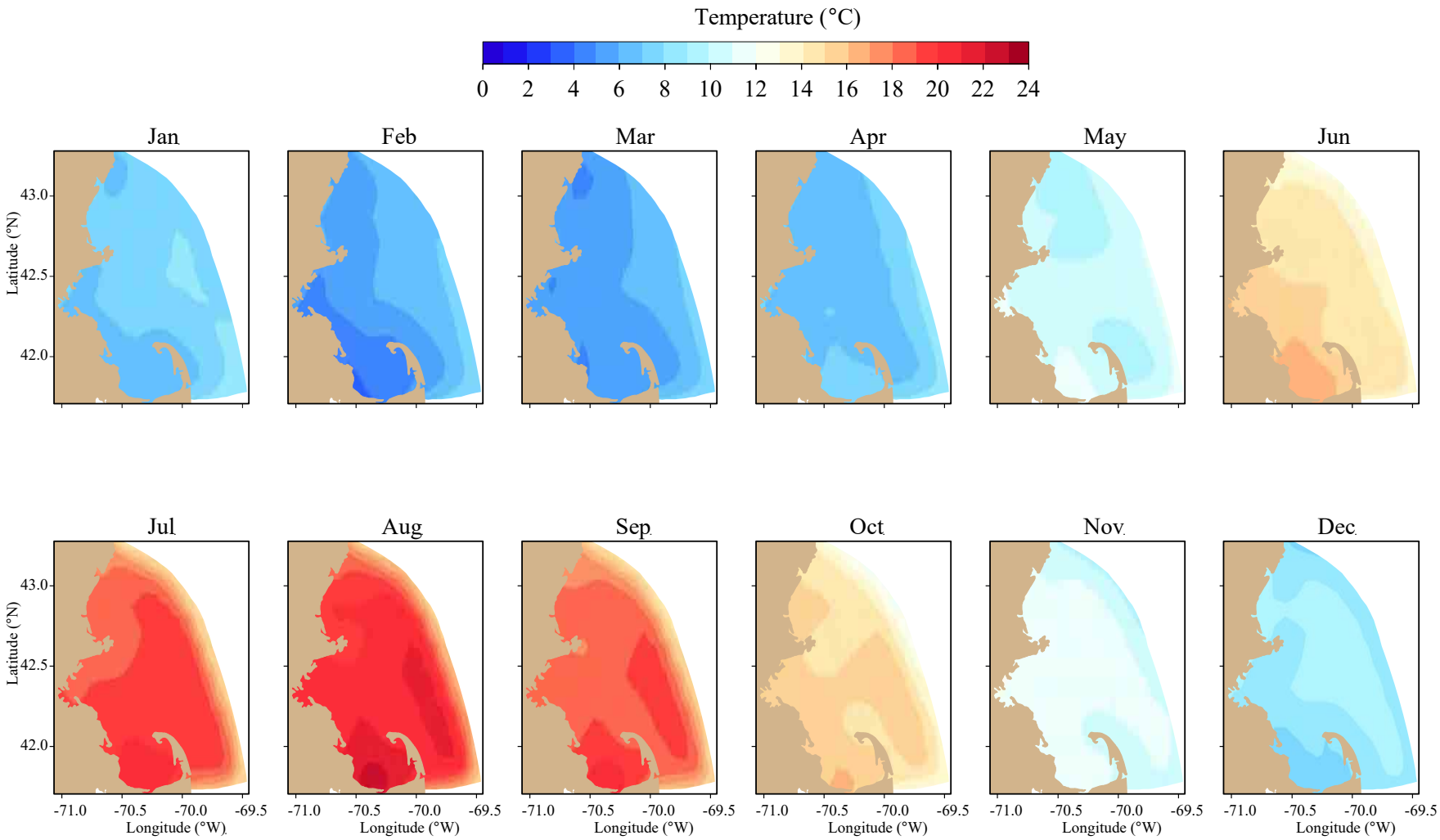

Figure 4-7a. Model temperature, monthly-mean spatial structure, at sea surface.

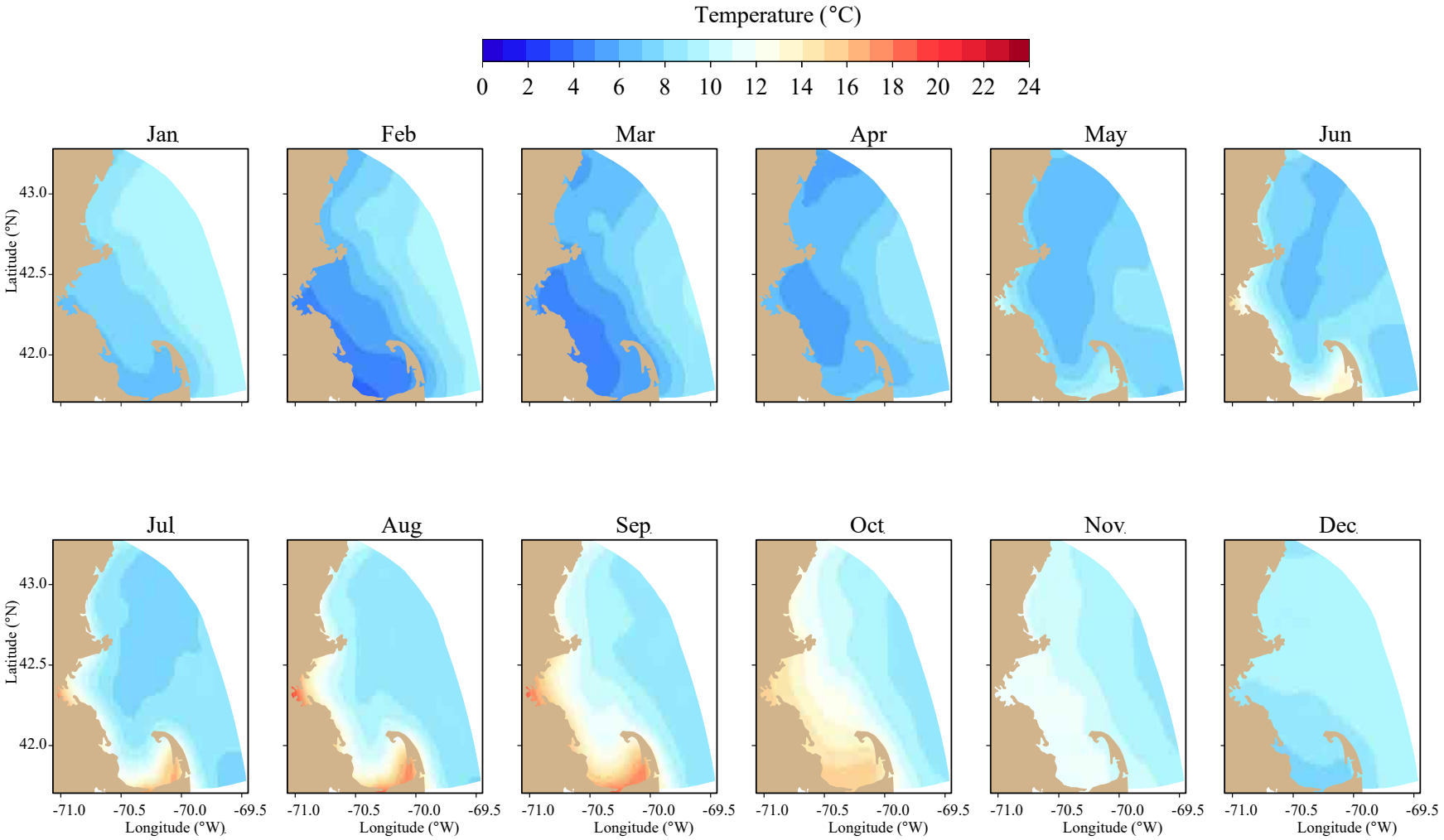

Figure 4-7b. Model temperature, monthly-mean spatial structure, at seafloor.

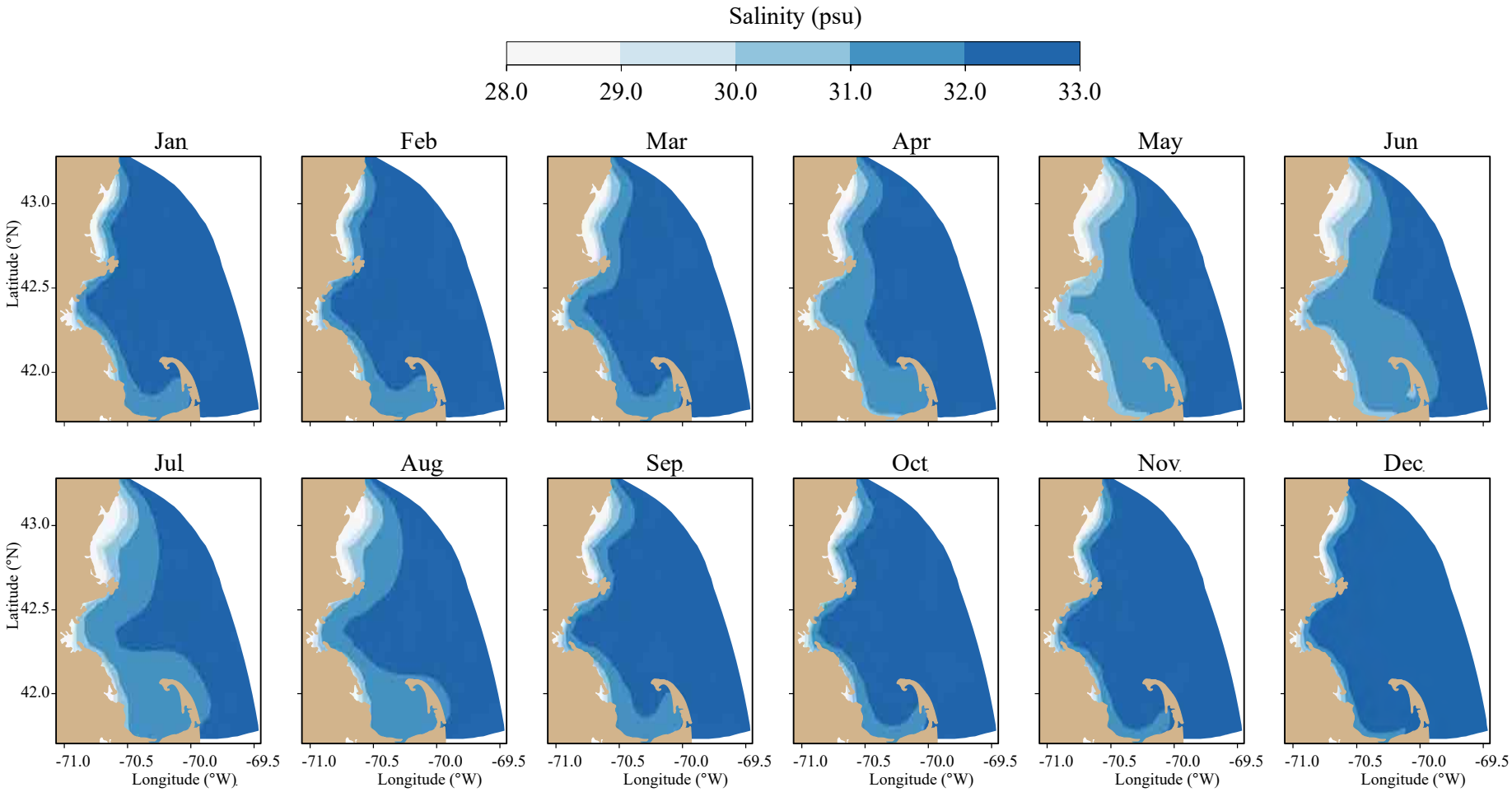

Figure 4-8a. Model salinity, monthly-mean spatial structure, at sea surface.

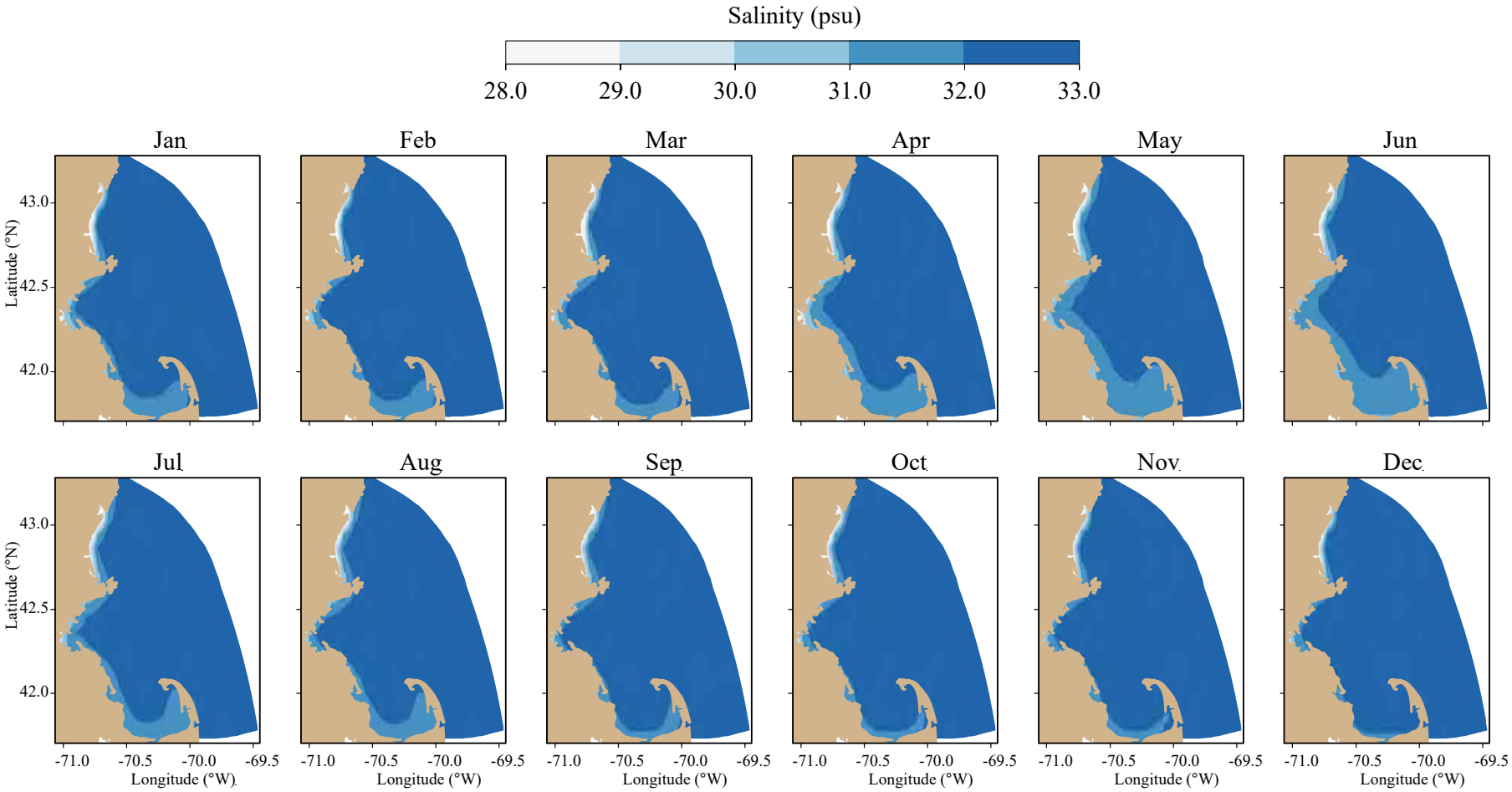

Figure 4-8b. Model salinity, monthly-mean spatial structure, at seafloor.

The temporal progression of the geographic pattern of 2016 monthly-mean model currents at the surface (Figure 4-9a) and at 15 m deep (Figure 4-9b) is consistent with the schematic for long-term mean flow in Figure 1-1 and characterized by the following main features. At the surface (Figure 4-9a), in January and September-December currents within the bays were generally weak. Southward flow within about 10-20 km of the western coast of Massachusetts Bay and Cape Cod Bay was strongest in December, reaching about 20 cm s^{-1}. Flow into Massachusetts Bay south of Cape Ann was evident from February through August and strongest in March through June. In March and April a single clockwise circulation occupied most of northern Massachusetts Bay, and in June the southward component of it bifurcated with one limb flowing southward in to Massachusetts Bay and then offshore. The latter counterclockwise flow persisted in July and August. From September to December the currents were strongest, reaching up to 30-40 cm s^{-1}, along the area offshore extending from Cape Ann to Cape Cod, having originated in the Western Maine Coastal Current north of Cape Ann. At 15 m deep (Figure 4-9b; blank areas, for example in southeastern Cape Cod Bay, are where the seafloor is shallower than 15 m) the flow patterns were generally similar to the surface, with the main difference being that currents are generally not stronger than about 10-15 cm/s, and are thus substantially weaker than currents at the surface.

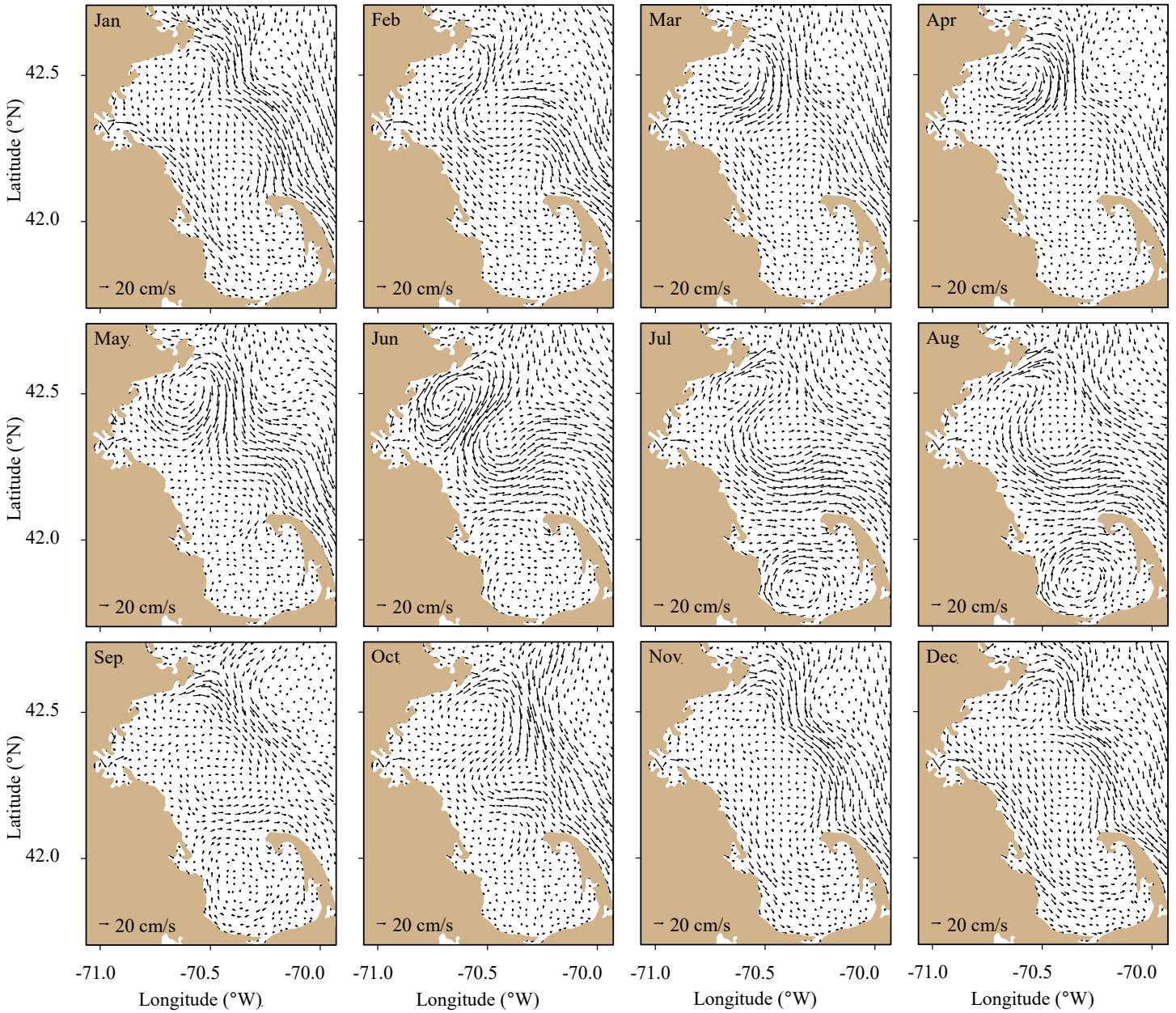

Figure 4-9a. Model currents, monthly-mean spatial structure, at sea surface.

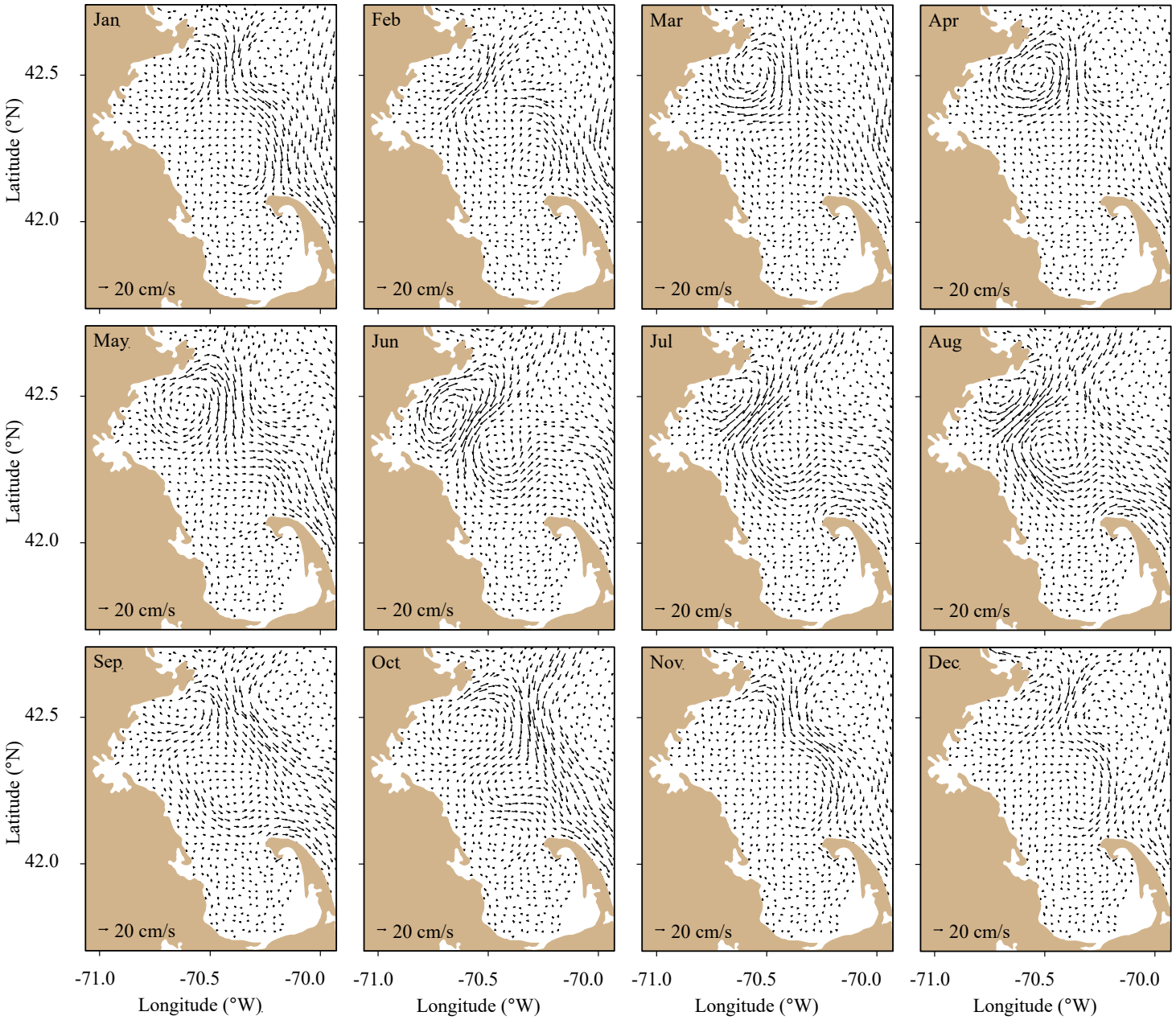

Figure 4-9b. Model currents, monthly-mean spatial structure, 15 m deep.

5. Water quality

Model-observation correlation and regression analyses of key water quality variables from the 2016 simulation are presented in Figure 5-1, including surface chlorophyll, surface inorganic nutrients (nitrate NO_3^-, ammonium NH_4^+, and silicate SiO_3^{2-}), bottom dissolved oxygen (DO) concentration (mg L^{-1}) and bottom DO saturation (%). These comparisons use observations from all Massachusetts Bay and Cape Cod Bay sites sampled by MWRA during 2016, comprising a total of 14 stations (see, for example, Figure 3-1 on page 8 of Werme et al. 2017). For clarity of presentation, as noted above, figures in the remainder of this section use a subset of 10 stations, as shown in Figure 3-6. In 2016 there was no meaningful correlation for near-surface chlorophyll, silicate, or ammonium. The model significantly underestimated chlorophyll when its concentration was higher than about 2-3 µg L^{-1}. For surface NO_3^- the correlation of 0.8 is lower than values near 0.9 in past years. For DO concentration the correlation coefficient is 0.90. The DO percent saturation was not directly modeled, rather it was calculated based on temperature, salinity and DO concentration using the approximate relation given in equation 2.3 of Zhao et al. (2012); biases in the simulation for these parameters could be factors that contribute to the lower correlation coefficient for DO percent saturation (0.67) than for DO concentration.

The remainder of this section describes the 2016 annual progressions of a representative set of water quality model variables from representative locations. Individual figures generally show results of model-observation comparisons for stations from one of the three groups in Figure 3-6 (northern, southern, and harbor), or monthly-mean model output along the east-west transect (shown in Figure 3-6) that originates at the coast, passes through the outfall site, and extends offshore across the Stellwagen Basin depression and the shoaling Stellwagen Bank.

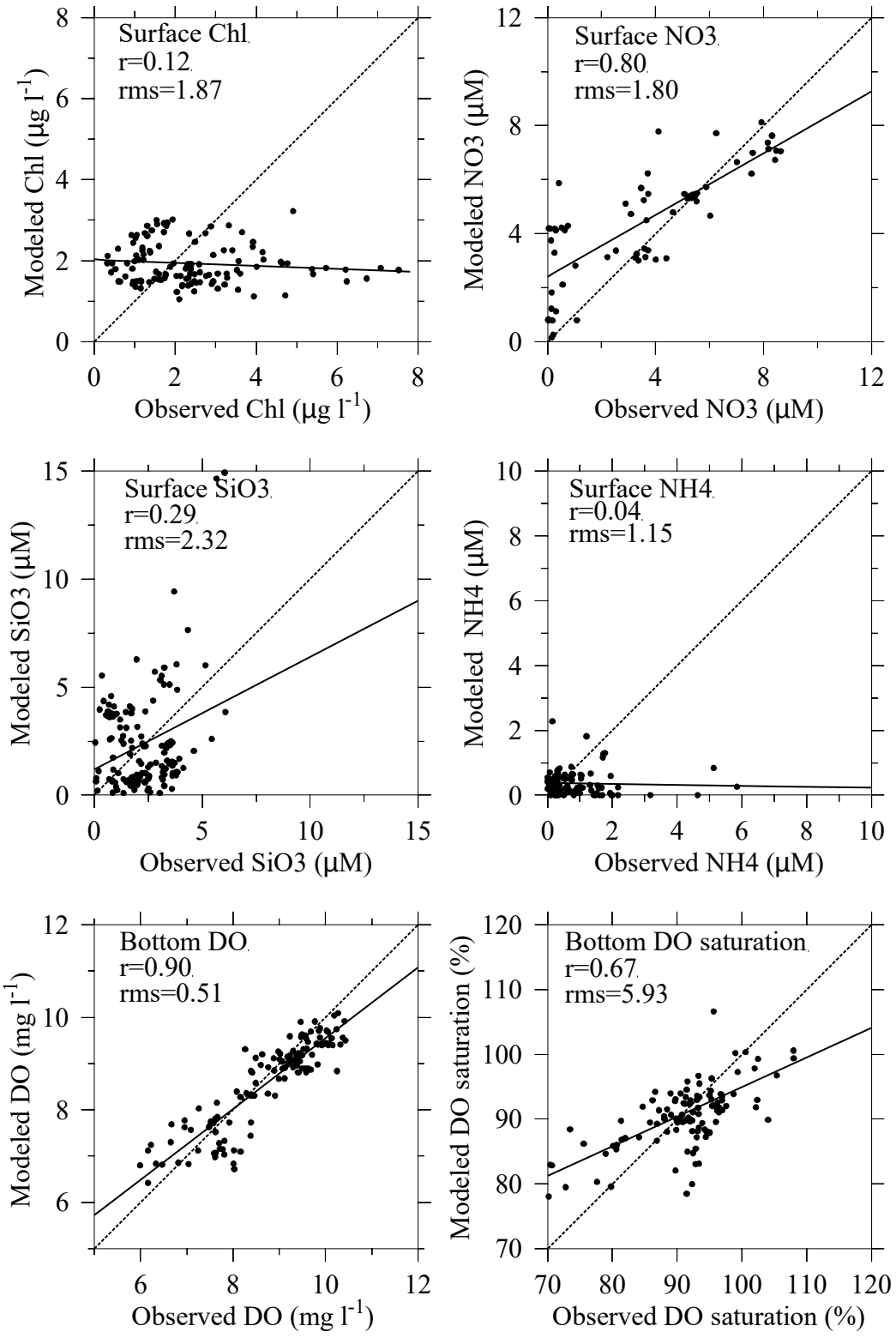

Figure 5-1. Model-observation correlations/regressions for key water quality parameters.

All stations outside Boston Harbor; regressions are solid lines, dashed lines indicate equality between observed and modeled results.

5.1 *Light*

For light, model-observation comparisons use extinction coefficients for attenuation of photosynthetically active radiation (PAR) in the water column, as described in Section 2.2 of Zhao et al. 2016a. At stations in the northern group (Figure 5-2a) and southern group (Figure 5-2b) spanning Massachusetts Bay and Cape Cod Bay, the model extinction coefficient results include annual-average values that differ modestly from site to site. Temporal variations during the year are minor, and the late-spring peak associated with chlorophyll self-shading (Hydroqual, 2001) typical in other years (e.g., see Zhao et al., 2016a) is modest or absent, except to some extent at the Cape Cod Bay stations, as consistent with the modest observed 2016 spring phytoplankton bloom. At all stations the range of temporal variability in the model is much lower than that in the observations. The modeled values are generally within the range of observations and model-observation bias is generally not pronounced.

The extinction coefficient results for the harbor group of stations (Figure 5-2c) are similar to those in the bays, with respect to site-to-site variations in the model being modest, and annual-average levels generally consistent with the observations. As expected, extinction is much more rapid (higher extinction coefficients) in the harbor than in the bay. At sites in the harbor where the temporal variability of observations is more pronounced (station 140, and to a lesser extent station 124), this leads to larger model-observation differences. At the other sites (024, 142, 139) there is evidence of modest positive bias in the model extinction coefficient relative to the observations.

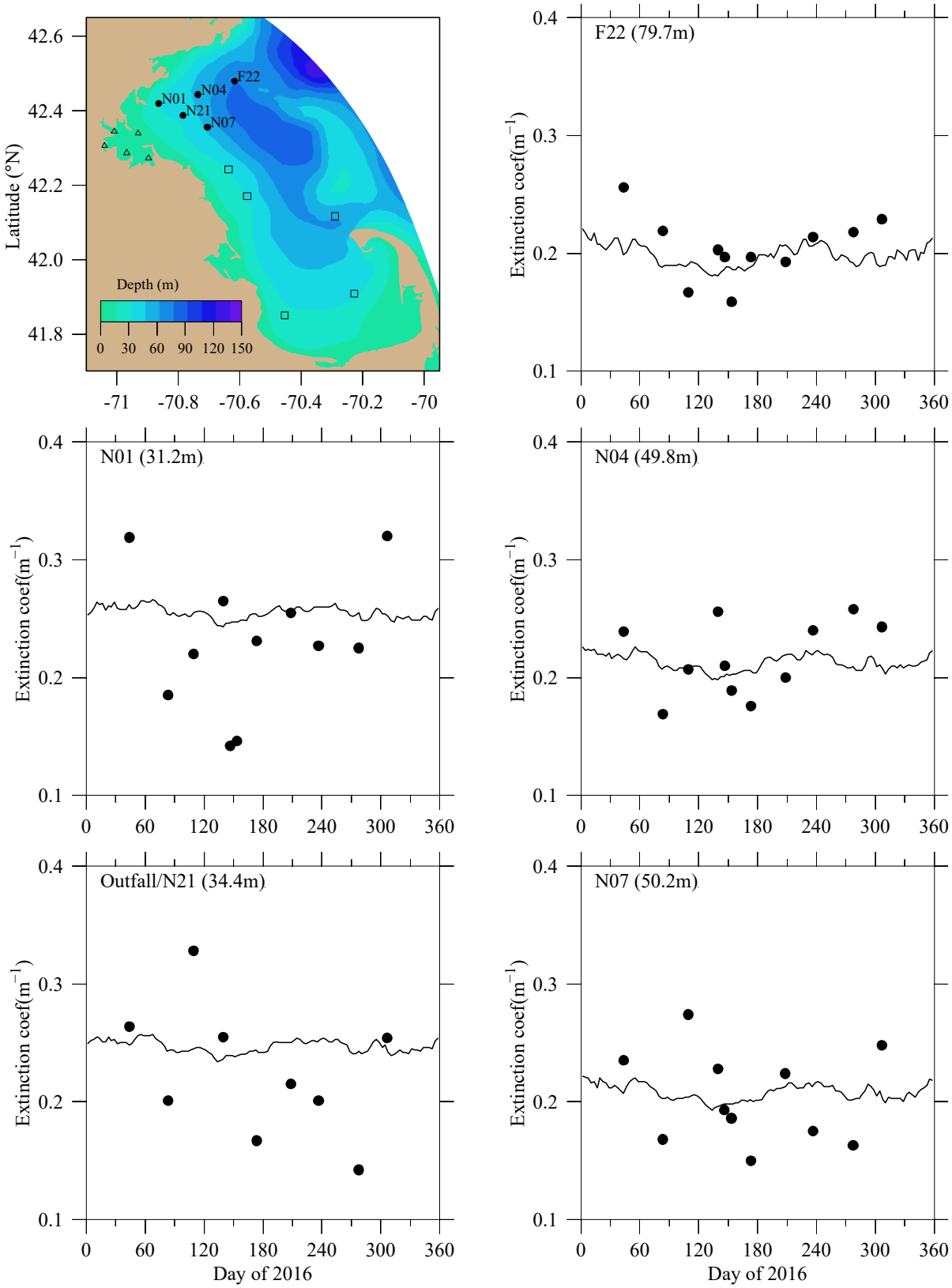

Figure 5-2a. Light extinction. Northern stations. Line: Model. Symbols: Observations.

In this and all similar plots to follow, upper left of frame shows "station name (bathymetric depth)".

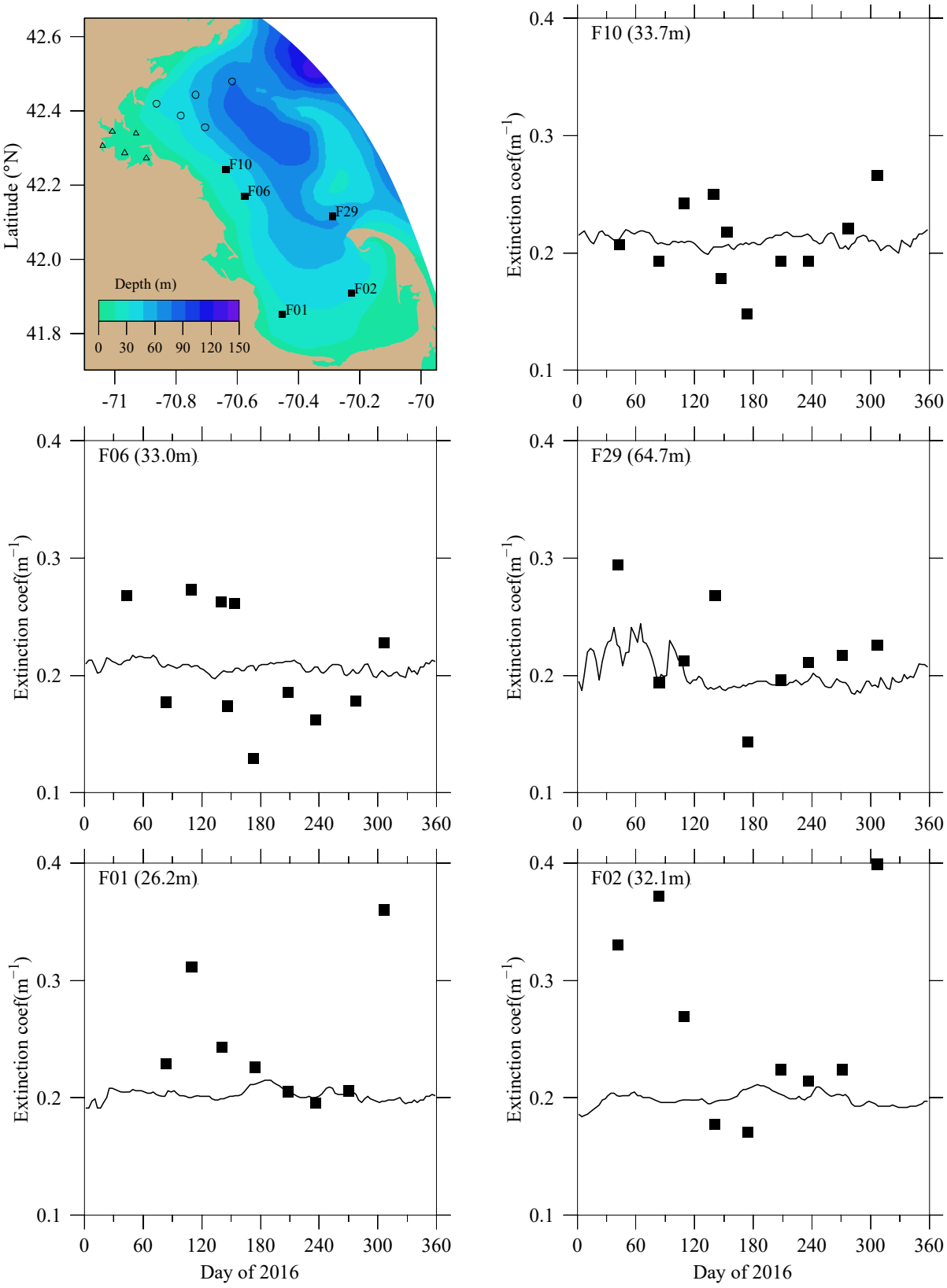

Figure 5-2b. Light extinction. Southern stations. Line: Model. Symbols: Observations.

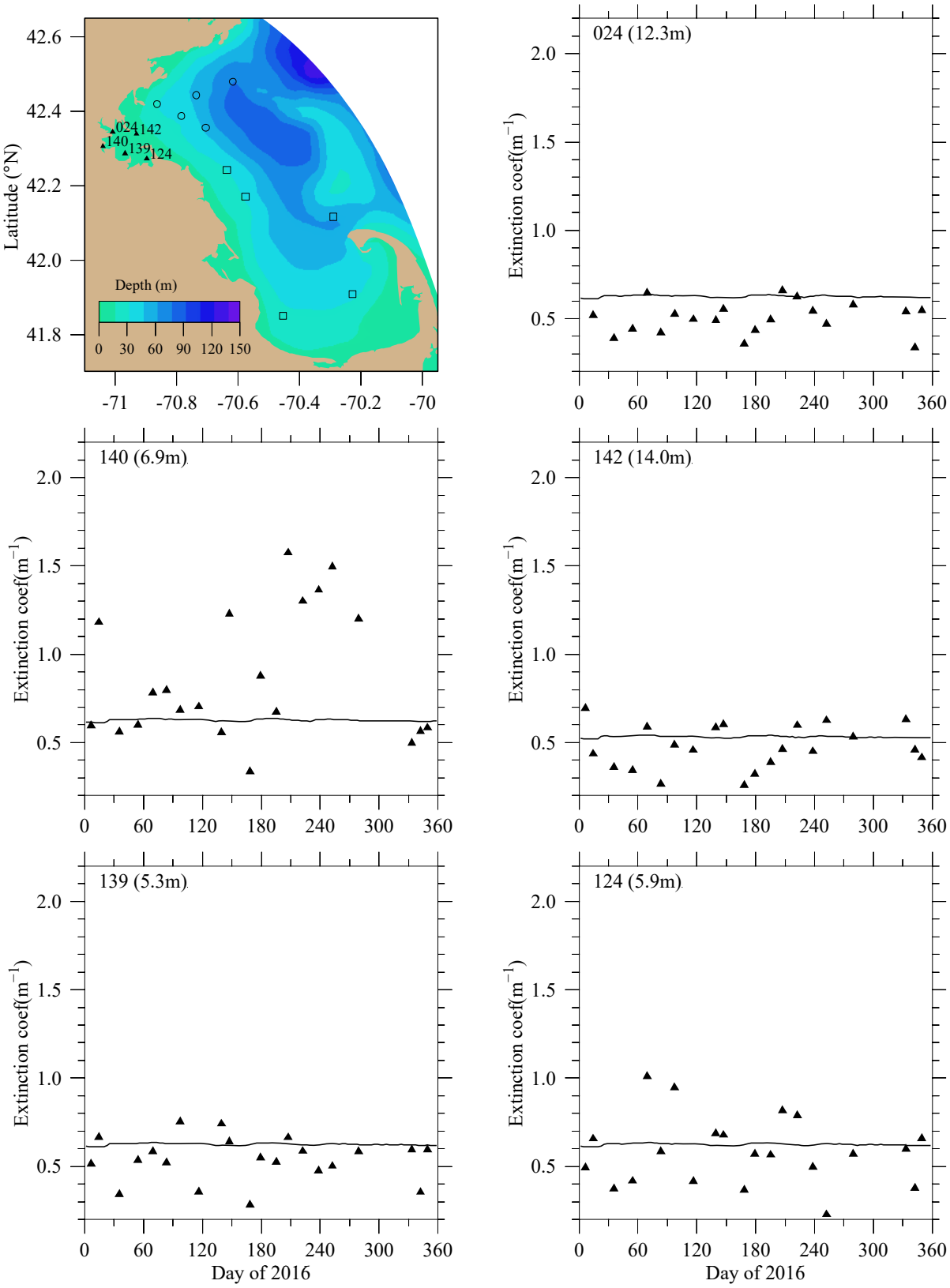

Figure 5-2c. Light extinction. Harbor stations. Line: Model. Symbols: Observations. Note different y-axis scale than for bay stations in Figure 5-2a and Figure 5-2b.

5.2 *Dissolved inorganic nitrogen*

Dissolved inorganic nitrogen (DIN) is the sum of the nitrogen in ammonium (NH_4), nitrate (NO_3), and nitrite (NO_2). Seasonal variations in modeled and observed DIN during 2016 at the northern and southern station groups were mostly typical of prior years (Figure 5-3a,b). At the start of the year the shallow and deep DIN concentrations were comparable. By May the shallow values were drawn down to nearly zero by phytoplankton consumption, and remained low through summer. Deep concentrations were also reduced in the summer, though by a much smaller amount. At stations in and near Cape Cod Bay (F29, F01, F02; Figure 5-3b) the measured early-year concentrations (until at least late April) were very low both near the surface and near the seafloor, which the model did not capture. At many stations, in particular the offshore station F22, the near-seafloor concentrations in the model underestimated the observed values.

As in past years, at the outfall/N21 site (Figure 5-3a) some observations (notably Feb, Apr, Oct, Nov) had higher concentrations near the surface, in contrast to other stations. The simulation did not match this feature, which is likely associated with small-scale variability of the effluent leaving the outfall in the mixing zone. While the model does not attempt to replicate each individual spatial and/or temporal fluctuation at these small scales, it is thought to capture their general statistical characteristics and thus their influences on the larger area surrounding the outfall.

For harbor stations the magnitudes and seasonal cycles of DIN in the model were generally similar to observations (Figure 5-3c). At most stations the observed differences between shallow and deep concentrations were minor (generally 2 μM or less) and surface-bottom differences in the model were smaller yet. At stations 140, 142, and 139 during the much of the springtime the model values were substantially higher than observed.

The modeled signature of the outfall in DIN is made clear by monthly-mean concentrations on the east-west transect (Figure 5-3d). The highest DIN levels generally occur near the seafloor, and within about 10 km of the outfall, year-round. High concentrations were also more common within 5-10 km of the coast from November through about March. Away from the outfall, during winter conditions (Jan-Feb, Nov, and to some extent Dec) vertical gradients are weak in association with more vigorous vertical mixing and reduced plankton uptake, while for the rest of the year concentrations in the upper water column are substantially lower than at depth due to uptake when stratification impedes vertical exchange. These patterns in 2016 were generally similar to simulations of prior years.

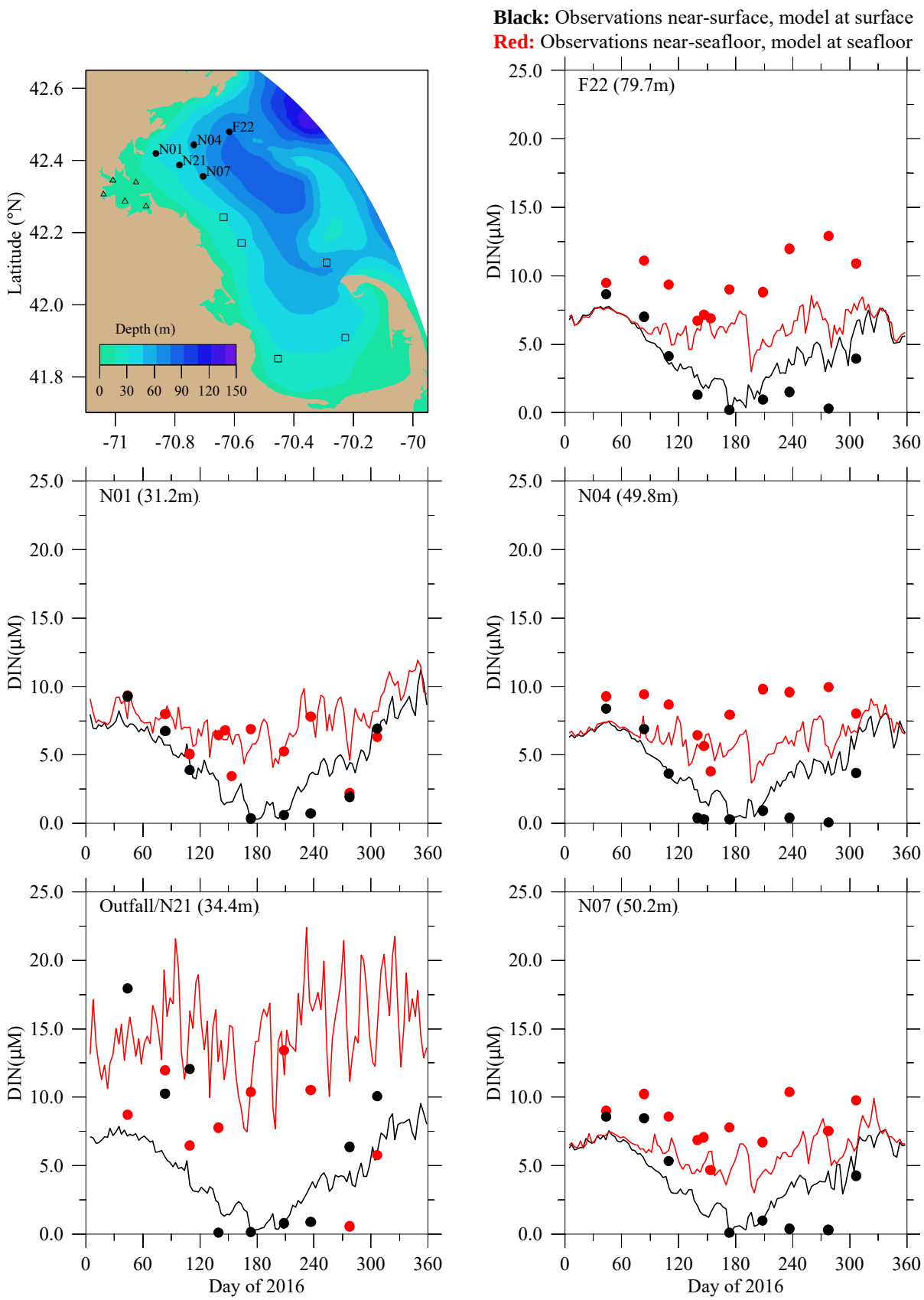

Figure 5-3a. Dissolved inorganic nitrogen. Northern stations. Model-observation comparisons.

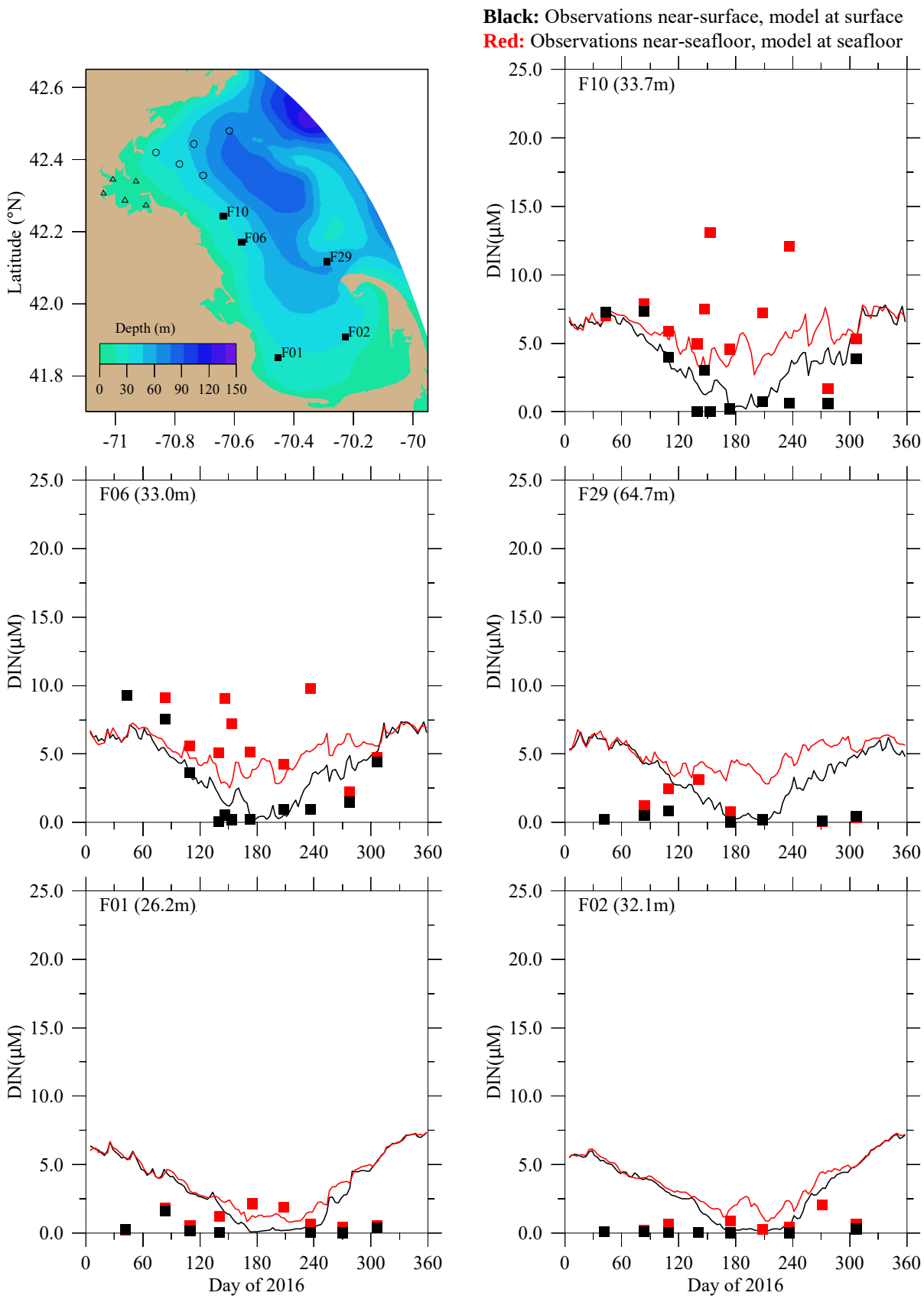

Figure 5-3b. Dissolved inorganic nitrogen. Southern stations. Model-observation comparisons.

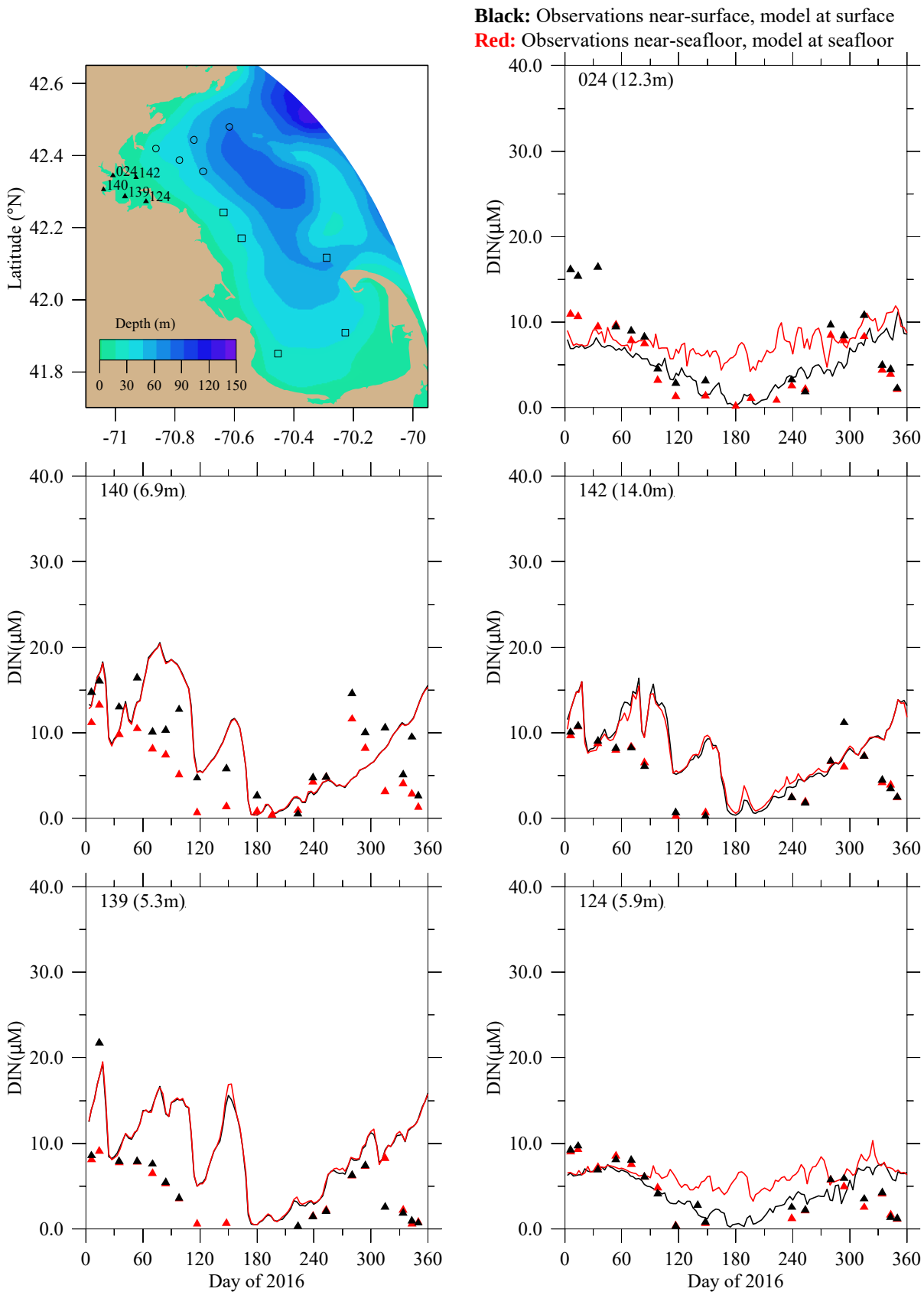

Figure 5-3c. Dissolved inorganic nitrogen. Harbor stations. Model-observation comparisons. Note different y-axis scale than for bay stations in Figure 5-3a and Figure 5-3b.

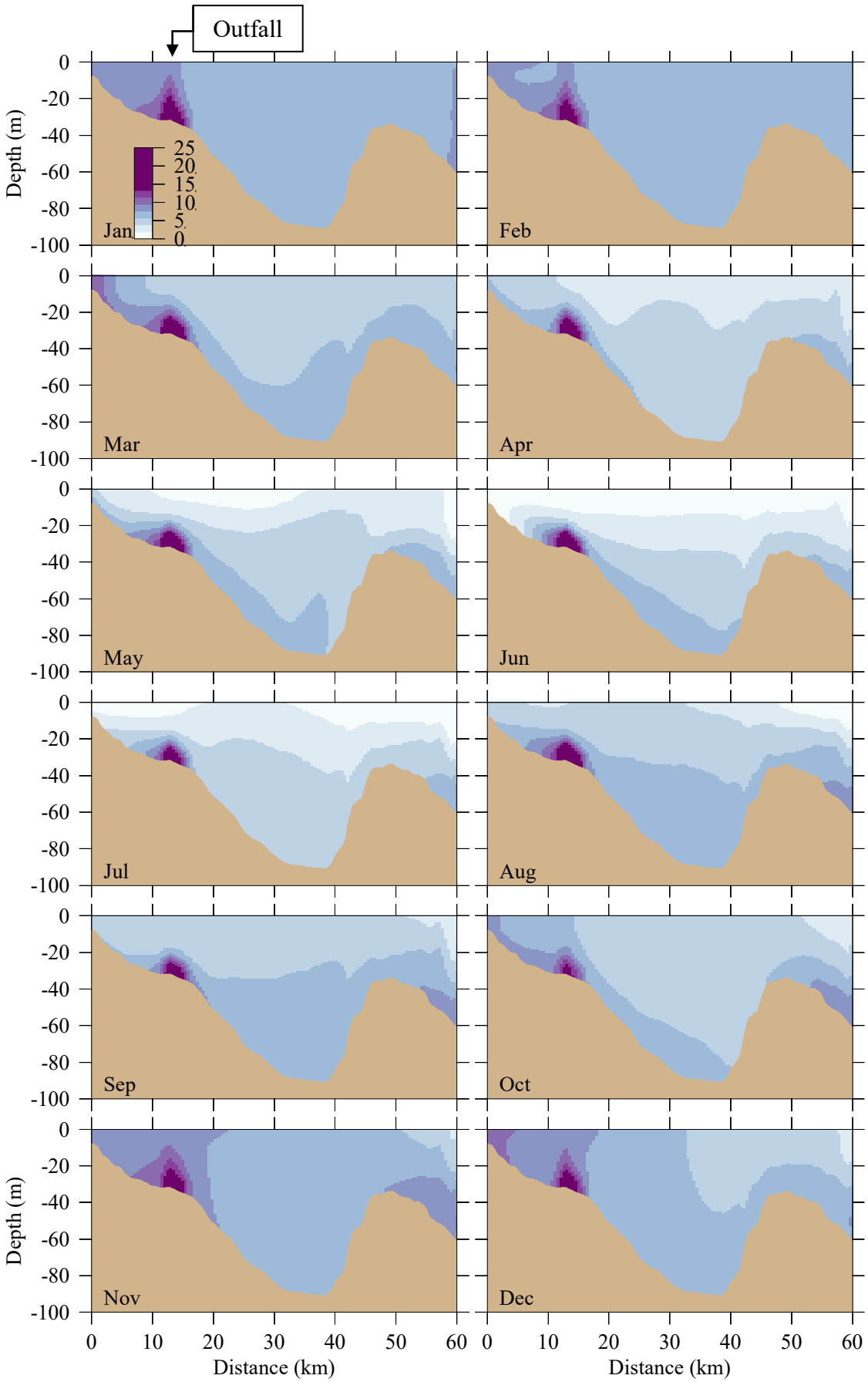

Figure 5-3d. Dissolved inorganic nitrogen (μM). Model results, east-west transect (Fig. 3-6). Horizontal axis is distance eastward from coast; outfall is on seafloor at approximately 13 km.

5.3 *Chlorophyll*

Model chlorophyll concentrations at Massachusetts Bay and Cape Cod Bay stations in 2016 (Figure 5-4a,b) showed modest temporal variations through the year. The model was generally within the observed ranges. However, at most stations the observations were notably higher near the surface than near the seafloor throughout most of the year, which was not the case in the model.

At most harbor stations (Figure 5-4c) the chlorophyll concentrations in the model underestimated observed levels, particularly in the summer and through the late fall and subsequent start of winter. In the model at stations 024 and 124, unlike the other stations, during much of the spring and summer the deep concentrations were lower than shallow concentrations. This was not a clear characteristic of the observations.

Model chlorophyll on the east-west transect (Figure 5-4d) had relatively high and vertically uniform concentrations early in the year. From March to June they were lower overall and decreased from inshore areas toward offshore. In July and August the concentrations were highest in a subsurface layer near the surface. Concentrations at the far offshore end of the transect were high in January, February, July, August, and December. In contrast to DIN, in model chlorophyll there was no signature of the outfall plume.

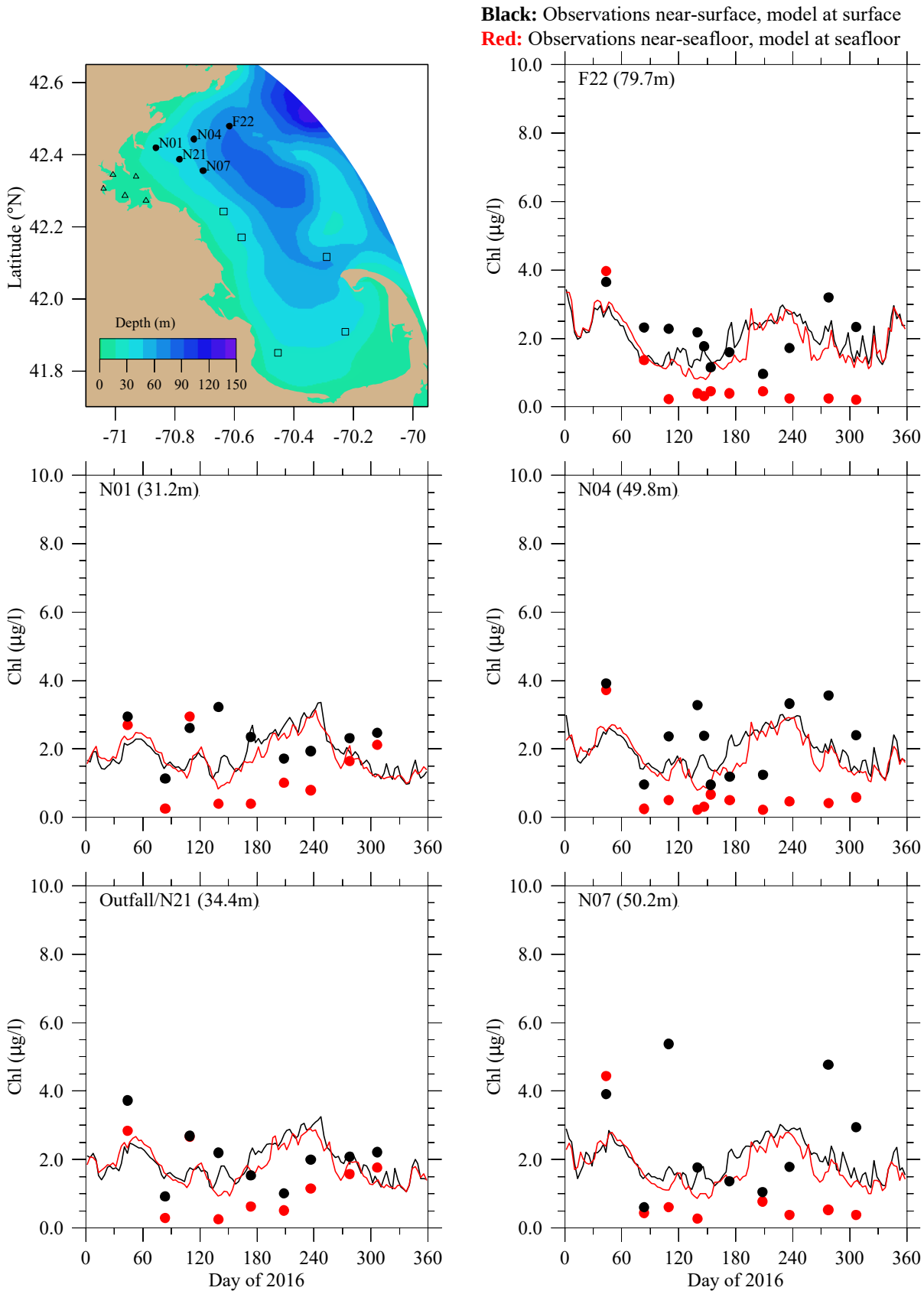

Figure 5-4a. Chlorophyll. Northern stations. Model-observation comparisons.

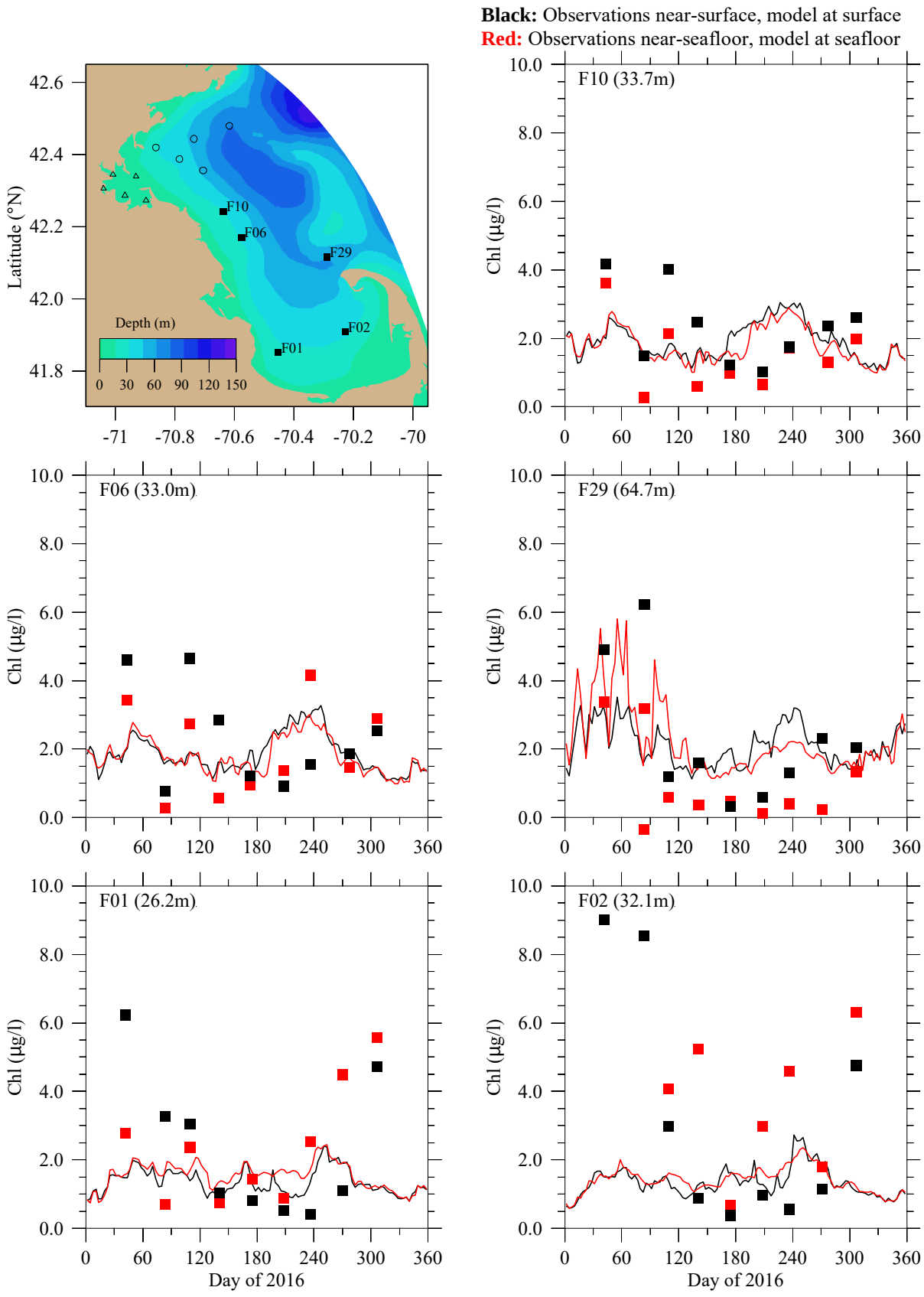

Figure 5-4b. Chlorophyll. Southern stations. Model-observation comparisons.

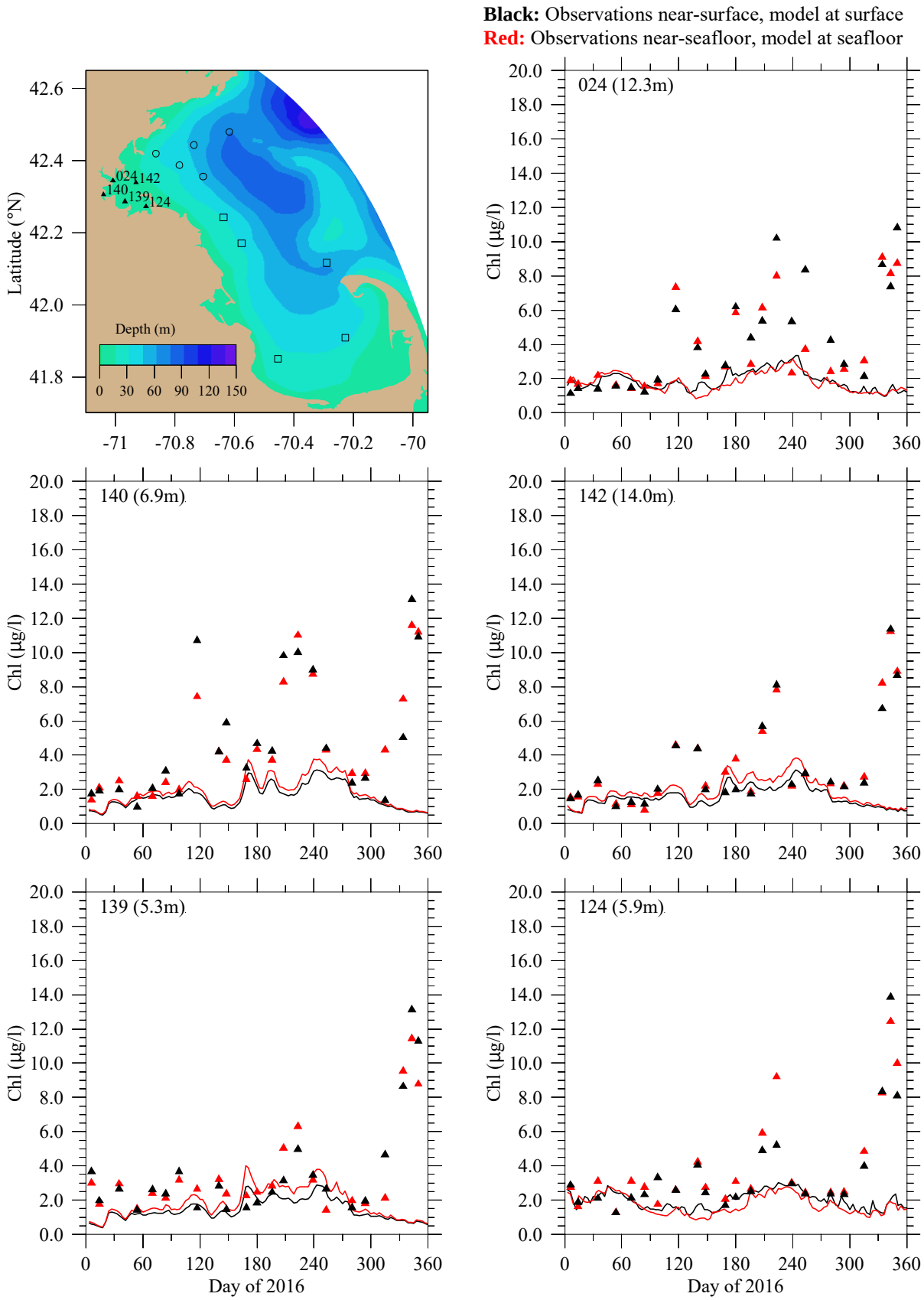

Figure 5-4c. Chlorophyll. Harbor stations. Model-observation comparisons.

Note different y-axis scale than for bay stations in Figure 5-4a and Figure 5-4b.

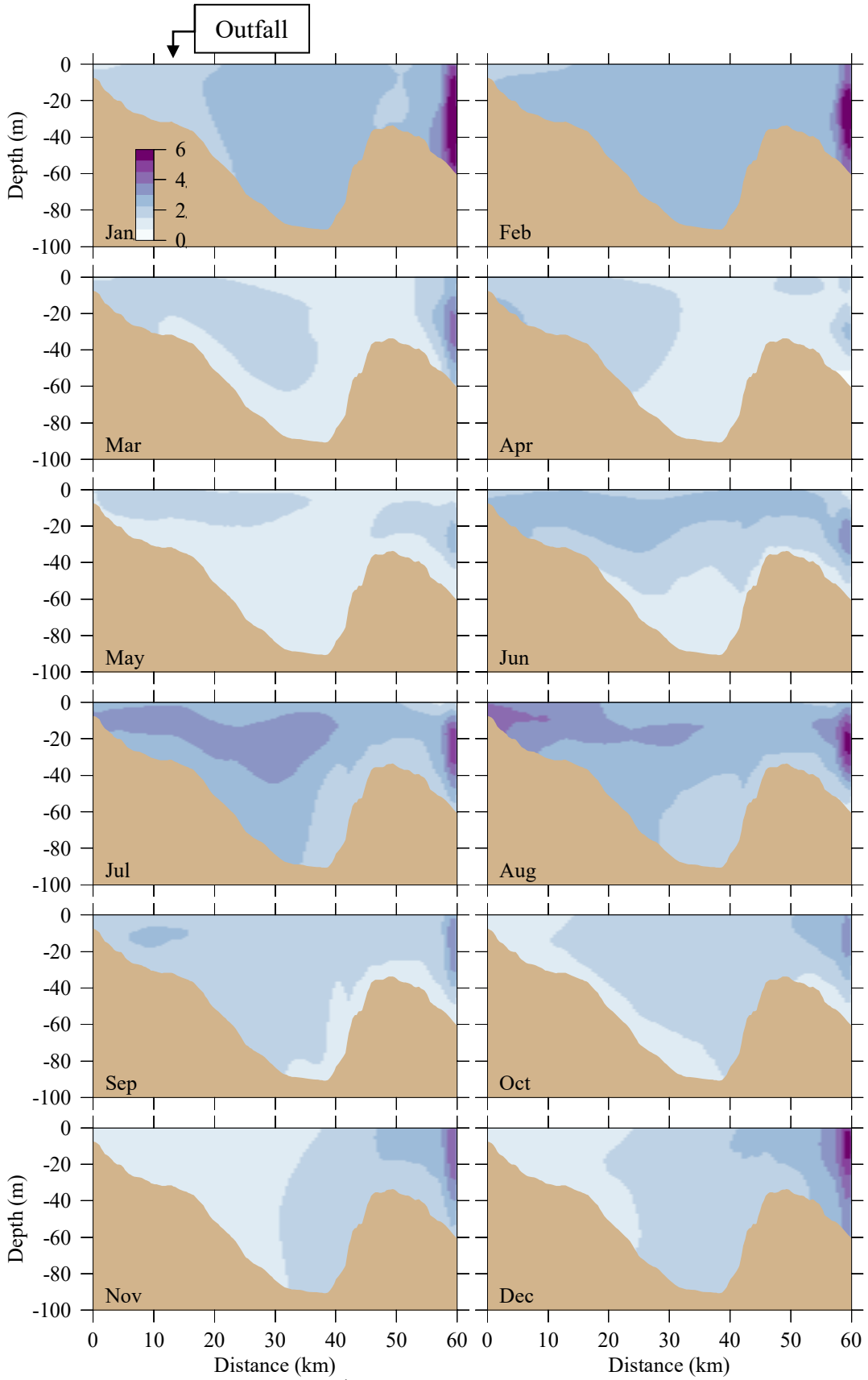

Figure 5-4d. Chlorophyll (µg L^{-1}). Model results, east-west transect (Fig. 3-6).

Horizontal axis is distance eastward from coast; outfall is on seafloor at approximately 13 km.

5.4 *Primary productivity*

Primary productivity in the 2016 model run is shown in Figure 5-5 at three monitoring stations (F23 at the mouth of Boston Harbor; N04 to the northeast of the outfall; and N18 nearest to the outfall) where observations of primary productivity had been made in past years. Ongoing field sampling no longer includes primary productivity measurements, but for context the observations from 1995-2010 are superimposed as box-whisker plots on the model outputs (a review of the field results is included as part of Keay et al., 2012; methods are described in Appendix C of Libby et al., 2005). The box-whisker plots consist of a box with the 25th and 75th percentiles at its lower and upper bounds and a horizontal line bisecting the box at the median (50th percentile), with whiskers that extend to the 9th and 91st percentiles. For most of the year, 2016 modeled primary productivity was within ranges of historic observations. At F23 the late summer levels were lower than observed in past years. Highest levels occurred during summer, particularly at N04 and N18, and in springtime the increase observed in past years was not seen in the model results. In fall, the modeled primary productivity decreased to low levels earlier than was observed in many past years. These features are all within similar ranges of results from model simulations of past years.

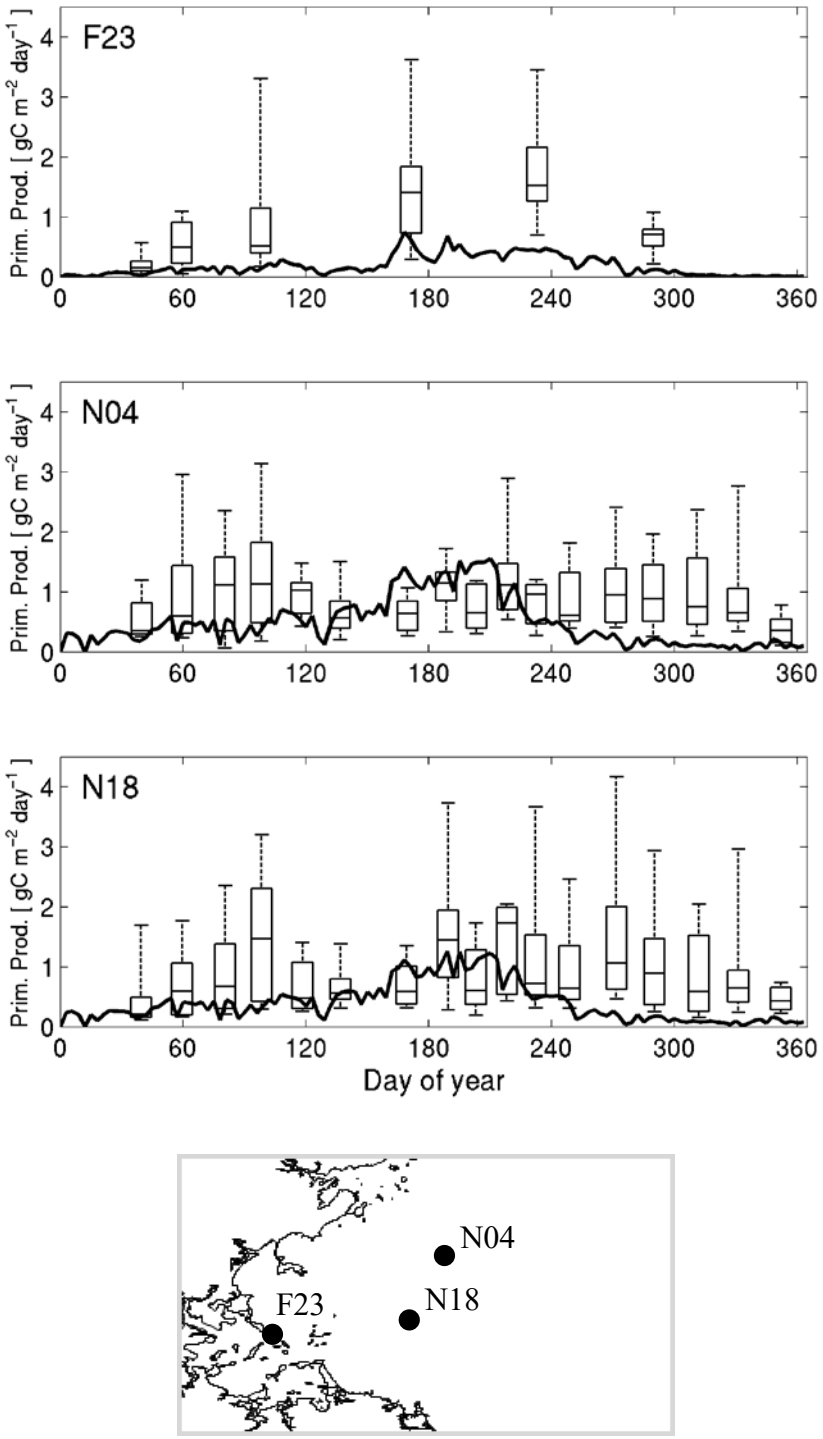

Figure 5-5. Primary production, vertically integrated, model-observation comparison.

Line is 2016 model result. Box-whiskers are 1995-2010 observations; box shows 25th, 50th, and 75th percentiles and whiskers are 9th and 91st percentiles.

5.5 *Dissolved and particulate organic nitrogen*

Model dissolved organic nitrogen (DON) levels during 2016 were generally within the range of variability of observations (Figure 5-6a,b). Temporal variations in the model were somewhat weaker than observations, and neither model nor observations included a strong seasonal signal. Model concentrations were highest in October through December, as evidenced in the east-west transect results (Figure 5-6c), and had modest vertical differences, with surface values slightly higher in the springtime.

Model particulate organic nitrogen (PON) during 2016 showed a stronger seasonal cycle than in DON, with low concentrations in winter and elevated levels in summer (Figure 5-7a,b); at most stations, deep concentrations were modestly less than shallow concentrations. The range of temporal variability in the model was less than in observations, and at most stations the deep observed values remained markedly lower than shallow values for all or most of the year, a feature the model did not capture. The east-west transect results for PON (Figure 5-7c) demonstrate that the seasonal changes and vertical structure just described generally occurred regionwide.

As noted for chlorophyll above, in both model and observations there was not a persistent anomalous signal near the outfall in either DON or PON. This is evidence supporting the conclusion that these variables are not detectably influenced by outfall effluent.

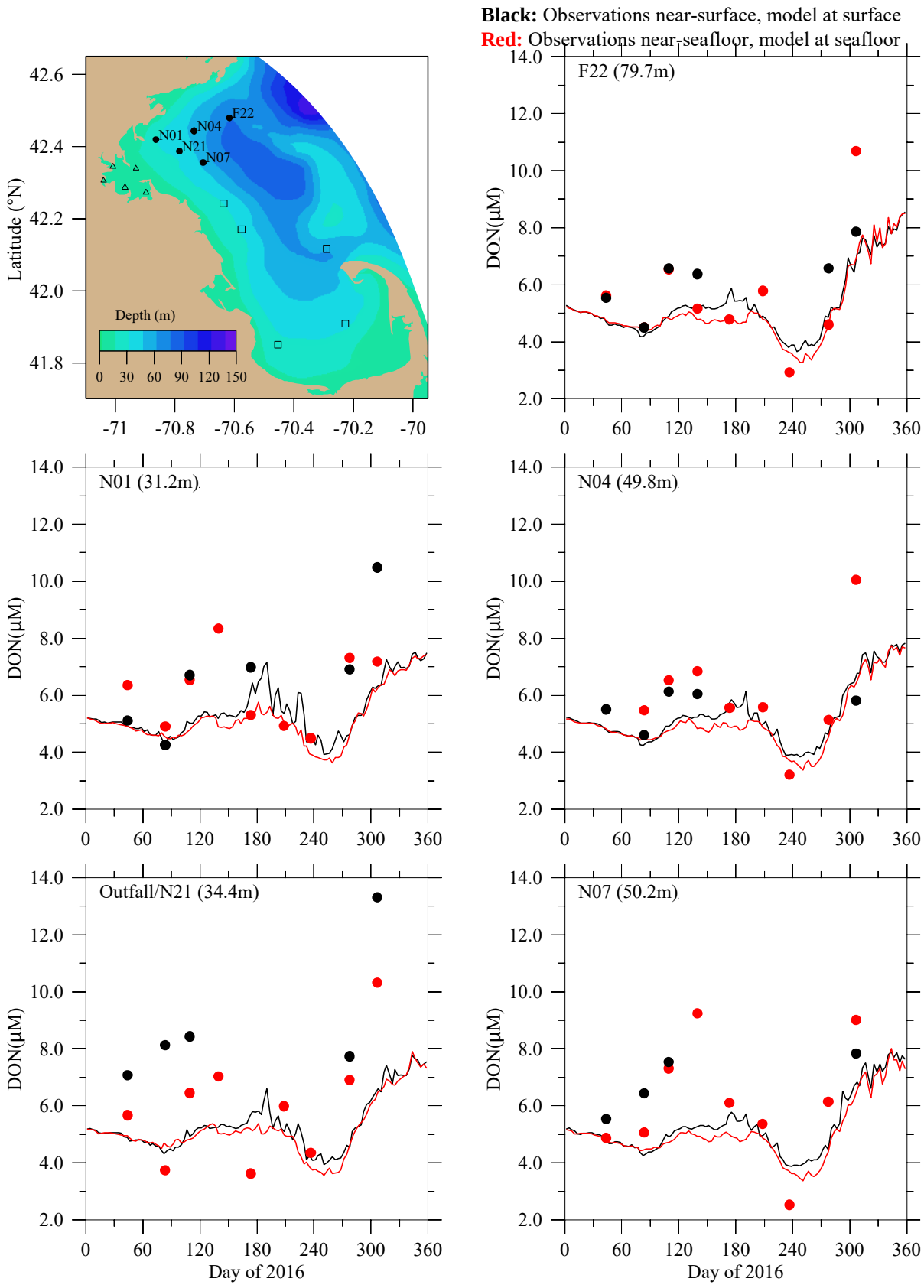

Figure 5-6a. Dissolved organic nitrogen. Northern stations. Model-observation comparisons.

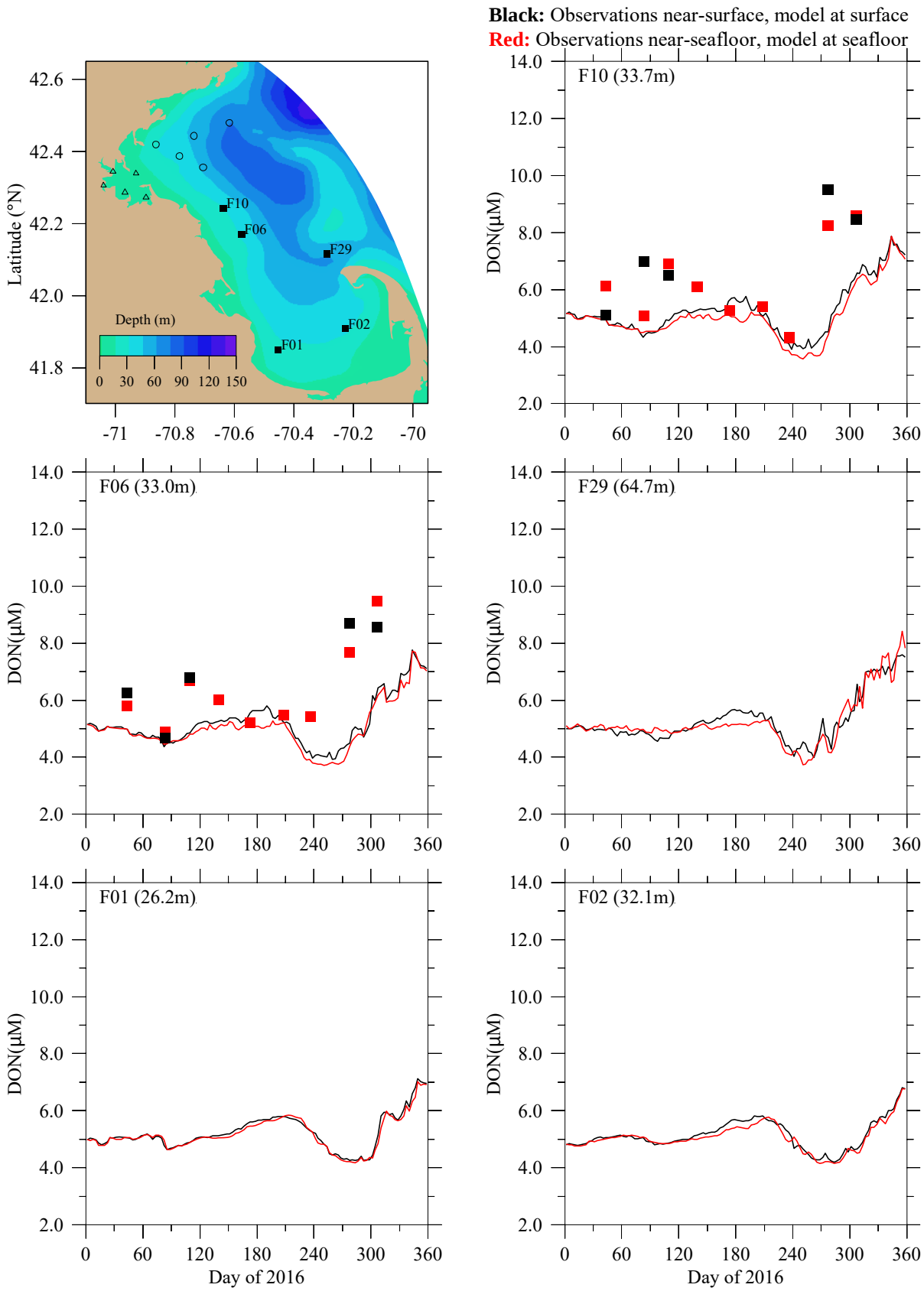

Figure 5-6b. Dissolved organic nitrogen. Southern stations. Model-observation comparisons. No observations were collected at stations F29, F01, or F02.

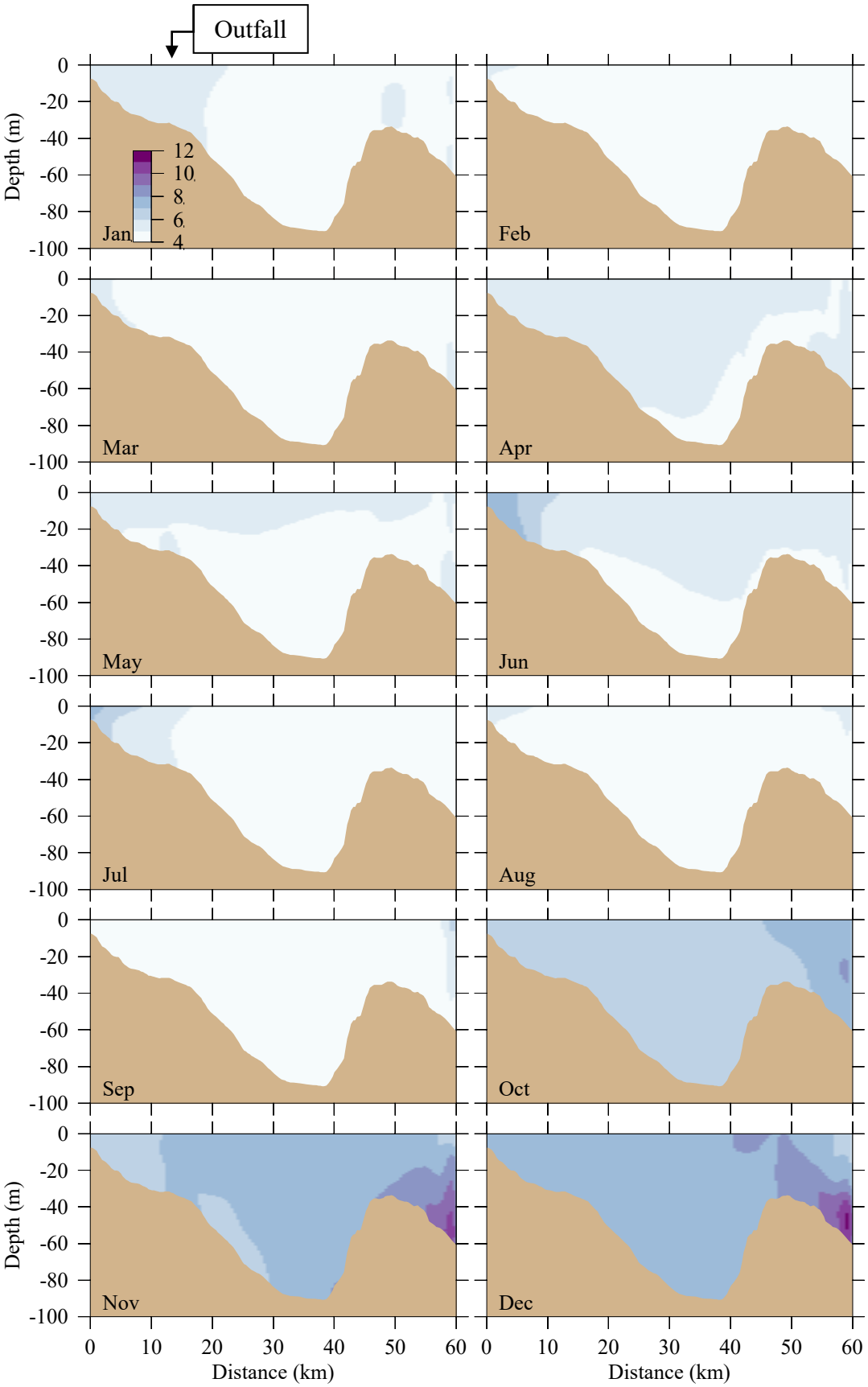

Figure 5-6c. Dissolved organic nitrogen (µM). Model results, east-west transect (Fig. 3-6). Horizontal axis is distance eastward from coast; outfall is on seafloor at approximately 13 km.

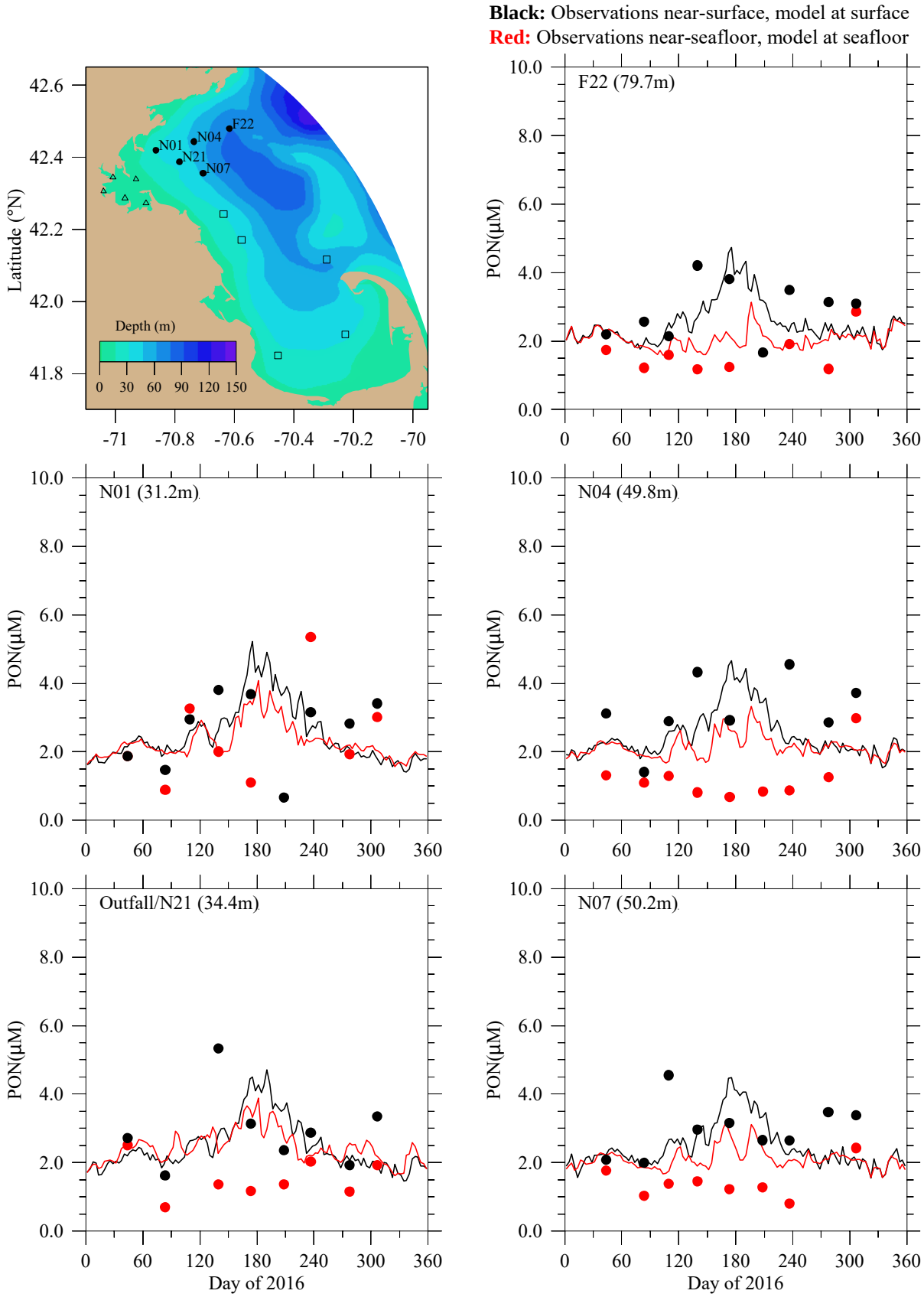

Figure 5-7a. Particulate organic nitrogen. Northern stations. Model-observation comparisons.

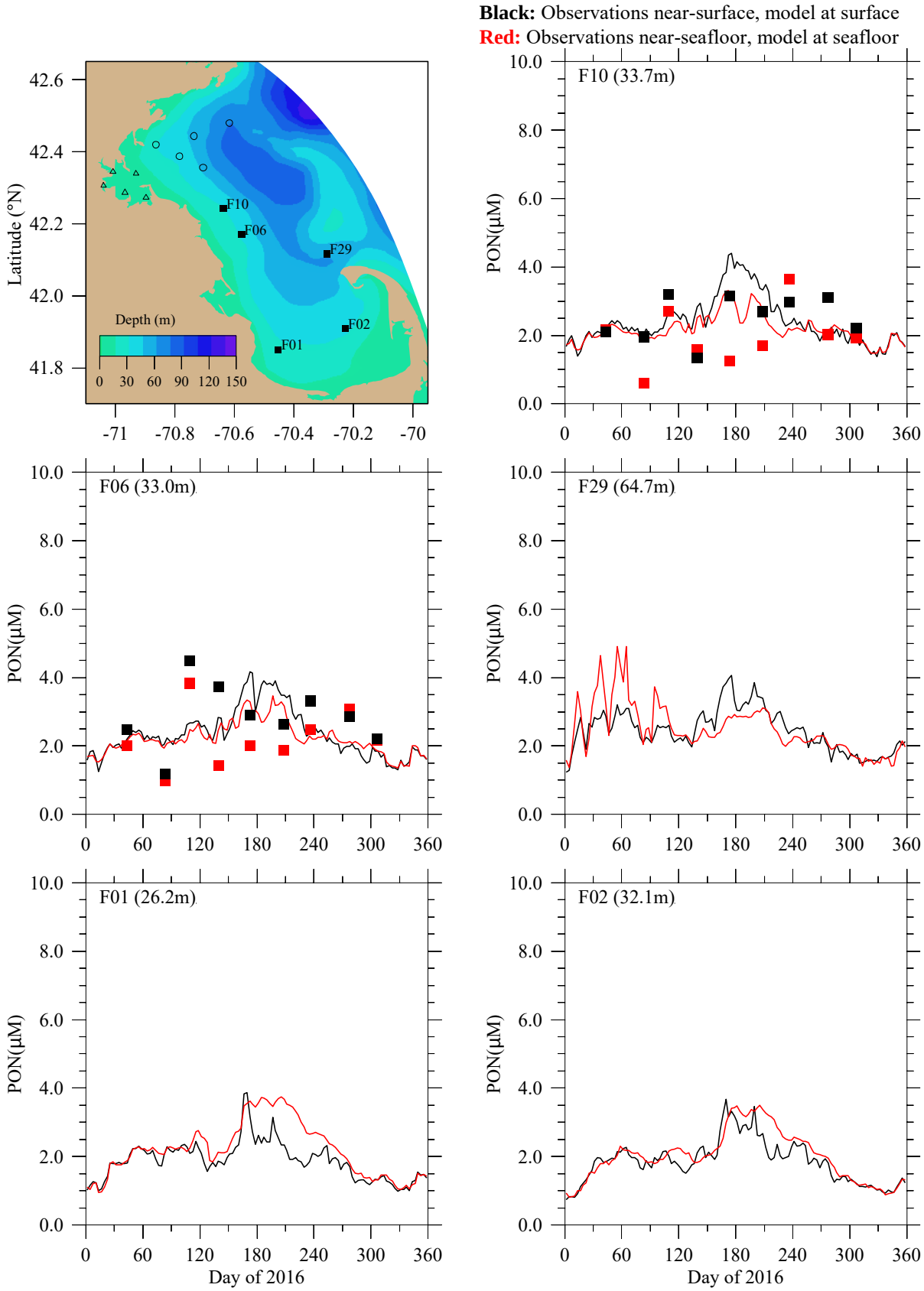

Figure 5-7b. Particulate organic nitrogen. Southern stations. Model-observation comparisons. No observations were collected at stations F29, F01, or F02.

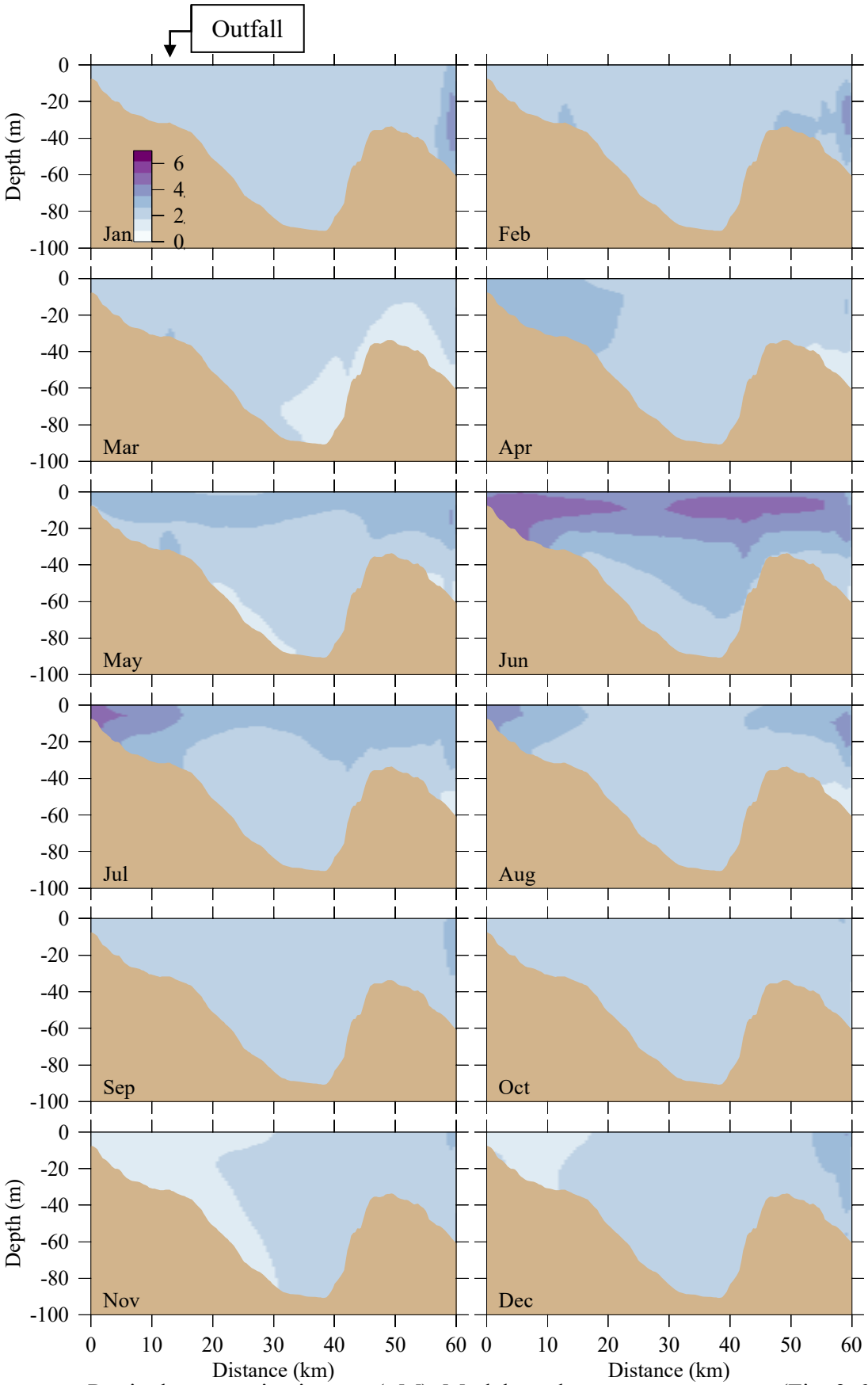

Figure 5-7c. Particulate organic nitrogen (µM). Model results, east-west transect (Fig. 3-6). Horizontal axis is distance eastward from coast; outfall is on seafloor at approximately 13 km.

5.6 *Particulate organic carbon*

The seasonal cycle in model particulate organic carbon (POC) during 2016 at Massachusetts Bay stations was pronounced (Figure 5-8a,b), with lowest values the spring, highest values in late summer and early fall, and intermediate values through the winter. The ranges of model values were generally near the range of observed values, but at many stations the model results were biased higher than observations. In the observations, deep concentrations were almost all substantially lower than shallow values, while the opposite was true for much of the year at many stations in the model. This mismatch between the vertical structure of POC in the model and observations is apparently due to parameterization of biogeochemical processes in UG-RCA, given that the hydrodynamic model is capturing observed variations of vertical structure (stratification) well, as described in Section 4.

Model POC on the east-west transect in 2016 (Figure 5-8c) showed generally higher concentrations from May through September, consistent with Figure 5-8a,b. Highest concentrations occurred subsurface in the upper water column. There were also high concentrations at the far offshore end of the transect during the spring and early fall.

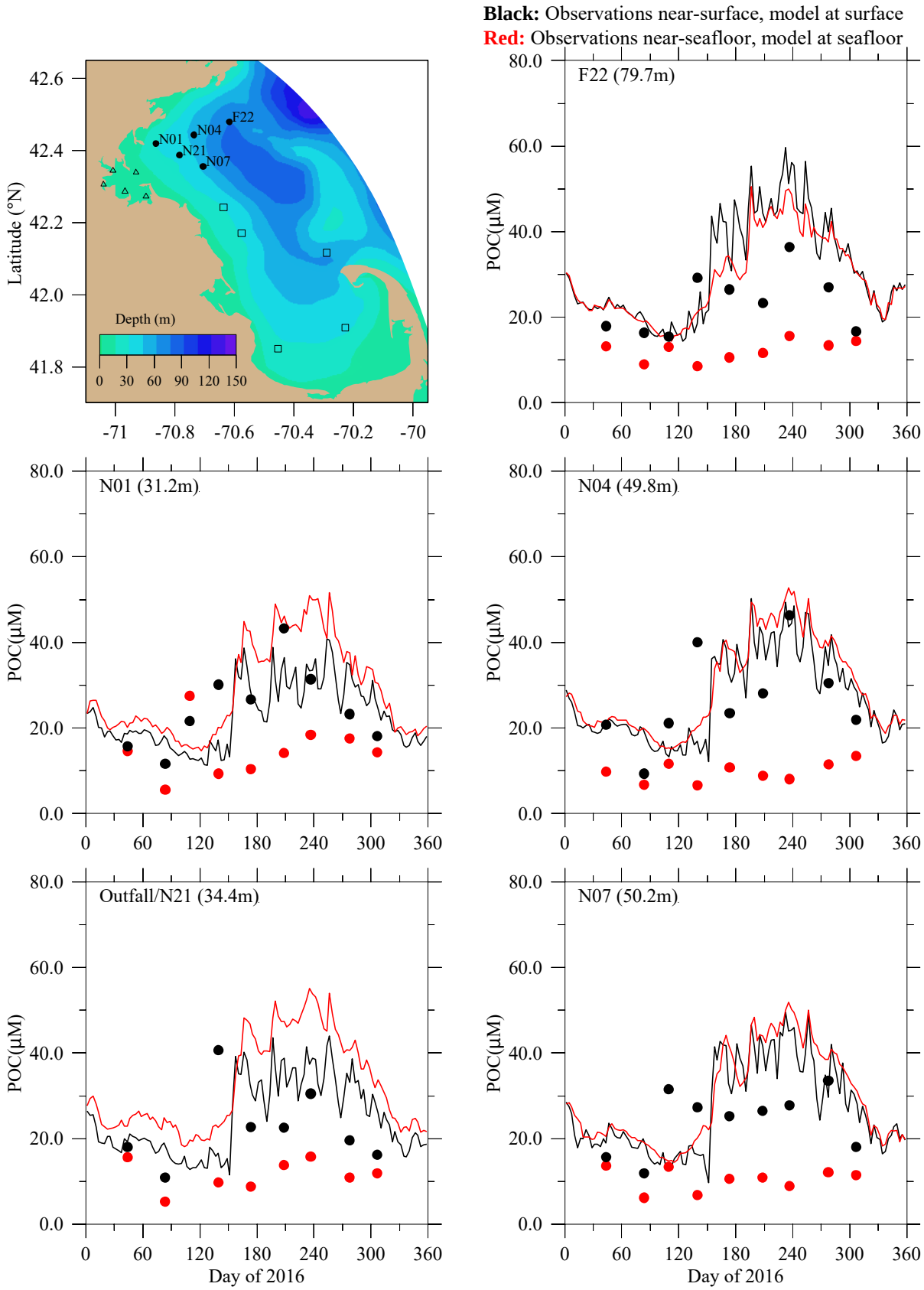

Figure 5-8a. Particulate organic carbon. Northern stations. Model-observation comparisons.

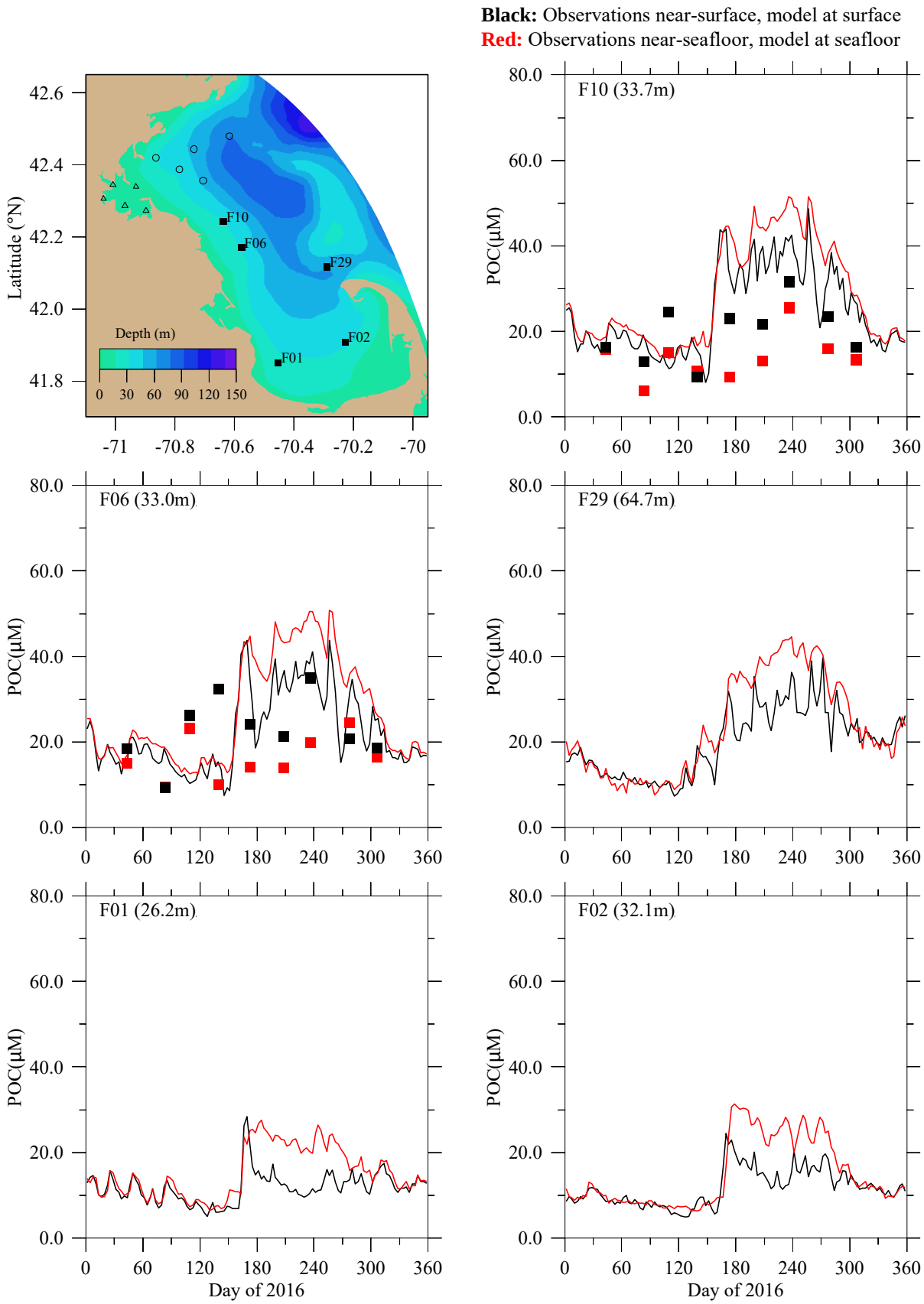

Figure 5-8b. Particulate organic carbon. Southern stations. Model-observation comparisons. No observations were collected at stations F29, F01, or F02.

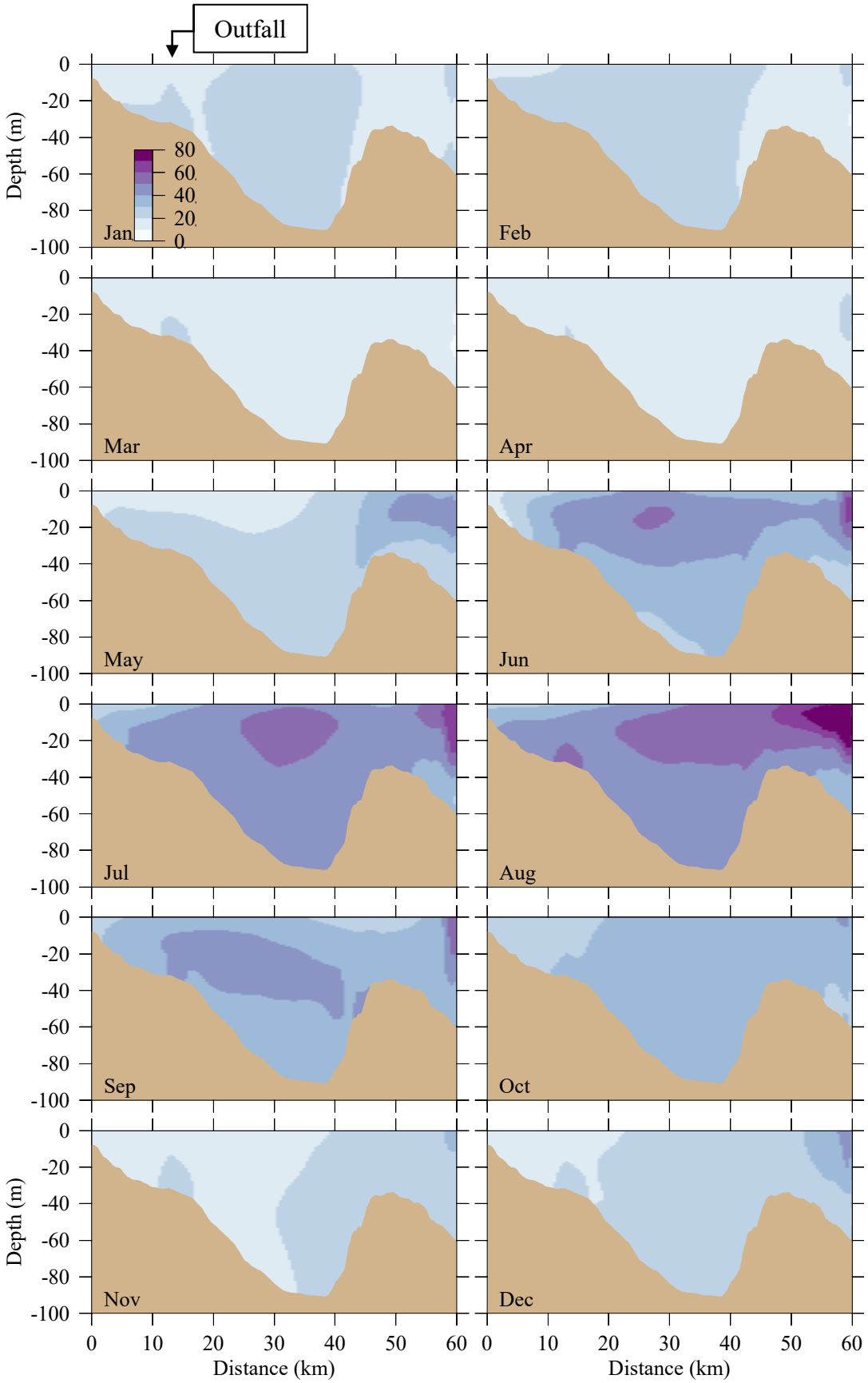

Figure 5-8c. Particulate organic carbon (µM). Model results, east-west transect (Fig. 3-6). Horizontal axis is distance eastward from coast; outfall is on seafloor at approximately 13 km.

5.7 *Dissolved oxygen*

The observed seasonal cycle in dissolved oxygen concentration (peak in spring, decrease through summer to minimum in late fall, then increase) in 2016 was reproduced well by the model at Massachusetts Bay and Cape Cod Bay stations (Figure 5-9a,b). As noted above (Figure 5-1) the correlation between modeled and observed DO concentrations was 0.90 near the bottom, with root-mean square (RMS) error of 0.51 mg L^{-1}. Concentrations are highest in spring and lowest in late summer, with values near the surface generally higher than near the bottom. The late summer and fall observed values at F02 and, to a lesser extent, F01 were substantially lower than at other stations, a feature the model did not capture. The model-observation differences in the 2016 simulation were similar in magnitude to those of previous years. Model DO concentration on the west-east transect (Figure 5-9c) showed the same general patterns as those found in previous years but with somewhat less-pronounced vertical structure, which could be due to the modest spring phytoplankton bloom that would have further increased near-surface concentrations if stronger.

DO percent saturation depends on temperature and salinity as well as oxygen concentration, and is a useful quantity to help understand the relative influence of temperature and photosynthesis on DO. Percent saturation above 100% can result from photosynthetic production. We computed DO saturation from model results for DO concentration, temperature, and salinity using the approximate relation given in equation 2.3 of Zhao et al. (2012). Comparisons between this result and observed DO saturation (Figure 5-10a, b) reveal reasonable agreement. The pattern is similar at most stations, and on the east-west transect (Figure 5-10c), with reaeration due to exchange between atmosphere and ocean playing a dominant role as described by Xue et al. (2014). In winter, DO saturation levels are modest due to weaker reaeration, and vertical mixing keeps them nearly vertically uniform; in spring, photosynthesis helps increase surface values, which remain higher through summer when reaeration is most active, while levels in deeper water steadily decrease because they are isolated by stratification. The deep minimum is reached in late summer, after which the fall overturn returns the system to winter conditions.

Finally, model DO concentration and percent saturation have also been compared (Figure 5-11) directly to the only available time series observations of DO, from near the surface (2 m deep) and 51 m deep at the Mooring A01 site (see Figure 1-1) in northeastern Massachusetts Bay. In order to minimize the influence of intermittent sensor noise due to bubble sweepdown, daily medians of the raw hourly near-surface measurements are used. The daily medians are averaged over 3 day

intervals to match the temporal resolution of the model output. The general patterns of seasonal variations in the model, as described above, are similar to the observations. However, the model oxygen concentration (upper frame, Figure 5-11) near the surface is systematically lower than observed; it is recognized that the observations can require calibration offsets at least as large as these differences, and the process of ground-truthing and correcting the observations for these offsets is still underway as of the time of publication of this report. As expected due to stronger winds and the associated vertical mixing, in the early part of the year the shallow and deep concentrations are very similar to each other in both the observations and the model. For DO percent saturation (lower frame, Figure 5-11) the relationships between model results and observations are similar to those for DO concentration. These model results, for both DO concentration and DO percent saturation, and for both annual-mean levels and seasonal variations about them, are similar to model simulations of past years.

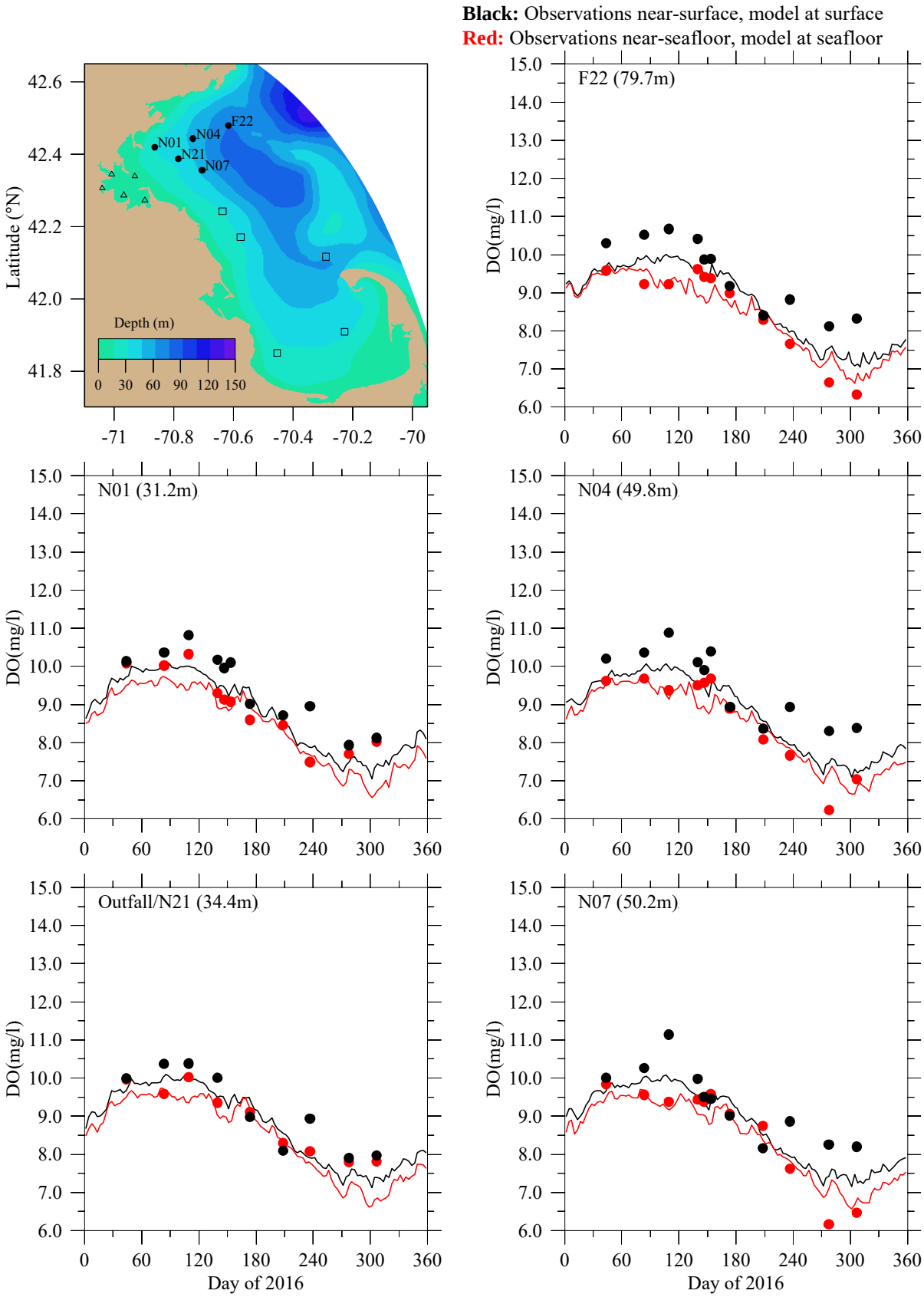

Figure 5-9a. Oxygen concentration. Northern stations. Model-observation comparisons.

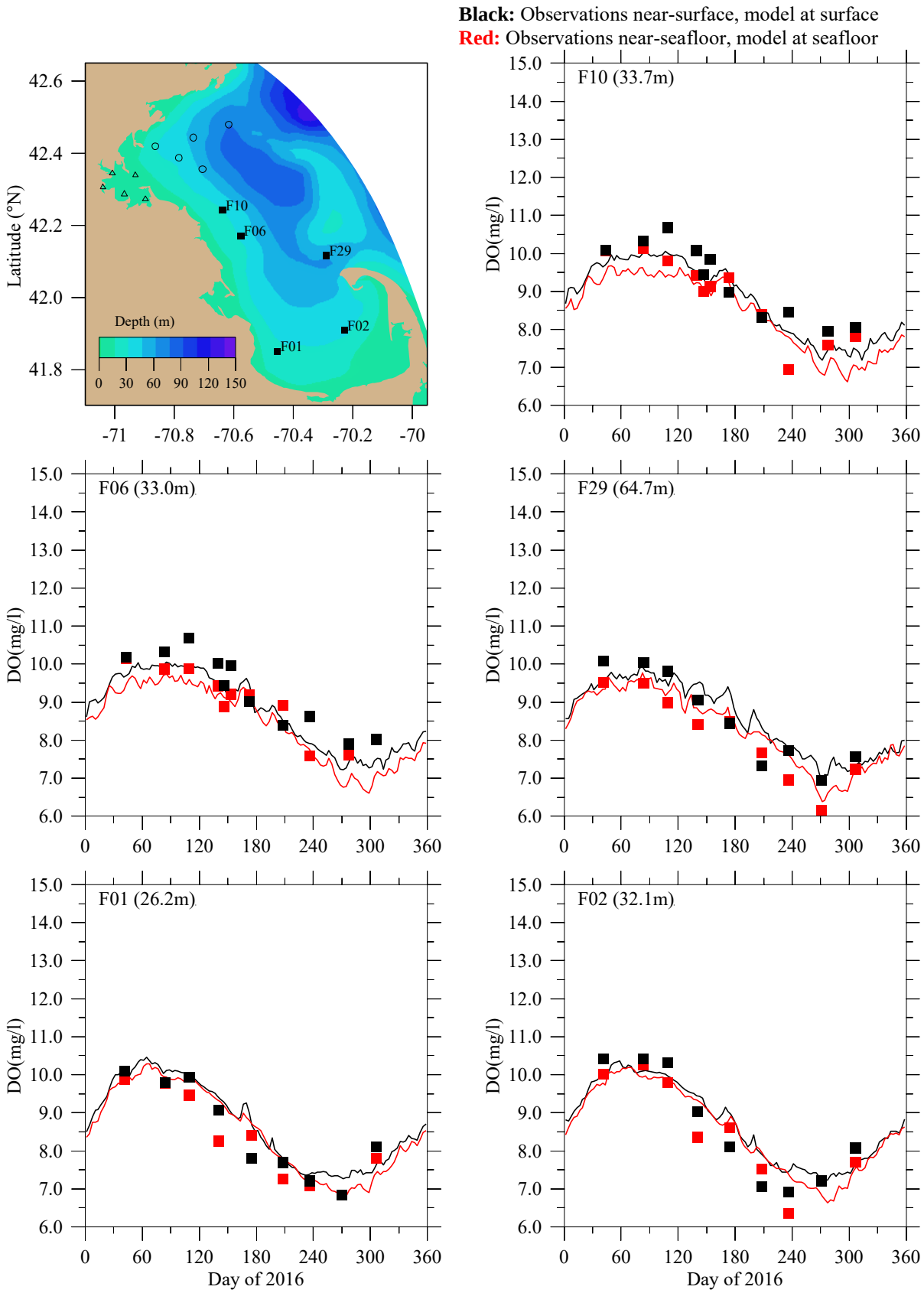

Figure 5-9b. Oxygen concentration. Southern stations. Model-observation comparisons.

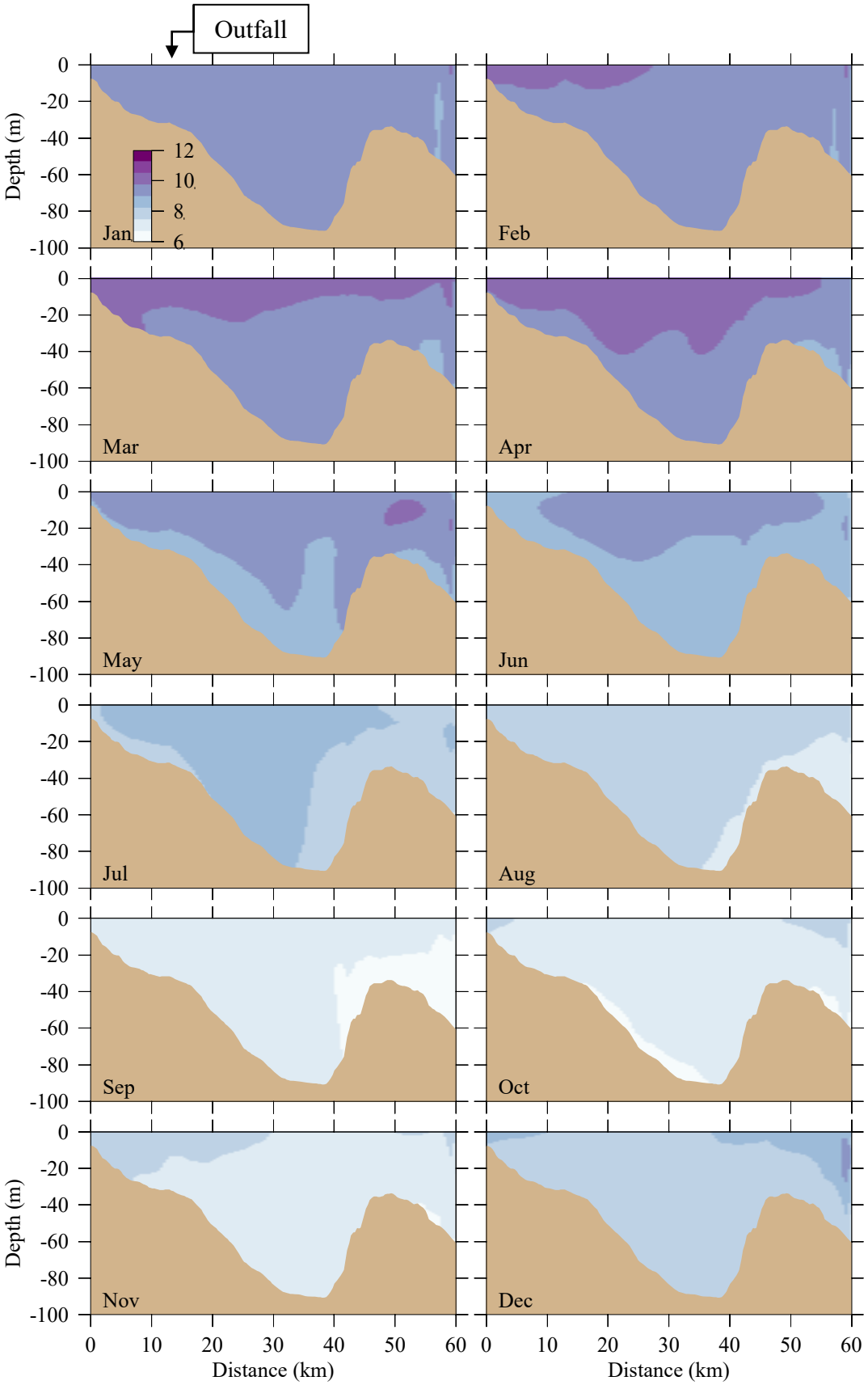

Figure 5-9c. Oxygen concentration (mg L^{-1}). Model results, east-west transect (Fig. 3-6). Horizontal axis is distance eastward from coast; outfall is on seafloor at approximately 13 km.

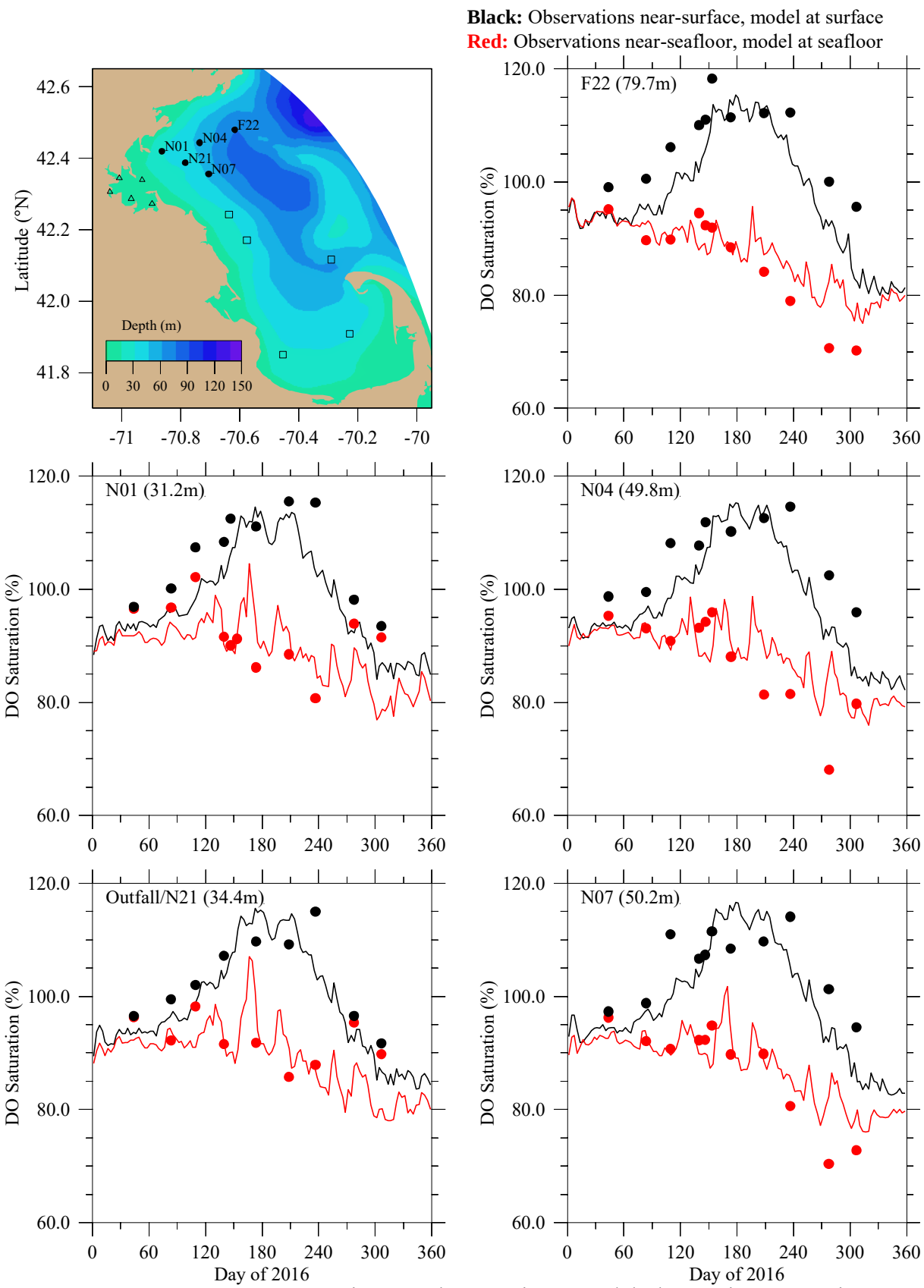

Figure 5-10a. Oxygen percent saturation. Northern stations. Model-observation comparisons.

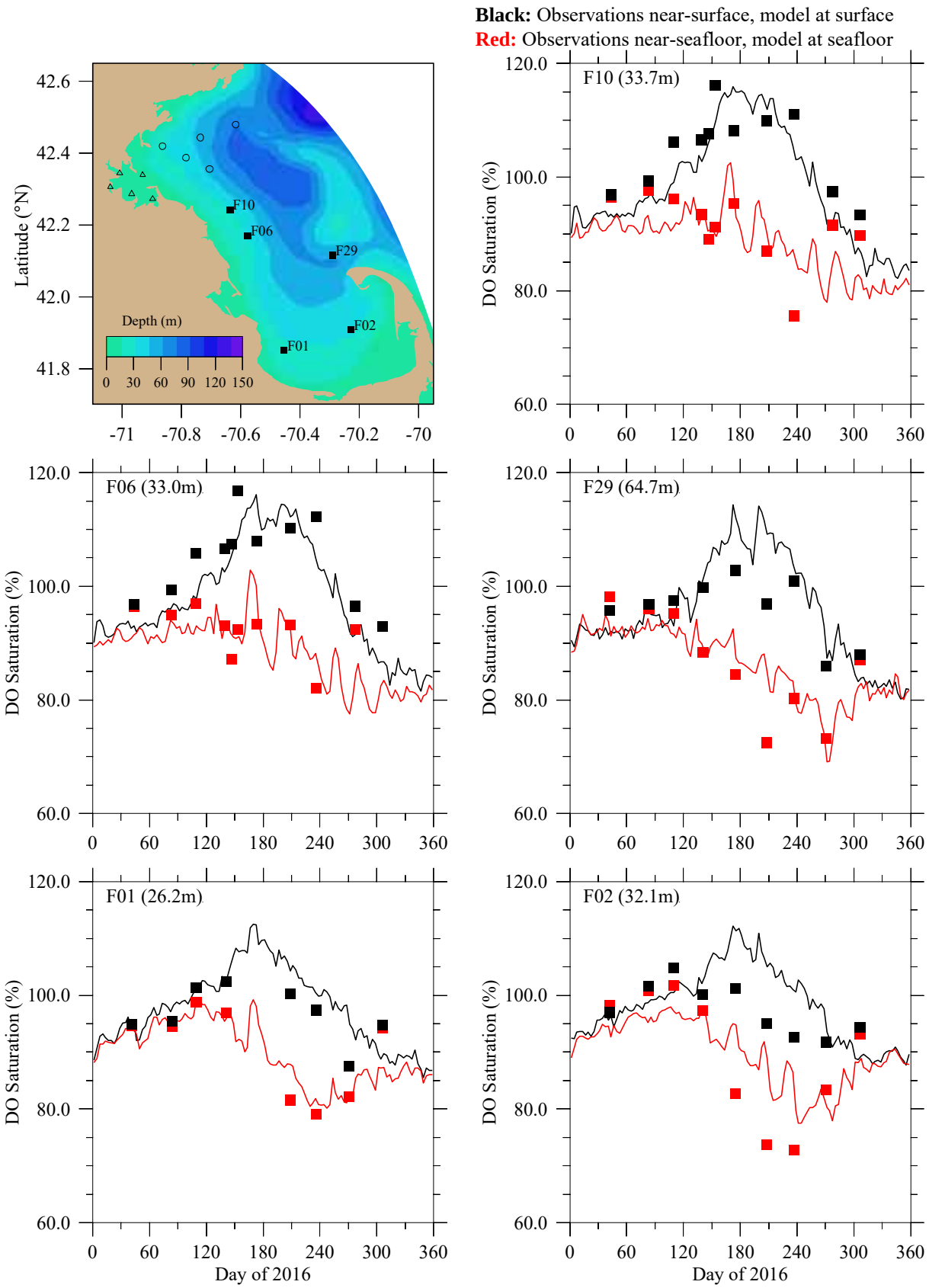

Figure 5-10b. Oxygen percent saturation. Southern stations. Model-observation comparisons.

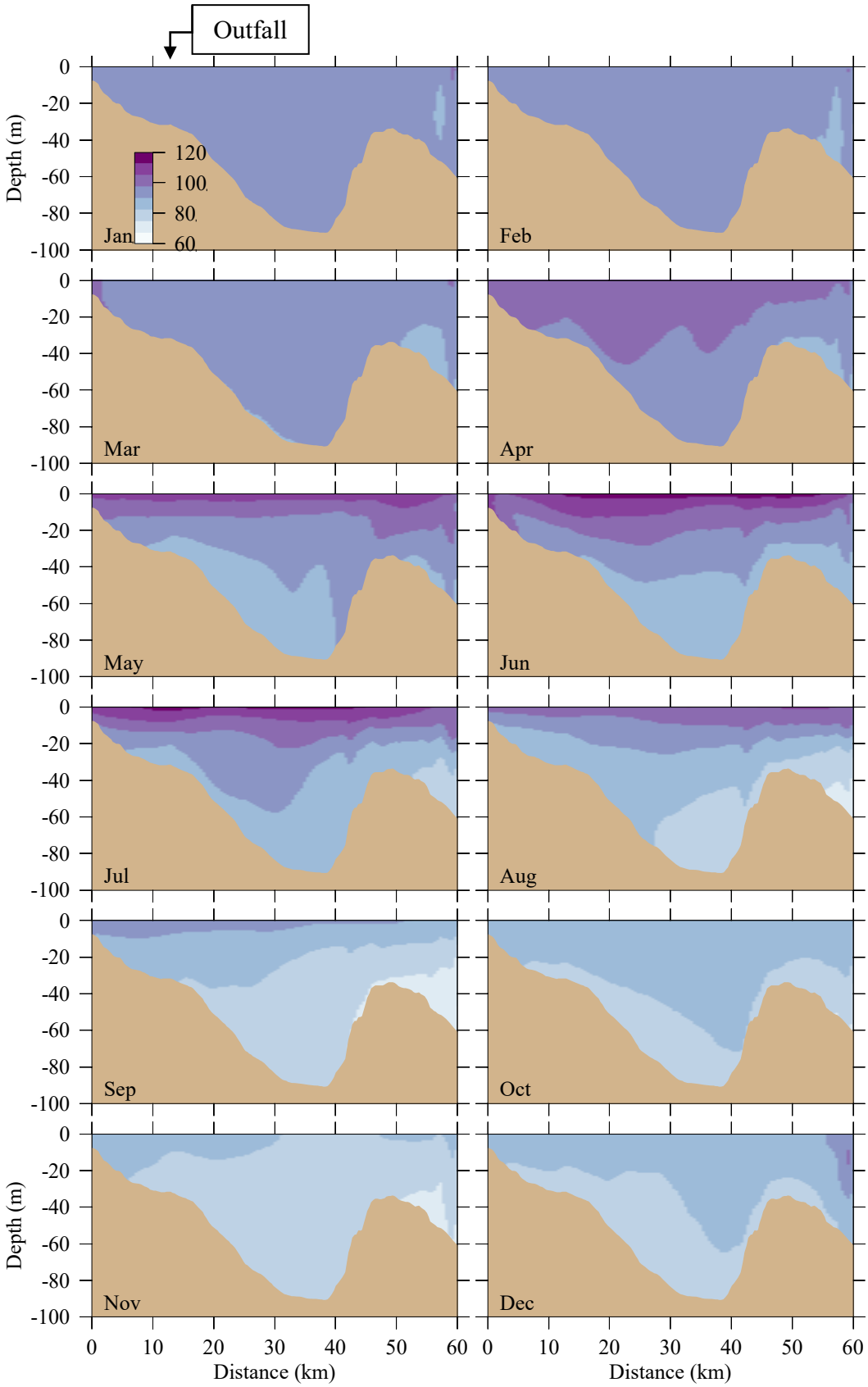

Figure 5-10c. Oxygen percent saturation. Model results, east-west transect (Fig. 3-6). Horizontal axis is distance eastward from coast; outfall is on seafloor at approximately 13 km.

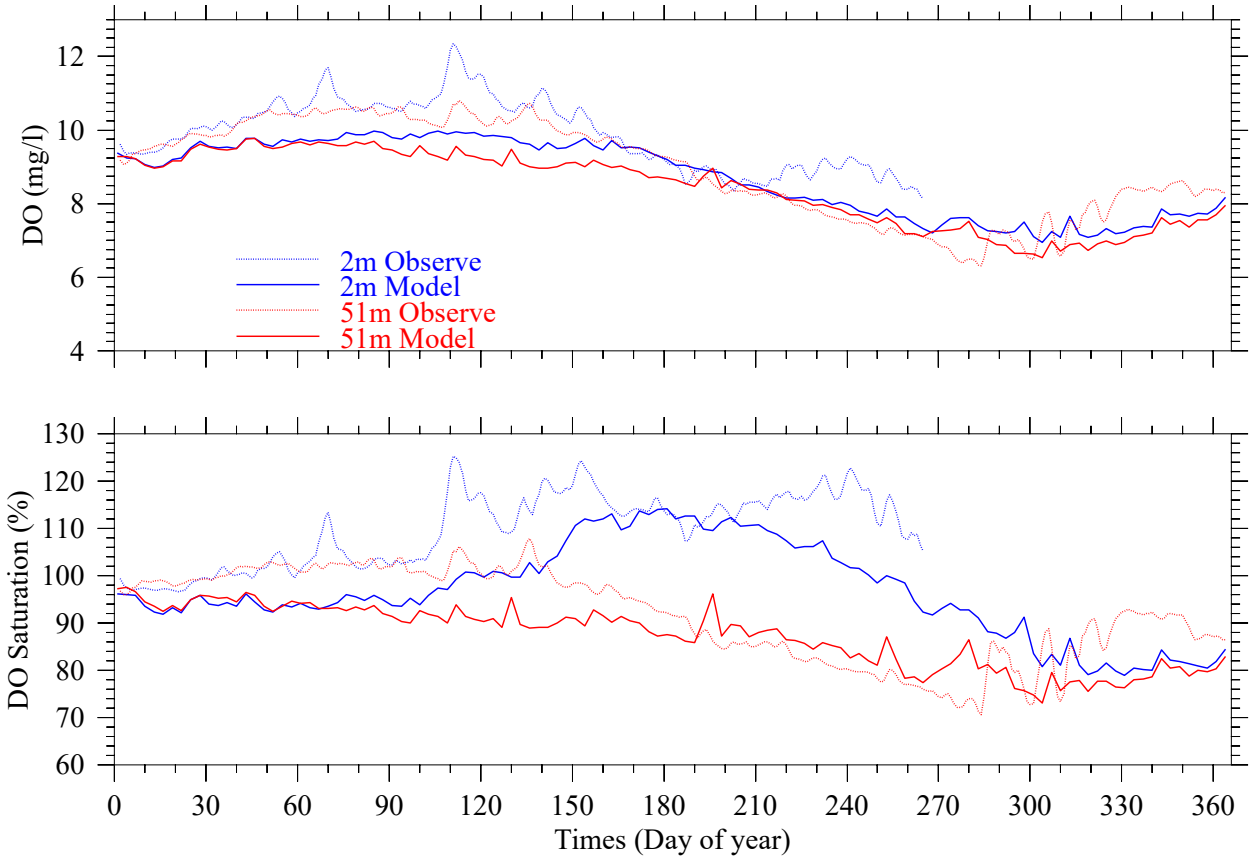

Figure 5-11. Oxygen time series, Mooring A01 site, model-observation comparison.

The 2-m deep observations after late September did not meet quality standards.

5.8 *Sediment fluxes*

Sediment NH_4^+ fluxes and sediment oxygen demand (SOD) from the 2016 simulation are shown in Figure 5-12 and Figure 5-13. Results are presented for the Massachusetts Bay and Boston Harbor stations where flux measurements had been made most consistently in earlier years, because they best facilitate model-observation comparisons. Ongoing field sampling no longer includes these benthic fluxes, but to provide context the observations from 2000-2010 are superimposed as box-whisker plots (as described in Section 5.4) on the model results (the field program and its results are described in MWRA technical reports, for example Tucker et al., 2010). Observations from prior to 2001 were not included, because diversion of the outfall to its current location occurred in 2000. At harbor stations the model NH_4^+ flux in 2016 was nearly zero except during about 5 months from summer to early fall, when it was positive but systematically lower than the central range of observed values except at BH03 during summer and early fall. At bay stations it was nearly zero except between May and December, when model values were generally within the range of historic observations, though they were higher than observations at MB05 in the fall. Model SOD at harbor stations exhibited seasonality, and bias toward low values, relative to observations, similar to the NH_4^+ flux there. At bay stations, model SOD had similar seasonality to the NH_4^+ flux there; relative to the range of observations, model values were low in the spring and early summer, near the lower end of the range in summer, and within or nearer to the range in fall. These characteristics and relationships to observations for the 2016 simulation are similar to those of simulations of recent years.

At harbor stations, the fluxes were becoming lower during the more recent years of the period when observations were collected (up to and including 2010), in association with the long-term decreases to productivity levels in response to decreased nutrient loads after the outfall was relocated offshore. In the years since 2010 fluxes have not been observed, but if that trend continued they would be lower than the box-whiskers in Figure 5-12 and Figure 5-13, and therefore generally consistent with the model results for recent years including 2016.

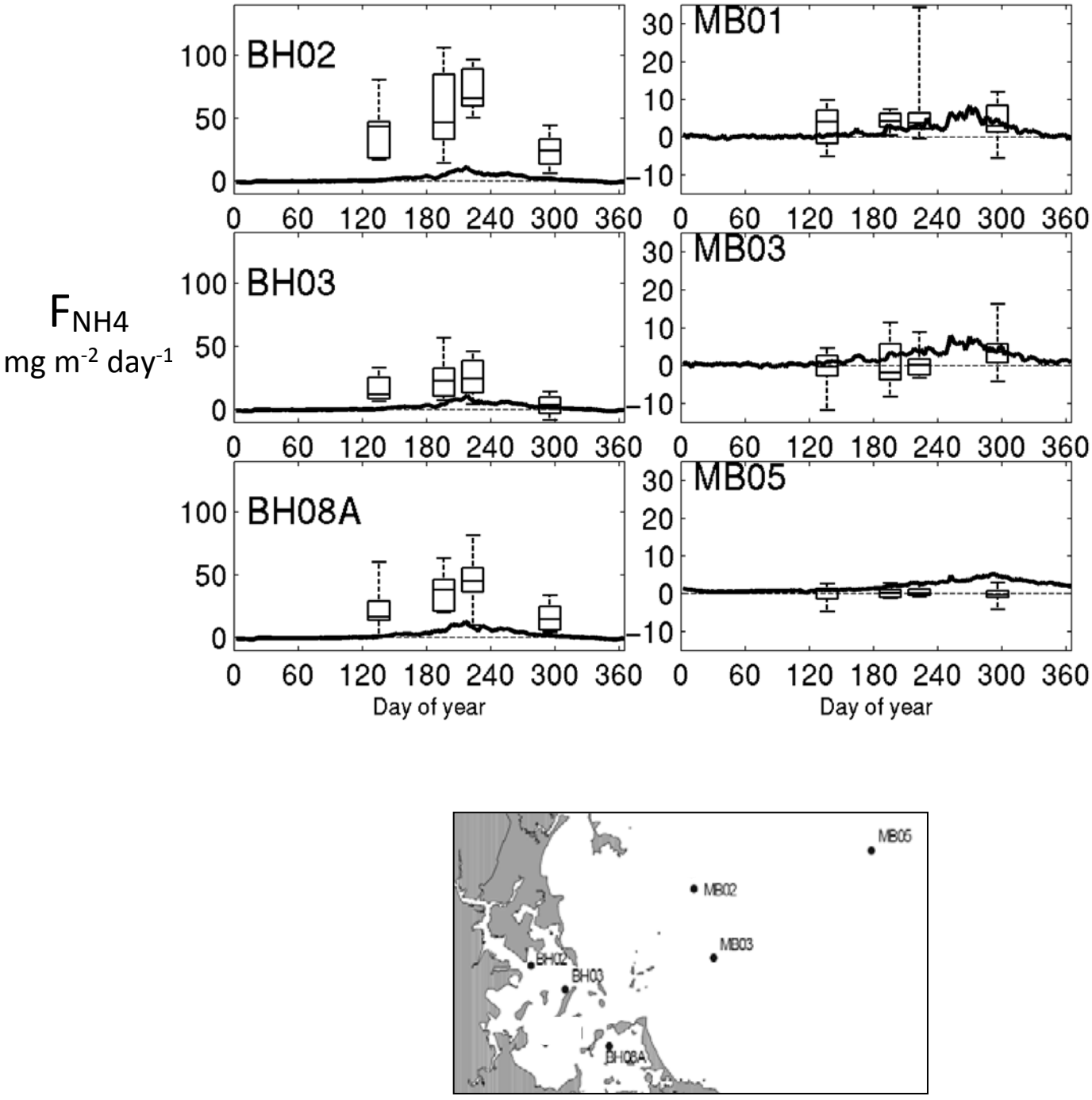

Figure 5-12. Sediment NH4+ flux. Model 2016 (line), observed 2001-2010 (box-whiskers). Select Boston Harbor stations (left column) and Massachusetts Bay stations (right column).

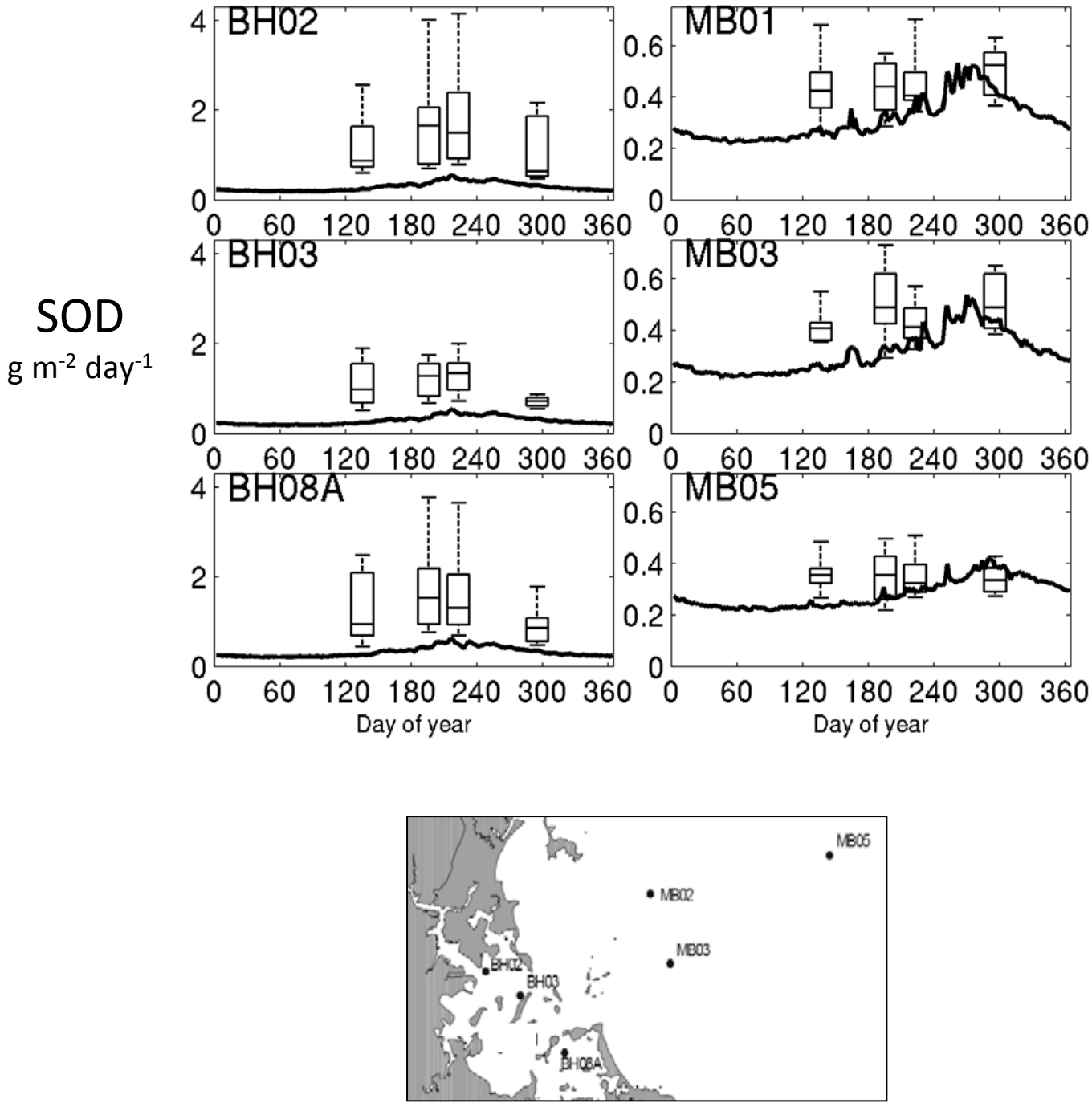

Figure 5-13. Sediment oxygen demand. Model 2016 (line), observed 2001-2010 (box-whiskers). Select Boston Harbor stations (left column) and Massachusetts Bay stations (right column).

5.9 *Summary*

In summary, the UG-RCA 2016 simulation captured many of the observed seasonal and vertical variations of an array of key water quality parameters examined here. Among water column parameters, agreement of the model with observations was generally strongest for DIN and DO, was modest for light, DON, and PON, and was weakest for POC and chlorophyll. Temporal and spatial variability in the model is typically less than observed, and at most stations surface-bottom differences in the model are smaller than observed. These results are typical of model-observation comparisons for the water quality parameters in BEM from prior years.

6. Synthesis/application: Sensitivity to effluent nutrient load

The synthesis/application simulations using 2016 conditions focus on the potential ecosystem impacts of nutrient loads due to the treated effluent released by MWRA through its outfall, located in the northern part of western Massachusetts Bay (see Figure 1-1). Nutrient loads, in this context, refer to nitrate, nitrite, ammonium, and phosphate delivered to the bay through the outfall. The nutrient load is the product of the nutrient concentration in the effluent and the effluent volume flow rate.

A motivation for this investigation is that, as noted above (Figure 3-5), the nitrogen load associated with effluent released at the outfall was slightly higher in 2016 than in recent years. The permit MWRA holds for operating its outfall has an Ambient Monitoring Plan attached to it, which includes a Contingency Plan (e.g., MWRA, 2001). The purpose of the Contingency Plan is to ensure that appropriate actions are taken in the event that the monitoring program observes conditions that change relative to defined thresholds. The Contingency Plan, developed in the late 1990s, included projections for future effluent nitrogen loads based on projected population growth in the Boston metro area and the associated increases anticipated for influent to the treatment plant. The estimate projected for 2020 conditions was 14,000 metric tons (MT) of nitrogen per year (MT yr^{-1}). This amount was denoted as a "Warning Level" in the contingency plan, with the purpose that an exceedance of this level prior to 2020 would indicate nitrogen loads had increased faster than expected based on population growth. The Contingency Plan also included a less stringent threshold denoted the "Caution Level", set arbitrarily at approximately 90% of the 2020 projection or 12,500 MT yr^{-1}. The main purpose of the Caution Level is as an informational trigger, such that an exceedance prior to 2020 would require MWRA to determine the causes and significance of the exceedance and identify what response, if any, was necessary. The 2016 nitrogen load was very nearly as high as the 12,500 MT yr^{-1} threshold.

Background. The topic of sensitivity to effluent nutrient loads has been investigated extensively in past BEM simulations. In a number of prior reports, comparisions were made between simulations that incorporated that year's observed effluent nutrient concentrations and companion simulations that were otherwise completely identical (including the effluent flow rate) except that the effluent nutrient concentrations (and therefore the nutrient loads) were fixed at zero (Hydroqual 1995; Jiang and Zhou, 2008; Tian et al., 2009; Chen et al., 2010; Tian et al., 2010; Zhao et al., 2011; Zhao et al., 2012, Zhao et al., 2015a; Zhao et al., 2015b). These comparisons have each concluded

that the removal of the effluent nutrient load (a) has negligible effect on bay-wide ecosystem function, in particular without important influence on water quality variables such as chlorophyll and dissolved oxygen, and (b) has one main impact, which is to modestly reduce the concentration of nutrients, primarily ammonium, within about 10-20 km of the outfall in the deeper portion of the water column. These findings support the conclusion that the main impact of the outfall nutrient loads on the bay is to cause modest increases in nutrient concentrations (mainly ammonium) near the seafloor in the local vicinity of the outfall, a result that has been arrived at independently through analysis of extensive observations collected by the outfall monitoring program (see, e.g., Werme et al., 2017). The reason the Massachusetts Bays system is not strongly sensitive to outfall nutrient loads is that the vast majority of its nutrients originate in the Gulf of Maine and are delivered by exchange with offshore waters (see, e.g., Figure 3-4 above). Nutrients from the outfall are only a small percentage of the total.

In addition, in the report on BEM simulations of 2013 conditions (Zhao et al., 2015b), a series of model runs was used to investigate sensitivity, in otherwise-identical simulations, to a broad range of nutrient loads from zero load to a load twice as high as the observed nutrient load that year. The latter case, a doubling of the nutrient loads, was included as an unrealistically high hypothetical limiting case, to help improve understanding of the system response. The investigation found that even in the case of doubling the nutrient loads, bay-wide ecosystem function was not significantly impacted. The main effects of the doubling were substantially higher DIN (by ~53%) local to the outfall and mainly at depth, minor increases (by ~7%) to chlorophyll concentrations, and changes of less than 0.5% in dissolved oxygen concentrations; conditions far from the outfall (for example, Cape Cod Bay) were essentially indistinguishable from the simulation with actual 2013 loading (Zhao et al., 2015b). Another important finding was that the impacts of changed nutrient loads varied in linear proportion with the loads: the magnitudes of the increases to DIN and to chlorophyll, and of the decreases to dissolved oxygen, varied in linear reponse to the amount by which nutrient loads changed. This linearity was demonstrated to apply for loads within the range from zero to at least twice the observed load.

Methods. The maximal-realism simulation (as described in the above sections of this report) of 2016 conditions using observed nutrient loads (denoted 1X; the control run) was repeated two times, using nutrient concentrations in the effluent that were reduced by 20% (denoted 0.8X) and increased by 20% (denoted 1.2X) but with all other aspects kept identical. Comparisons were made

between the results of these new runs and the control run. The comparisons use year-long time series of DIN at the surface and seafloor, surface chlorophyll, bottom dissolved oxygen, and surface dissolved oxygen percent concentration at seven locations spanning Massachusetts Bay, Cape Cod Bay, and the mouth of Boston Harbor, including the outfall location. The comparisons also use maps and vertical sections of *differences* of ammonium concentration, the parameter that outfall nutrient loads most strongly influence, between the 1.2X and 1X cases and between the 1X and 0.8X cases, as monthly averages through the 12 months of the year. Finally, the differences between the 1.2X and 1X cases, and between the 1X and 0.8X cases, were tabulated at three representative stations and normalized by the 1X case to yield Δ values, reported as percentages, for the month of August when the differences are among the largest during the year.

Results. Timeseries of surface DIN concentration (Figure 6-1) through the year for the three simulations (0.8X, 1X, and 1.2X) at the 7 stations make evident the differences among the runs. As expected, concentrations are higher in the 1.2X run and lower in the 0.8X run. The differences are minor, even over the outfall, not exceeding about 1 μM. Timeseries for bottom DIN concentration presented in the same way (Figure 6-2) are similar to the surface DIN results at the non-outfall sites, while at the outfall the changes are larger in magnitude and reach as much as about 3 μM. As expected, the effect on surface chlorophyll (Figure 6-3) is extremely small, and the effects on bottom dissolved oxygen concentration (Figure 6-4) and surface oxygen percent saturation (Figure 6-5) are effectively imperceptible.

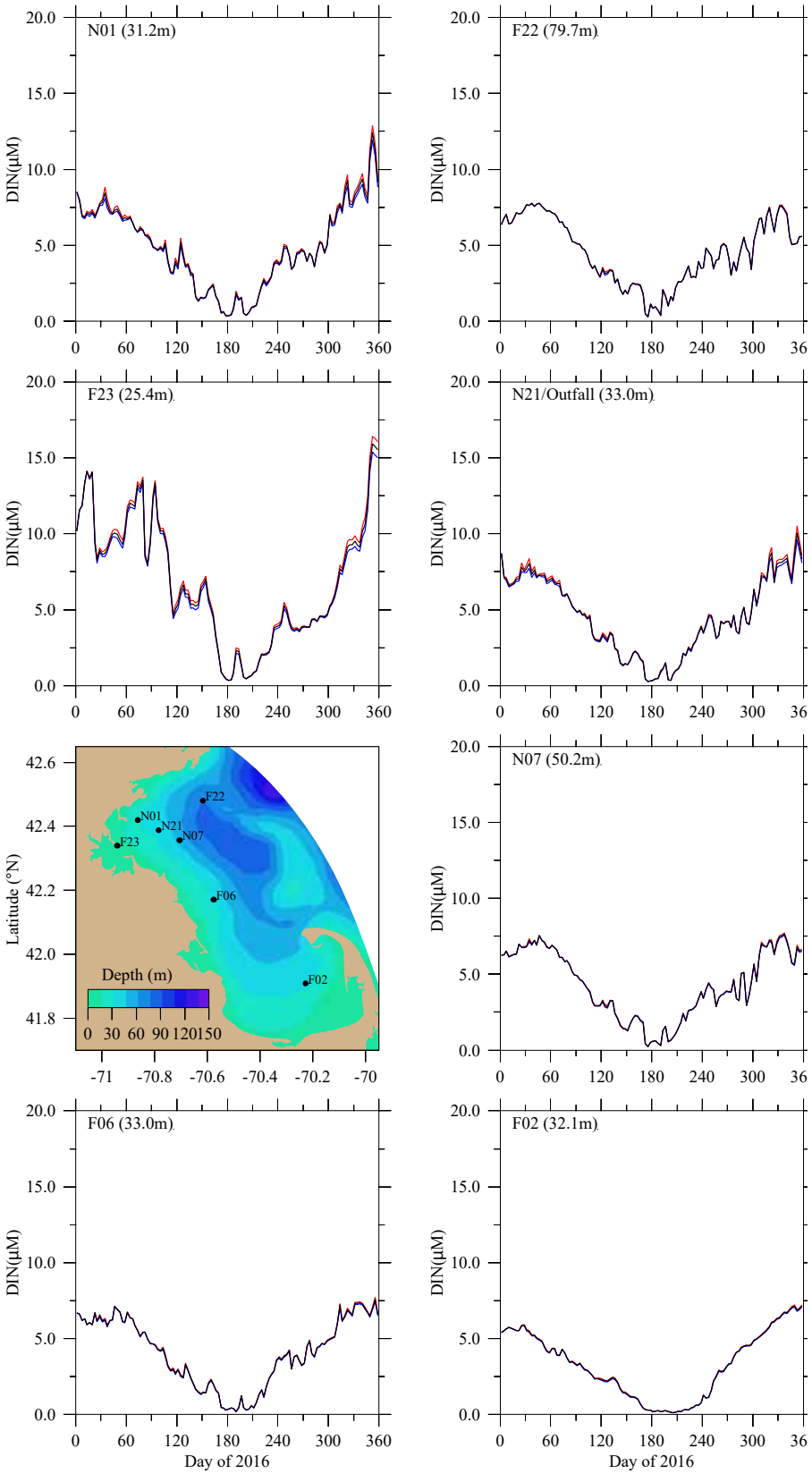

Figure 6-1. Surface DIN time series under 0.8X (blue), 1X (black), and 1.2X (red) nutrient loads. Where the black line and blue/red lines overlap, the black overlies the others.

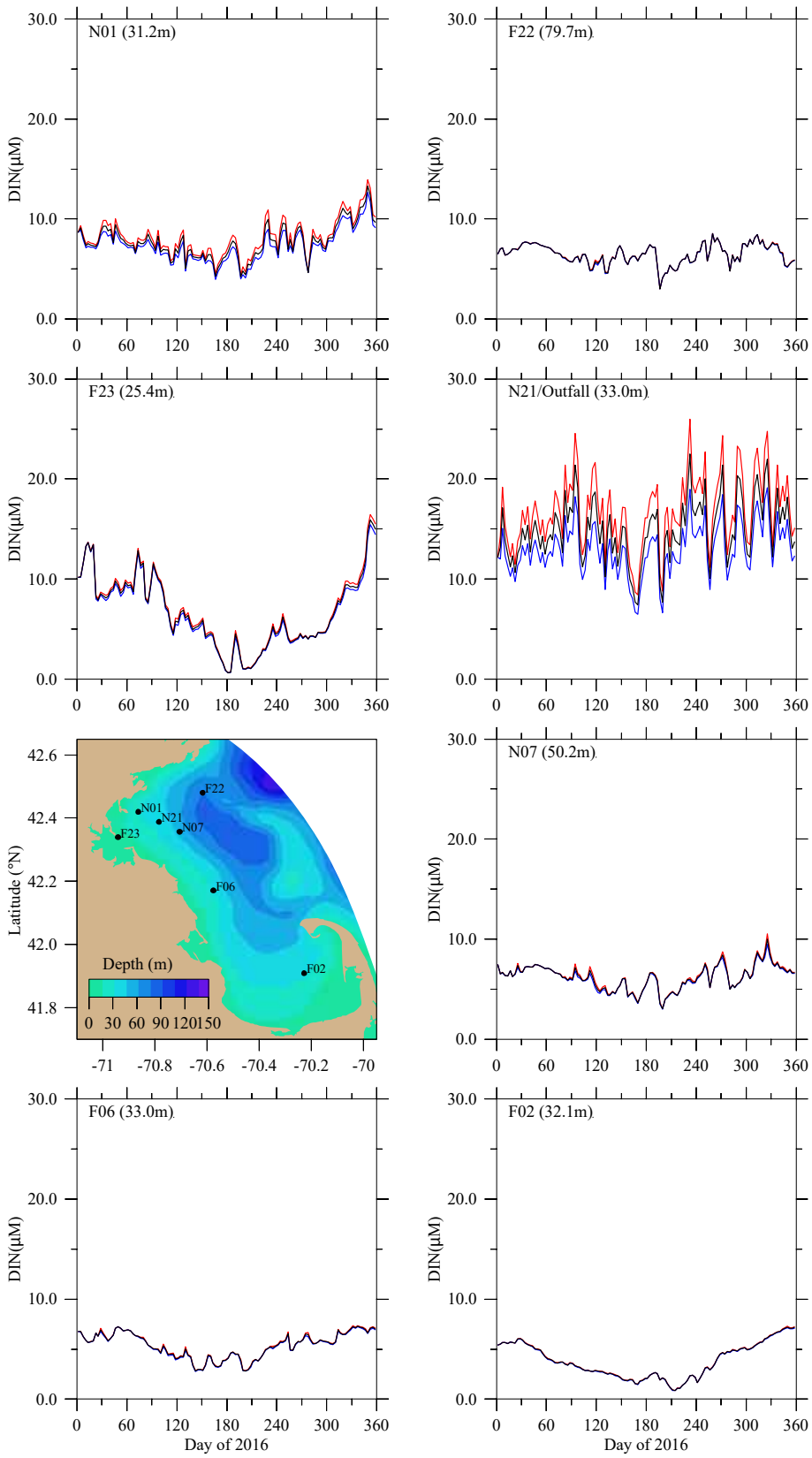

Figure 6-2. Seafloor DIN concentrations, presented as in Figure 6-1.

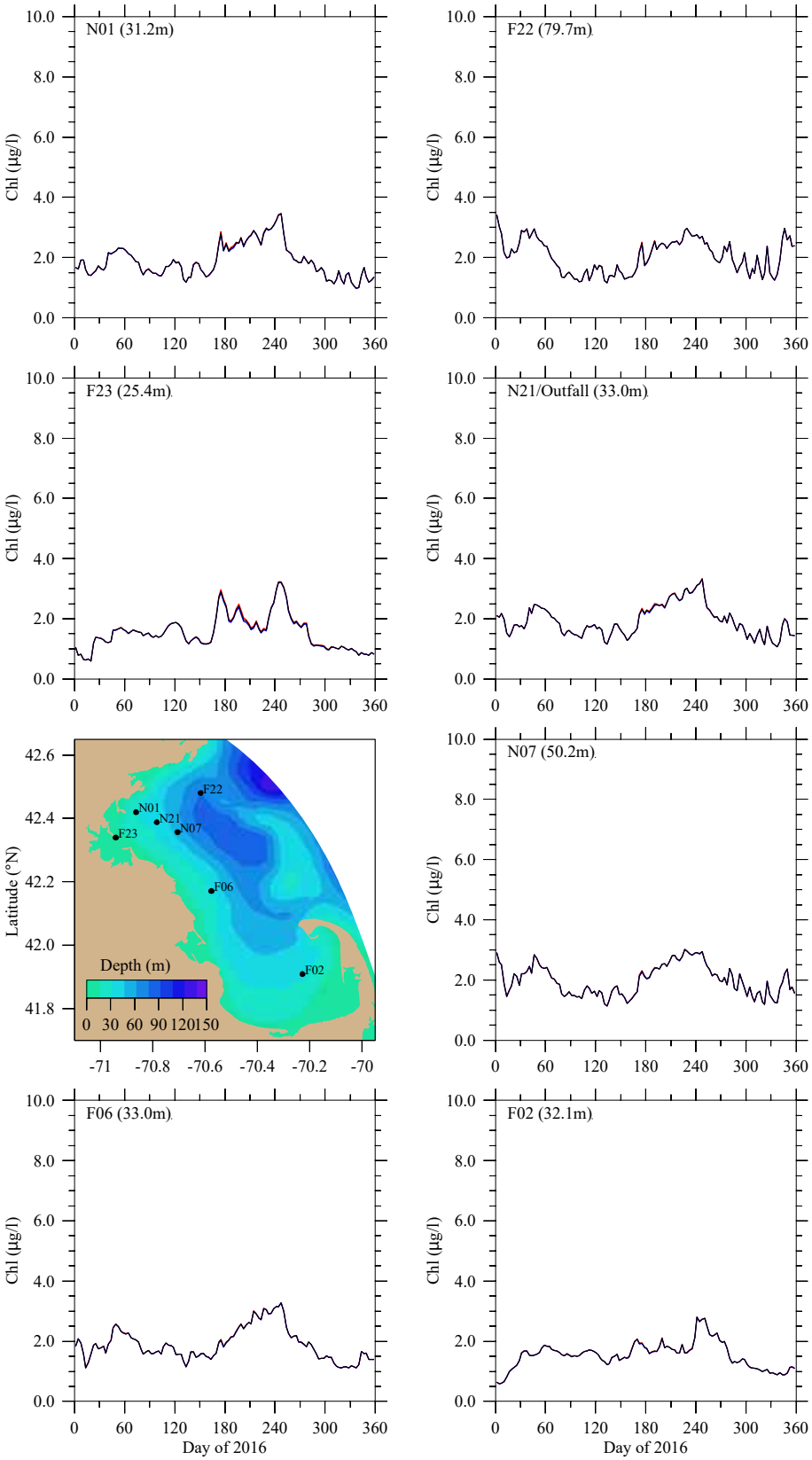

Figure 6-3. Surface chlorophyll concentrations, presented as in Figure 6-1.

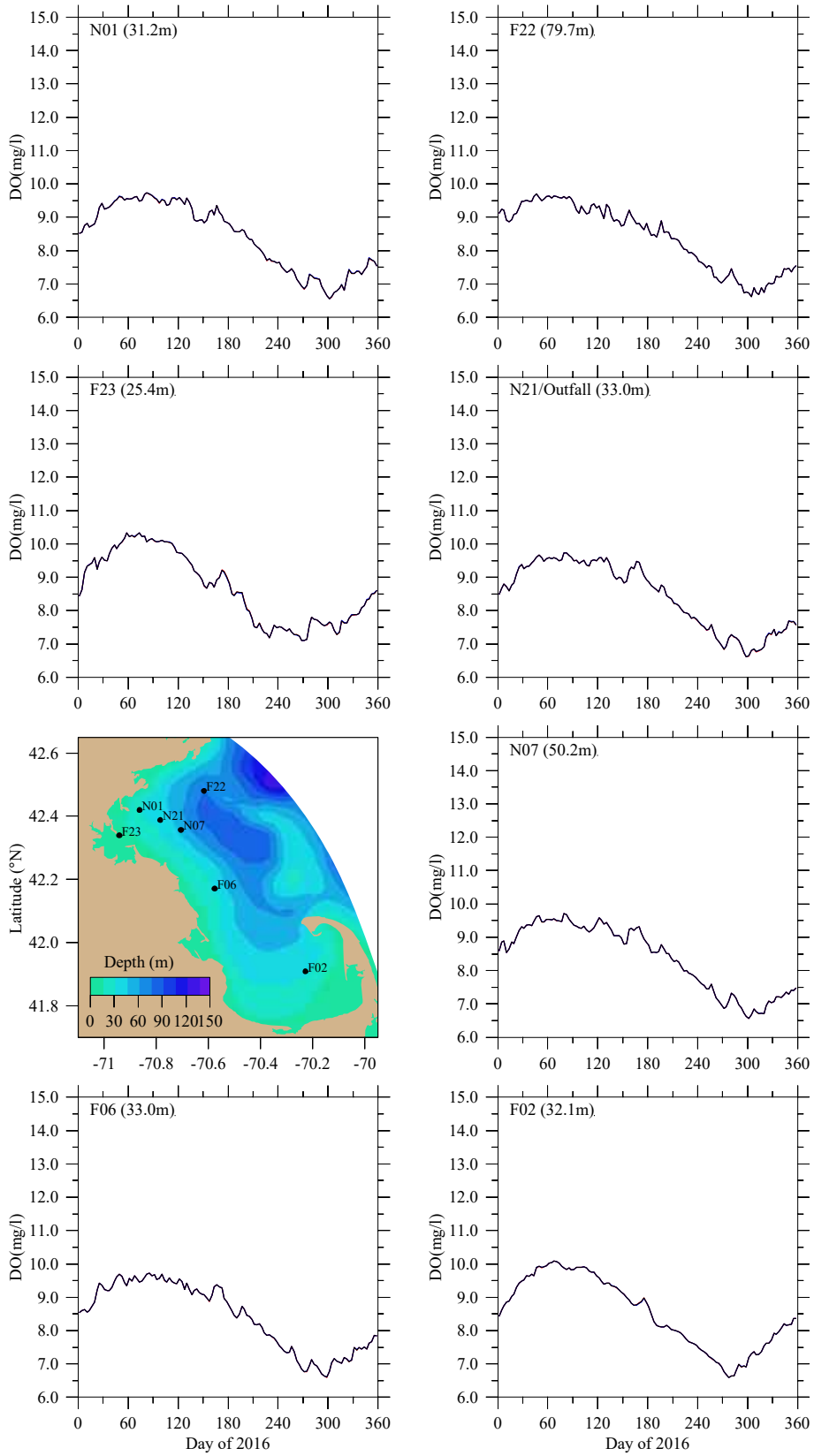

Figure 6-4. Seafloor dissolved oxygen concentrations, presented as in Figure 6-1.

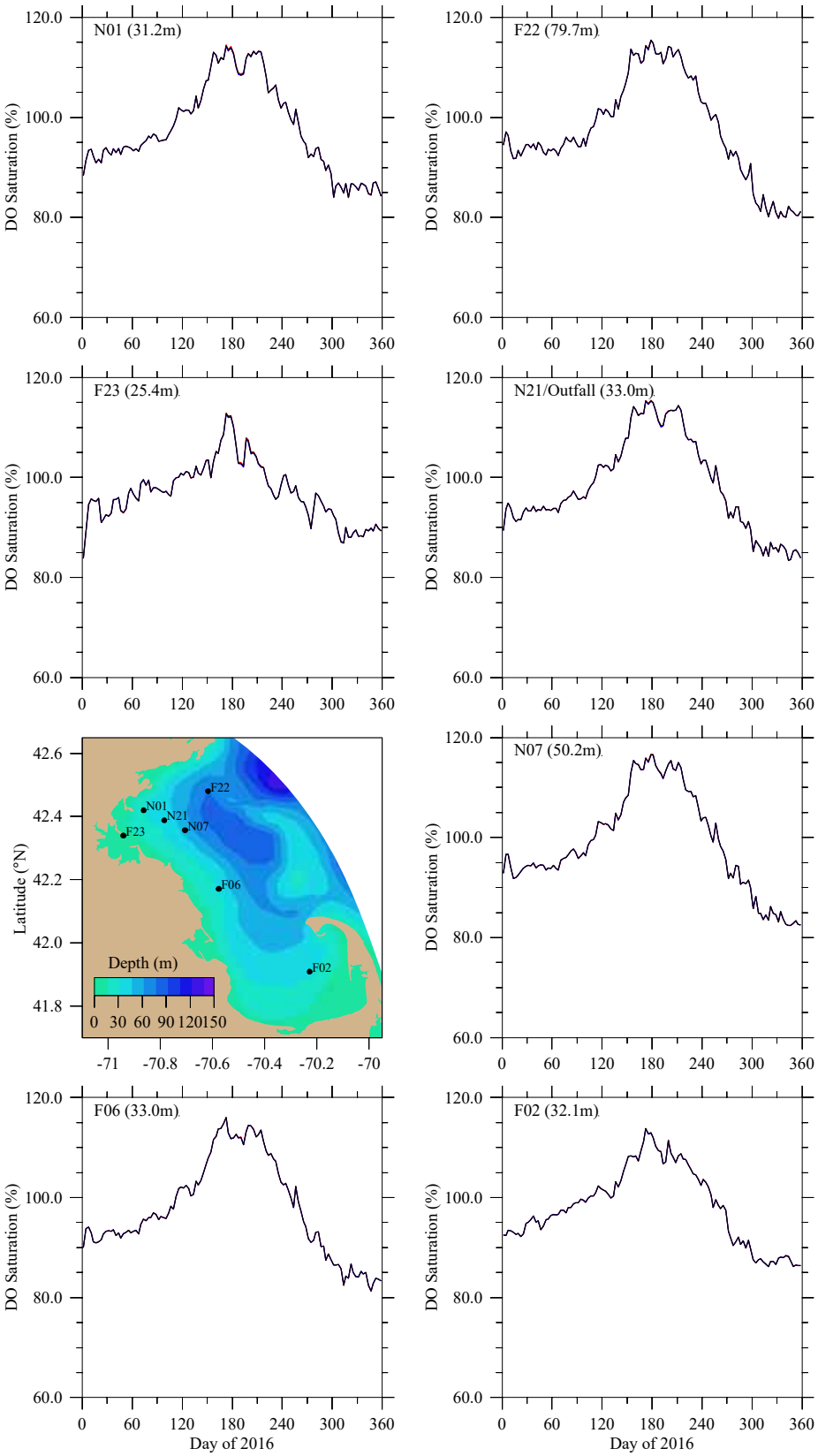

Figure 6-5. Surface dissolved oxygen percent saturation, presented as in Figure 6-1.

Ammonium concentration, which the field monitoring program and prior BEM simulations have determined is the most sensitive parameter to outfall nutrient load increases, is examined to help focus further on these effects. The *differences* between ammonium concentration in the 1.2X run and the 1X run at the seafloor (Figure 6-6), and along the west-east transect (see Figure 3-6) passing through the outfall (Figure 6-7), show that increasing the load to 20% higher than observed causes concentration increases that are confined to an area in the local vicinity of the outfall. The amount of the increases is at most a few μM, on the seafloor at the outfall location, and drops off with distance away from there horizontally and vertically.

The *difference* between ammonium concentration in the 1X and 0.8X runs is presented similarly in Figure 6-8 and Figure 6-9, respectively. The results are virtually identical to the differences between the 1.2X and 1X runs (Figure 6-6 and Figure 6-7). This graphically demonstrates the linearity of the response to nutrient load changes. A 20% increase *or* decrease in nutrient loads, relative to the observed 2016 load, causes increases *or* decreases to ammonium concentrations in the bay, respectively, that have effectively identical magnitudes and spatial distributions horizontally and vertically. This is consistent with the result of Zhao et al. (2015b) that the response is linear between zero load and a load of at least 100% higher than observed.

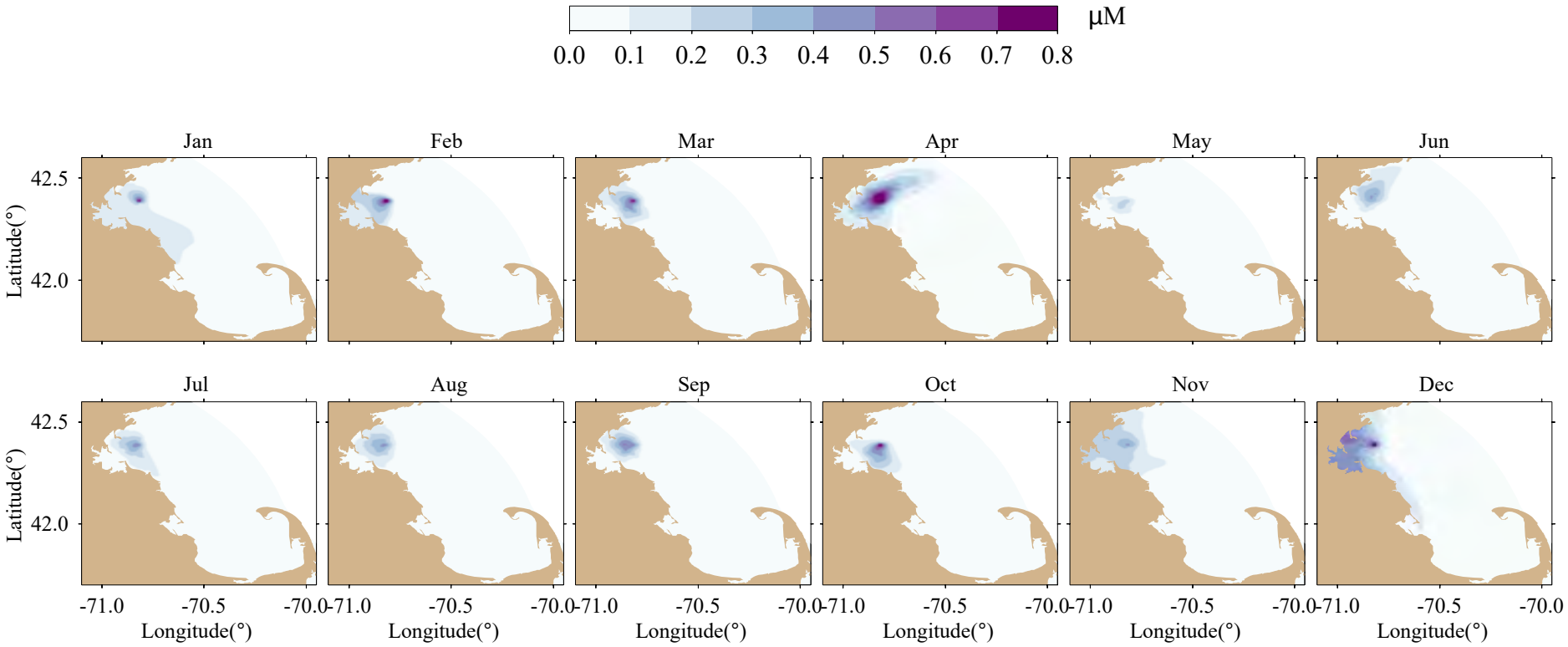

Figure 6-6. *Difference* of seafloor NH4 between 1.2X and 1X runs, monthly means.

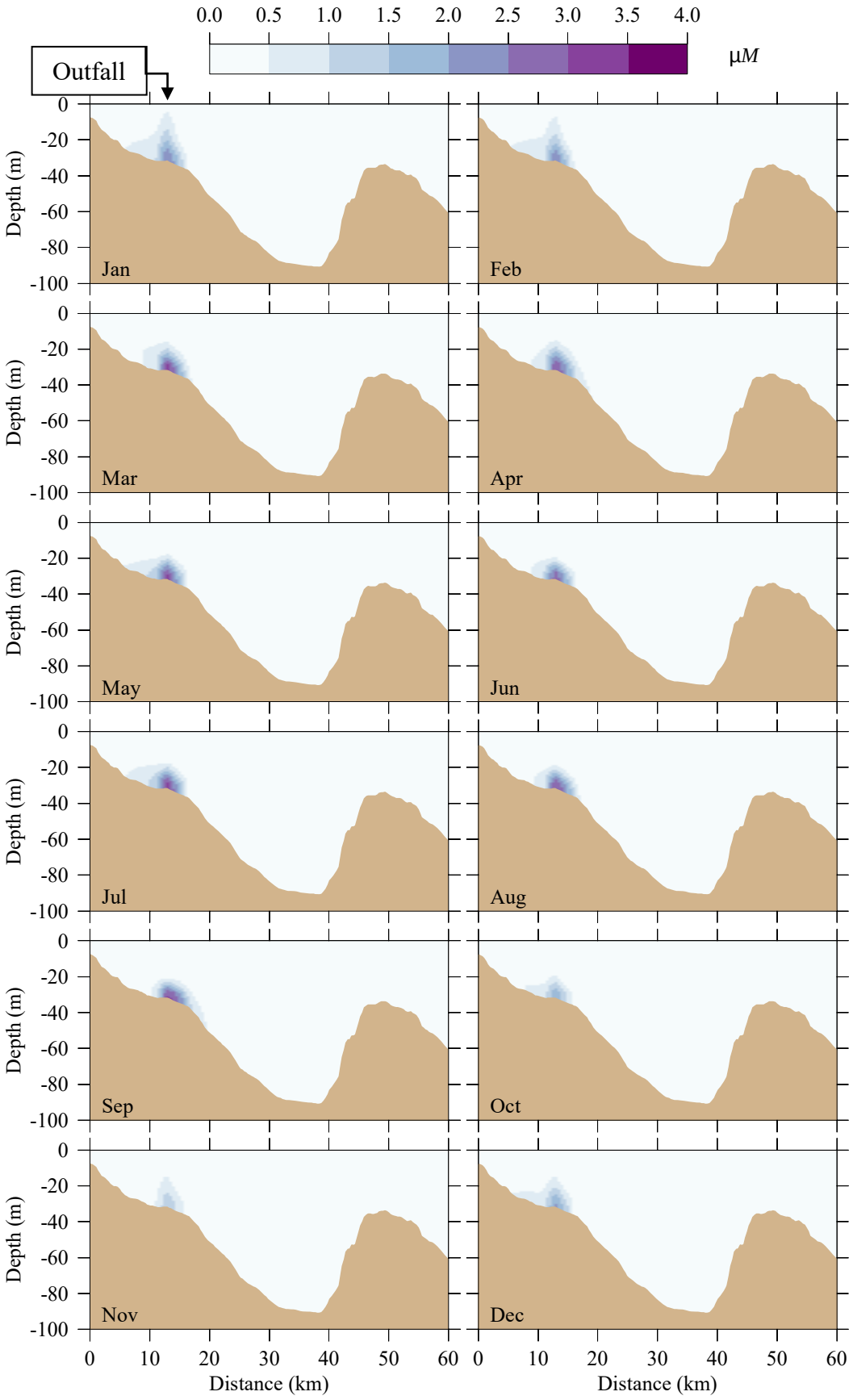

Figure 6-7. *Difference* of NH4 between 1.2X and 1X runs, east-west transect, monthly means.

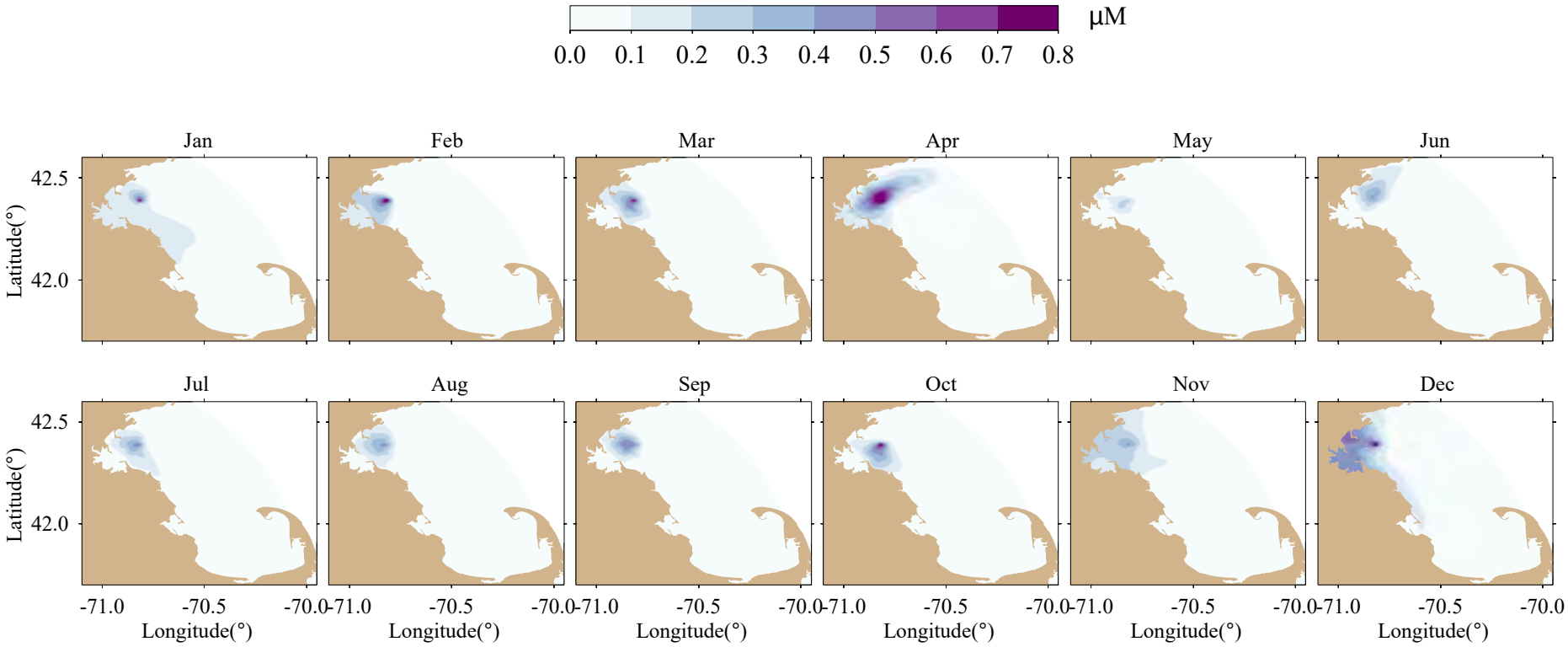

Figure 6-8. *Difference* of seafloor NH4 between 1X and 0.8X runs, monthly means.

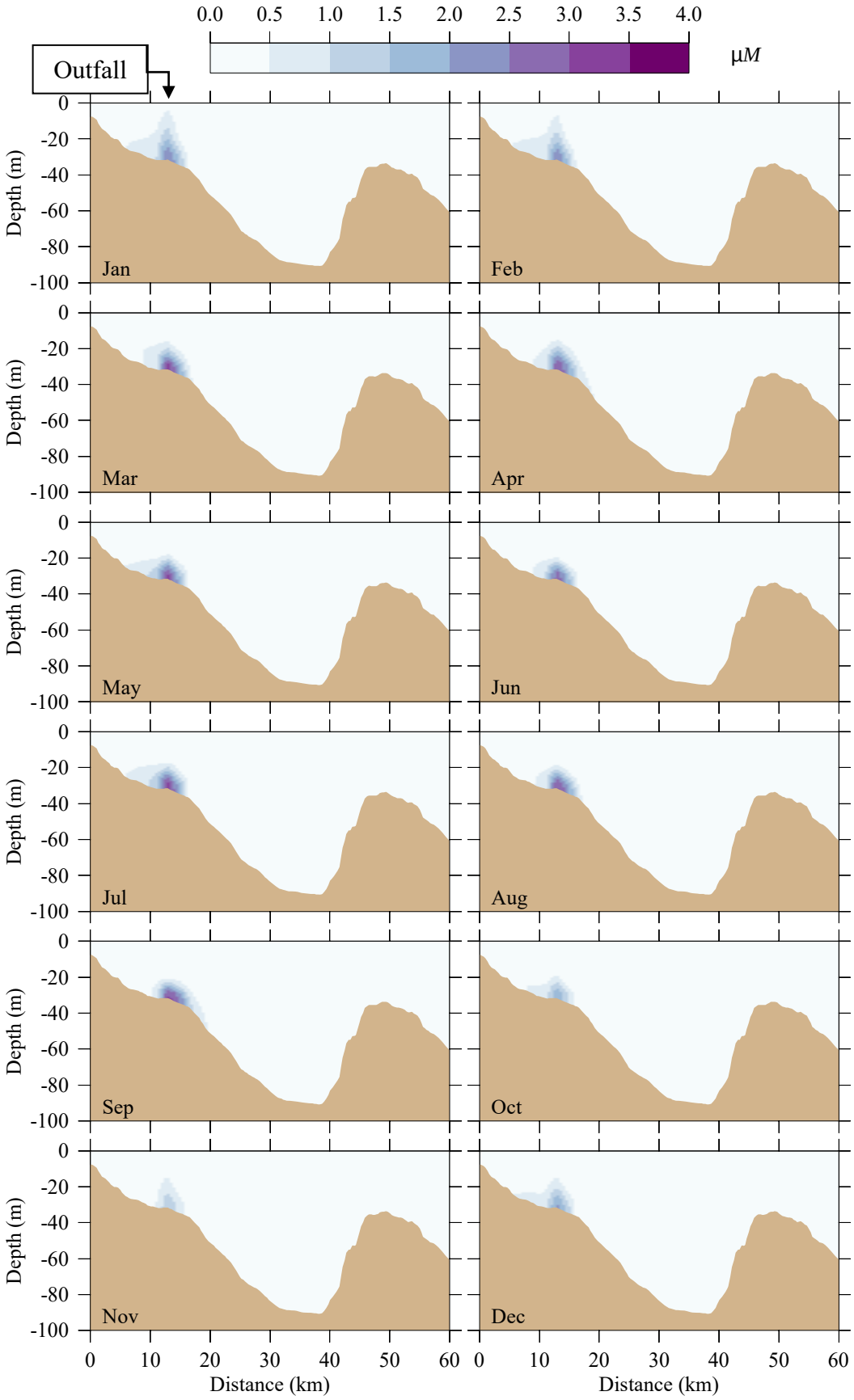

Figure 6-9. *Difference* of NH4 between 1X and 0.8X runs, east-west transect, monthly means.

Table 6-1 shows monthly means from August at three representative stations, and the fractional differences Δ for the 1.2X and 0.8X run relative to the control run, for the same five parameters as examined above. The month of August is representative of other months and is during stratified conditions when ecosystem attributes potentially influenced by eutrophication through nutrient loads, such as dissolved oxygen, can be expected to respond at least as strongly as other times of year. The 20% increase or decrease to the outfall nutrient load led to DIN fractional differences that are largest at the outfall site at the bottom, where they reach magnitudes of about 7.9%. At the outfall site at the surface, they reach magnitudes of about 1.3%, and at other sites they are less than 1% in magnitude. At all sites, magnitudes of fractional differences in chlorophyll are much smaller (0.3% or less), and for oxygen concentration and percent saturation they are trivial (0.03% or less). The symmetry (effectively same magnitudes, with opposite signs) of the Δ values for the 0.8X and 1.2X cases further demonstrates the linear nature of the system response, as described above.

In addition to verifying the expectation that the effects of outfall nutrient loads are limited even for 2016 conditions, when the effluent nitrogen load was slightly higher than in recent years, these results shed light on the nitrogen load thresholds in the Contingency Plan. Both thresholds (12,500 and 14,000 MT yr^{-1}) are well less than twice a typical load observed in recent years, and therefore within the range for which the response of the system is linearly proportional to increases or decreases in load (Zhao et al., 2015b). In 2016 the actual load was under, but very near to, the 12,500 MT yr^{-1} threshold. Based on these synthesis simulations it can be concluded that, in the event that the load in a future year exceeds the 12,500 MT yr^{-1} threshold by as much as 20%, to reach 15,000 MT yr^{-1} (and therefore exceeds even the 14,000 MT yr^{-1} threshold), effects on the system will be limited to minor increases (less than about 8%) in deep DIN concentrations local to the outfall and will not lead to important influences on other ecosystem characteristics such as chlorophyll and oxygen. As noted above, the reason for the relative insensitivity of the system to outfall nutrient loads is that the vast majority of nutrients are provided by exchange with offshore water of the Gulf of Maine, not the outfall.

Table 6-1. August 2016 means and fractional differences Δ at three representative stations.

		Surface Chlorophyll		Surface DIN		Bottom DIN		Bottom DO Concentration		Surface DO Saturation	
		[µg L^{-1}]	**Δ%**	[µM]	**Δ%**	[µM]	**Δ%**	[mg L^{-1}]	**Δ%**	[%]	**Δ%**
Station N18: Near outfall	0.8X	2.8573	**-0.21**	2.6037	**-1.24**	7.1279	**-7.86**	7.8894	**+0.03**	107.3217	**-0.01**
	Control	2.8632		2.6365		7.7359		7.8874		107.3308	
	1.2X	2.8696	**+0.22**	2.6693	**+1.24**	8.3441	**+7.86**	7.8857	**-0.02**	107.3399	**+0.01**

		Surface Chlorophyll		Surface DIN		Bottom DIN		Bottom DO Concentration		Surface DO Saturation	
		[µg L^{-1}]	**Δ%**	[µM]	**Δ%**	[µM]	**Δ%**	[mg L^{-1}]	**Δ%**	[%]	**Δ%**
Station F06: West-central MB	0.8X	2.9545	**-0.11**	2.1821	**-0.77**	4.7100	**-0.90**	7.8955	**+0.01**	107.6676	**-0.00**
	Control	2.9577		2.1990		4.7530		7.8950		107.6728	
	1.2X	2.9606	**+0.10**	2.2160	**+0.77**	4.7956	**+0.90**	7.8945	**-0.01**	107.6778	**+0.00**

		Surface Chlorophyll		Surface DIN		Bottom DIN		Bottom DO Concentration		Surface DO Saturation	
		[µg L^{-1}]	**Δ%**	[µM]	**Δ%**	[µM]	**Δ%**	[mg L^{-1}]	**Δ%**	[%]	**Δ%**
Station F02: Cape Cod Bay	0.8X	1.8360	**-0.27**	0.5279	**-0.30**	1.6455	**-0.33**	7.7352	**-0.01**	105.5162	**-0.01**
	Control	1.8409		0.5295		1.6509		7.7358		105.5277	
	1.2X	1.8456	**0.26**	0.5309	**+0.26**	1.6560	**+0.31**	7.7361	**+0.00**	105.5379	**+0.01**

7. Summary

The Marine Ecosystem Dynamics Modeling Laboratory at University of Massachusetts Dartmouth simulated hydrodynamic and water quality parameters for calendar year 2016 in Massachusetts Bay, Cape Cod Bay, and Boston Harbor using the unstructured-grid Bays Eutrophication Model (BEM). BEM consists of a system of nested models including data-assimilative hydrodynamic simulations at global (Global-FVCOM), regional (GOM4-FVCOM), and coastal embayment (MB-FVCOM) scales, together with the UG-RCA water quality model applied within a subset of the latter. The methods were the same as in the prior year's simulation (described in Zhao et al., 2016b) except that resolution of a northern portion of the grid for the regional model was increased.

The main features of observed seasonal cycles in temperature and salinity were captured well by the hydrodynamic model. The seasonal cycle of stratification in the model also agreed well with observations. Comparisons to observed currents were favorable.

Overall patterns in seasonal variations and vertical structure of many water quality parameters in the model were in good agreement with observations. In comparison to field measurements, the model typically showed a smaller range of values, and smaller surface-bottom differences during the stratified season. The well-known observed spring/summer reduction in shallow DIN concentrations due to phytoplankton uptake, and later fall replenishment due to enhanced mixing when stratification breaks down, were apparent in the model and consistent with observations. The model also reproduced the main characteristics of the observed seasonal cycle of DO, with peaks in spring when shallow values increase due to phytoplankton growth, followed by continuous decreases at depth through summer and early fall, with replenishment during the winter mixed period. In addition to these bay-wide patterns, near the seafloor local to the outfall (within 10-20 km) dissolved inorganic nitrogen was elevated, but this was not the case for other water quality parameters including chlorophyll. Agreement of model DON and PON with observations was modest, and model POC showed relatively poor agreement with measurements, particularly with regard to vertical structure. In summary, model-observation agreement was generally strongest for DIN and DO, modest for DON and PON, and weakest for POC and chlorophyll. Overall, the simulations support the conclusions of the field monitoring program, that the outfall does not have an appreciable influence on bay-wide ecosystem function.

Agreement with observations was generally better for the hydrodynamic model than for the water quality model. This is not unusual, in the context of current research methods for simulations of coastal waterbodies such as Massachusetts Bay and Cape Cod Bay. In part this is a result of the less complete scientific understanding of the complex biological and chemical processes that are represented in water quality models. The model must include such processes but can only use substantially simplified formulations for them, leading to larger differences when compared to observations. In addition, for the biological and chemical parameters of the water quality model, observations available to drive and verify the model are less spatially and temporally extensive compared to parameters important to the hydrodynamic model. An example of the latter is that water temperatures, and the strength and direction of winds, are monitored at least hourly at multiple Gulf of Maine locations. In contrast, the most substantial field sampling effort for water quality parameters has been the MWRA Ambient Monitoring program, which consists of vessel-based surveys 3-4 weeks apart and focuses on measuring and understanding outfall effects, so can only partially characterize the regional nutrient and plankton dynamics.

To investigate sensitivity to nutrient loads from the MWRA outfall, two synthesis/application simulations were carried out. They were configured identically to the maximal-realism case except that they incorporated effluent nutrient concentrations (and therefore loads) increased or decreased by 20%. They confirmed the expectation that changed outfall load effects (a) are limited to minor changes to nutrient concentrations in the vicinity of the outfall and do not cause important changes to other ecosystem characteristics such as chlorophyll and dissolved oxygen, and (b) occur in linear proportion to the magnitude of the changed load. In 2016 the outfall nitrogen load was higher than in recent years; it was below but very close to the 12,500 metric tons per year threshold in the Contingency Plan attached to MWRA's permit for operating the outfall. The conclusion from these simulations is that if the outfall nitrogen load were to be higher by as much as 20% in some future year, reaching up to 15,000 metric tons per year and therefore exceeding the 14,000 metric tons per year threshold in the Contingency Plan, the effects on bay-wide ecosystem function would remain linearly proportional to the amount of the increase and be limited to minor increases in nutrient concentrations local to the outfall (maximum increase of up to about 8%, near the bottom). This insensitivity to outfall nutrients is due to the fact that the outfall nutrient load contributes a small percentage to the nutrients in the bays system, which originate dominantly from exchange with offshore Gulf of Maine waters.

References

Beardsley RC, EE Adams, D Harleman, A Giblin, JR Kelly, JE O'Reilly, and JF Paul, 1995. Report of the MWRA hydrodynamic and water quality model evaluation group. MWRA Enviro. Quality Dept. Misc. Rpt. No. ms-37. Boston: Massachusetts Water Resource Authority. 58pp. http://www.mwra.state.ma.us/harbor/enquad/pdf/1995-ms-37.pdf

Becker S, 1992. The seasonal distribution of nutrients in Massachusetts and Cape Cod Bays. Masters Thesis, University of New Hampshire, Durham. 127pp.

Blumberg A, Z Ji, and CK Ziegler, 1996. Modeling outfall plume behavior using a far field model, *J. Hydraulic Engineering*, 112: 610-616.

Chen C, B Beardsley, GW Cowles, J Qi, Z Lai, G Gao, D Stuebe, Q Xu, P Xue, J Ge, R Hu, R Ji, R Tian, H Huang, H Wu, H Lin, Y Sun, and L Zhao, 2013. An Unstructured grid, Finite-Volume Community Ocean Model-FVCOM User Community-FVCOM user manual, School for Marine Science and Technology, University of Massachusetts Dartmouth, New Bedford, Fourth Edition. SMAST/UMASSD Technical Report-13-0701, 404pp.

Chen, C, H Haung, RC Beardsley, Q Xu, R Limeburner, GW Gowles, Y Sun, J Qi and H Lin, 2011. Tidal dynamics in the Gulf of Maine and New England Shelf: An application of FVCOM. *J. Geophys. Res., 116*. C12010, doi: 10.1029/2011JC007054.

Chen, C, G Gao, Y Zhang, R Beardsley, Z Lai, J Qi, H Lin. 2016. Circulation in the Arctic Ocean: Results from a high-resolution coupled ice-sea nested Global-FVCOM and Arctic-FVCOM system. *Prog. Oceanogr.* 141 (2016), 60-80.

Chen C, R Tian, RC Beardsley, J Qi, and Q Xu, 2010. Modeling 2008 in Massachusetts Bay using an upgraded unstructured-grid Bays Eutrophication Model. Boston: Massachusetts Water Resources Authority. Report 2010-15. 127pp. http://www.mwra.state.ma.us/harbor/enquad/pdf/2010-15.pdf

Cowles, GW, SJ Lentz, C Chen, Q Xu, and RC Beardsley, 2008, Comparison of observed and model-computed low-frequency circulation and hydrography on the New England Shelf, *J. Geophys. Res.*, 113, C09015, doi:10.1029/2007JC004394.

Fitzpatrick JJ and RA Isleib, 2003. Post-audit analysis of the impacts of wastewater treatment plant outfall relocation on Boston Harbor, Massachusetts Bay and Cape Cod Bay water quality Proceedings of the Water Environment Federation, WEFTEC 2003, pp. 530-555.

Geyer, WR, PS Libby, and AE Giblin, 2002. Influence of physical controls on dissolved oxygen variation at the outfall site. Boston: Massachusetts Water Resources Authority. Letter Report, Task Order 35. 20 pp.

Geyer, WR, G Gardner, W Brown, J Irish, B Butman, T Loder, R Signell, 1992. Physical oceanographic investigation of Massachusetts and Cape Cod Bays. Massachusetts Bays Program. U.S. EPA Region I / Massachusetts Coastal Zone Management Office, Boston, Massachusetts. Technical Report MBP-92-03. 497pp.

Hunt CD, RK Kropp, JJ Fitzpatrick, P Yodzis, and RE Ulanowicz, 1999**.** A Review of Issues Related to the Development of a Food Web Model for Important Prey of Endangered Species in

Massachusetts and Cape Cod Bays. Boston: Massachusetts Water Resources Authority. Report ENQUAD 99-14. 62 pp. http://www.mwra.state.ma.us/harbor/enquad/pdf/1999-14.pdf

HydroQual, 1993. A water quality model for Massachusetts and Cape Cod Bays. Boston: Massachusetts Water Resources Authority. Report 1993-05. 222pp. http://www.mwra.state.ma.us/harbor/enquad/pdf/1993-05.pdf

HydroQual, 1995. A water quality model for Massachusetts and Cape Cod Bays: Calibration of the Bay Eutrophication Model (BEM). Boston: Massachusetts Water Resources Authority. Report 1995-08. 402pp. http://www.mwra.state.ma.us/harbor/enquad/pdf/1995-08.pdf

HydroQual, 2000. Bays Eutrophication Model (BEM): modeling analysis for the period 1992-1994. Boston: Massachusetts Water Resources Authority. Report 2000-02. 158pp. http://www.mwra.state.ma.us/harbor/enquad/pdf/2000-02.pdf

HydroQual, 2001. Analysis of the addition of a third algal group to the Bays Eutrophication Model (BEM) kinetics. Boston: Massachusetts Water Resources Authority. Report ENQUAD 2001-15. 110pp.

HydroQual, 2002a. Sensitivity of the Bays Eutrophication Model (BEM) to changes in algal model coefficients. Boston: Massachusetts Water Resources Authority Report 2002-16. 236pp. http://www.mwra.state.ma.us/harbor/enquad/pdf/2002-16.pdf

HydroQual, 2002b. Addendum to the 1998-1999 hydrodynamic modeling report. Boston: Massachusetts Water Resources Authority. Report 2002-17. 82pp. http://www.mwra.state.ma.us/harbor/enquad/pdf/2002-17.pdf

HydroQual, 2004. “User’s Guide for RCA, Release 3.0”, Hydroqual, Inc, New Jersey.

Jiang M, GT Wallace, M Zhou, PS Libby and CD Hunt, 2007. Summer formation of a high-nutrient low-oxygen pool in Cape Cod Bay, USA, *J. Geophys. Res.*, **112**, C05006, doi:10.1029/2006JC003889.

Jiang M, and M Zhou, 2004. Calibration of the Massachusetts and Cape Cod Bays hydrodynamic model: 2000-2001. Boston: Massachusetts Water Resources Authority. Report 2004-08. 71pp. http://www.mwra.state.ma.us/harbor/enquad/pdf/2004-08.pdf

Jiang, M and M Zhou, 2008. Massachusetts Bay Eutrophication Model: 2005 Simulation. Boston: Massachusetts Water Resources Authority. Report 2008-13. 82 pp. http://www.mwra.state.ma.us/harbor/enquad/pdf/2008-13.pdf

Keay KE, WS Leo, and PS Libby, 2012. Comparisons of Model-Predicted and Measured Productivity in Massachusetts Bay. Boston: Massachusetts Water Resources Authority. Report 2012-03. 11 p. plus Appendix. http://www.mwra.state.ma.us/harbor/enquad/pdf/2012-03.pdf

Li Y, PS Fratantoni, C Chen, JA Hare, Y Sun, RC Beardsley, R Ji, 2015. Spatio-temporal patterns of stratification on the Northwest Atlantic shelf. Prog. Oceanog. 134, p123-137. http://dx.doi.org/10.1016/j.pocean.2015.01.003

Libby PS, DG Borkman, WR Geyer, JT Turner, AS Costa, J Wang, DL Codiga, DI Taylor. 2017. 2016 Water column monitoring results. Boston: Massachusetts Water Resources Authority. Report 2017-11. 56 pp. http://www.mwra.state.ma.us/harbor/enquad/pdf/2017-11.pdf

Libby PS, C Gagnon, C Albro, M Mickelson, A Keller, D Borkman, J Turner, and CA Oviatt, 2005. Combined work/quality assurance plan for baseline water quality monitoring: 2004-2005. Boston: Massachusetts Water Resources Authority. Report 2005-09. Version 1. 76 pp., plus appendices. http://www.mwra.state.ma.us/harbor/enquad/pdf/2005-09.pdf

Limeburner, R (Editor), 1985. CODE-2: Moored Array and Large-Scale Data Report. Woods Hole Oceanographic Institution Technical Report 85-35, 234pp.

Menzie CA, JJ Cura, Jr, JS Freshman, and B Potocki, 1991. Boston Harbor: estimates of loadings. Boston: Massachusetts Water Resources Authority. Report 1991-04. 108pp. http://www.mwra.state.ma.us/harbor/enquad/pdf/1991-04.pdf

Menzie-Cura and Associates, 1991. Sources and loadings of pollutants to the Massachusetts Bay. Report to the Massachusetts Bays Program. Report No. MBP-1991-01.

Montoya JP, KM Rathbun, and CS Mayo, 2003. Information Briefing to Outfall Monitoring Science Advisory Panel. Recent nitrogen isotope data from Massachusetts and Cape Cod Bays. January 6, 2003. 8 pp.

MWRA, 2001. Massachusetts Water Resources Authority Contingency Plan Revision 1. Boston: Massachusetts Water Resources Authority. Report ENQUAD ms-071. 47 p. http://www.mwra.state.ma.us/harbor/enquad/pdf/2001-ms-71.pdf

Sun C, & co-authors, 2010. "The Data Management System for the Global Temperature and Salinity Profile Programme" in Proceedings of OceanObs.09: Sustained Ocean Observations and Information for Society (Vol. 2), Venice, Italy, 21-25 September 2009. Hall, J, DE Harrison, and D Stammer, Eds., ESA Publication WPP-306, doi:10.5270/OceanObs09.cwp.86.

Sun Y, C Chen, RC Beardsley, D Ullman, B Butman, and H Lin, 2016. Surface circulation in Block Island Sound and adjacent coastal and shelf regions: A FVCOM-CODAR comparison, *Progr. Oceanogr.*, 143, p 26-45, DOI:10.1016/j.pocean.2016.02.005.

Taylor DI, 2015. Boston Harbor Water Quality 1994-2014. Boston: Massachusetts Water Resources Authority. Report 2015-05. 11 p. http://www.mwra.state.ma.us/harbor/enquad/pdf/2015-05.pdf

Tian, RC, C Chen, Q Xu, PF Xue, GW Cowles, RC Beardsley, and B Rothschild, 2009. Massachusetts Bay Eutrophication Model: 2006-2007 Simulation. Boston: Massachusetts Water Resources Authority. Report 2009-11. 147pp. http://www.mwra.state.ma.us/harbor/enquad/pdf/2009-11.pdf

Tian, RC, C Chen, LZ Zhao, P Xue, WS Leo, MJ Mickelson, 2010. Modeling 2009 in Massachusetts Bay using the unstructured-grid Bays Eutrophication Model. Boston: Massachusetts Water Resources Authority. Report 2010-22. 100pp. http://www.mwra.state.ma.us/harbor/enquad/pdf/2010-22.pdf

Tucker J, and AE Giblin, 2002. Stable isotope analyses of sediment and invertebrate samples from Boston Harbor and Massachusetts Bay. Boston: Massachusetts Water Resources Authority. Report 2002-21. 24 p. http://www.mwra.state.ma.us/harbor/enquad/pdf/2002-21.pdf

Tucker J, AE Giblin, CS Hopkinson, Jr, and D Vasiliou, 2000. Benthic nutrient cycling in Boston Harbor and Massachusetts Bay: 1999 annual report. Boston: Massachusetts Water Resources Authority. Report 2000-11. 63 p. http://www.mwra.state.ma.us/harbor/enquad/pdf/2000-11.pdf

Tucker J, S Kelsey, and AE Giblin, 2010. 2009 benthic nutrient flux annual report. Boston: Massachusetts Water Resources Authority. Report 2010-10. 27 p. http://www.mwra.state.ma.us/harbor/enquad/pdf/2010-10.pdf

Werme C, KE Keay, PS Libby, DL Codiga, DI Taylor, D Wu, L Charelstra. 2017. 2016 Outfall monitoring overview. Boston: Massachusetts Water Resources Authority. Report 2017-12. 49 p. http://www.mwra.state.ma.us/harbor/enquad/pdf/2016-12.pdf

Xue, P, C Chen, J Qi, RC Beardsley, R Tian, L Zhao, and H Lin, 2014. Mechanism studies of seasonal variability of dissolved oxygen in Mass Bay: A multi-scale FVCOM/UG-RCA application. *Journal of Marine Systems*. 131, 102-119.

Zhao L, C Chen, RC Beardsley, DL Codiga, WS Leo, and MJ Mickelson, 2015a. Modeling 2012 in Massachusetts Bay Using the Unstructured-Grid Bays Eutrophication Model. Boston: Massachusetts Water Resources Authority. Report 2015-02. 102p. http://www.mwra.state.ma.us/harbor/enquad/pdf/2015-02.pdf

Zhao L, C Chen, RC Beardsley, DL Codiga, WS Leo, and MJ Mickelson, 2015b. Modeling 2013 in Massachusetts Bay Using the Unstructured-Grid Bays Eutrophication Model. Boston: Massachusetts Water Resources Authority. Report 2015-03. 102p. http://www.mwra.state.ma.us/harbor/enquad/pdf/2015-03.pdf

Zhao L, Chen C, Beardsley RC, Codiga DL, Leo W. 2016a. Simulations of Hydrodynamics and Water Quality in the Massachusetts Bay System during 2014 using the Bays Eutrophication Model. Boston: Massachusetts Water Resources Authority. Report 2016-03. 105p. http://www.mwra.state.ma.us/harbor/enquad/pdf/2016-03.pdf

Zhao L, Chen C, Beardsley RC, Codiga DL, Leo W. 2016b. Simulations of Hydrodynamics and Water Quality in the Massachusetts Bay System during 2015 using the Bays Eutrophication Model. Boston: Massachusetts Water Resources Authority. Report 2016-16. 112p. http://www.mwra.state.ma.us/harbor/enquad/pdf/2016-16.pdf

Zhao, L, C Chen, WS Leo, and MJ Mickelson, 2012. Modeling 2011 in Massachusetts Bay using the unstructured-grid Bays Eutrophication Model. Boston: Massachusetts Water Resources Authority. Report 2012-13. 135pp. http://www.mwra.state.ma.us/harbor/enquad/pdf/2012-13.pdf

Zhao L, R Tian, P Xue, C Chen, WS Leo, and MJ Mickelson, 2011. Modeling 2010 in Massachusetts Bay using the unstructured grid Bay Eutrophication Model. Boston: Massachusetts Water Resources Authority. Report 2011-09. 118 p. http://www.mwra.state.ma.us/harbor/enquad/pdf/2011-09.pdf

Massachusetts Water Resources Authority
Charlestown Navy Yard
100 First Avenue
Boston, MA 02129
(617) 242-6000
www.mwra.com